processes

MDPI

*Review*

# Recent Progress of Non-Pt Catalysts for Oxygen Reduction Reaction in Fuel Cells

**Qing Chen, Zhou Zhang, Ruiquan Zhang, Maocong Hu *, Ling Shi * and Zhenhua Yao ***

Hubei Key Laboratory of Industrial Fume and Dust Pollution Control, Jianghan University, Wuhan 430056, China

* Correspondence: maocong.hu@jhun.edu.cn (M.H.); shiling@jhun.edu.cn (L.S.); zhenhua.yao@jhun.edu.cn (Z.Y.)

**Abstract:** In recent years, non-Pt-based ORR catalysts have been developing rapidly and have achieved performance comparable to or even surpassing Pt precious metal catalysts in specific reactions, offering new possibilities for Pt-based catalyst replacement and showing great promise for application. This paper reviews the recent research progress of non-Pt-based fuel cell ORR catalysts. The latest research progress of non-Pt-based ORR SACs (including single metal active site ORR SACs, multi-metal active site ORR SACs, and non-Pt-based noble metal catalyst ORR SACs), non-metallic ORR catalysts, alloy-based ORR catalysts, high-entropy alloy ORR catalysts, and other non-Pt-based fuel cell ORR catalysts are presented in detail. This paper discusses in detail the synthesis methods, characterization means, optimization of performance, and application prospects of these non-Pt-based ORR catalysts. In addition, this review details the excellent performance of these catalysts in terms of compositional and structural controllability, electrical conductivity, and chemical stability, as well as their ability to exhibit ORR activity comparable to that of commercial Pt/C catalysts. This field is full of opportunities and challenges. In summary, non-Pt-based fuel cells show great potential in ORR. With the continuous improvement of preparation and characterization technologies, catalysts have broad application and market prospects. In addition, the development trend of non-precious metal fuel cell catalysts is reviewed.

**Keywords:** single-atom catalysts (SACs); alloy catalysts; high-entropy alloy catalysts; non-metallic catalysts; ORR

**Citation:** Chen, Q.; Zhang, Z.; Zhang, R.; Hu, M.; Shi, L.; Yao, Z. Recent Progress of Non-Pt Catalysts for Oxygen Reduction Reaction in Fuel Cells. *Processes* **2023**, *11*, 361. https://doi.org/10.3390/pr11020361

Academic Editor: Qunjie Xu

Received: 22 November 2022
Revised: 27 December 2022
Accepted: 7 January 2023
Published: 23 January 2023



## 1. Introduction

The growing global energy crisis and environmental pollution pose a great threat to human survival and development [1]. In response, scholars have developed clean, efficient, safe, and sustainable energy sources to address this crisis [2]. The most important of these energy sources are advanced electrochemical energy storage and conversion devices [3], such as direct methanol fuel cells (DMFCs), direct methanol fuel cells (DEFCs), and proton exchange membrane fuel cells (PEMFCs) [4,5], in which the increasing conversion of electrochemical energy to energy reduces the environmental pollution from conventional catalysts [6,7]. The oxygen reduction reaction (ORR) is the cathodic reaction in the above-mentioned electrochemical devices, which may proceed via a two-electron pathway or a four-electron pathway [8]. ORR is a multi-electron reaction with a much more complex mechanism than nitrogen reduction and hydrogen reduction reactions, and contains multiple initial reactions as well as multiple intermediate reactions. The mechanism proposed by Wroblowa in 1976 is perhaps the most effective explanation of the ORR process [9], allowing the formation of (two-electron pathway) or no (four-electron pathway) intermediate $H_2O_2$ through the activation of oxygen molecules electrically reduced to water. Experimental results show that the theoretical potential of the direct four-channel is 1.23 V, while the theoretical potential of the two-channel is 0.7

V. In general, the four-electron reaction has a higher reduction potential than the two-electron reaction. Certain catalysts are less stable when a two-electron or mixed two-electron and four-electron reaction occurs, causing the destruction of the catalyst and the proton exchange membrane by peroxide [10]. Four-electron reaction pathways can completely reduce $O_2$ to $H_2O$, and exhibit a higher output voltage. Therefore, the development of ORR catalysts with four-electron pathways is preferred. However, the slow reaction kinetics of ORR is a constraint on the development of the above electrochemical devices [11–13]. Therefore, there is a need to develop ORR catalysts with excellent electrocatalytic activity and high stability in order to improve the ORR kinetics. The development of efficient and stable ORR catalysts is an effective way to improve the performance of fuel cells [14]. Pt/C is currently the most efficient ORR catalyst for fuel cells [15,16]; however, this catalyst suffers from poor stability and is prone to CO poisoning, leading to the deactivation of its active center [17–19]. In addition, Pt-based ORR catalysts are more difficult to develop commercially for large-scale applications due to the high price and low reserves of Pt. Therefore, it is crucial to explore the development of inexpensive and efficient non-Pt catalysts that can be used for ORR. In summary, this paper reviews the recent research progress of non-Pt-based fuel cell ORR catalysts in recent years. These catalysts, such as non-Pt-based ORR SACs (including monometallic active site ORR SACs, multi-metallic active site ORR SACs, and non-Pt-based noble metal catalyst ORR SACs), non-metallic ORR catalysts, alloy-based ORR catalysts, high-entropy alloy ORR catalysts, and other non-Pt-based fuel cell ORR catalysts, have been the subject of recent research.

Recently, a review of high-performance M-N-C catalyst designs for ORR was published by Ye [20]; another review of non-precious metal-based ORR electrocatalysts was published recently by Sanket D. Bhoyate [21]; a review of 2D material-supported transition metal single-atom ORR catalysts was published by Niu [22]; and Zhang [23], Huang [24], and Huo [25] all published reviews of high-entropy alloy catalytic materials for ORR. Obviously, these are relatively recent and excellent articles; however, they all cover a narrow field. At present, there does not exist any systematic review of fuel cell ORR catalysts involving a complete range of all types. For example, in addition to the above-mentioned types, alloys, non-Pt noble metals, oxides, and a number of other unconventional materials are involved in ORR electrocatalysts; as such, the present review article is meant to help readers quickly understand the related fields. The description of the preparation process, characterization, and application prospects of the materials is more important for review articles [26–30]. In this paper, we systematically introduce a wide and diverse range of ORR catalysts for fuel cells (Figure 1). In addition, we present a detailed discussion and insights into the synthesis methods, characterization methods, performance optimization, application prospects, and challenges of these non-Pt ORR catalysts, focusing on several hot research areas in recent years, such as non-precious metal single-atom catalysts, high-entropy alloy catalysts, and non-metallic ORR catalysts (Supplementary Table S1). This review provides key information for the design of various catalysts and the preparation of new non-Pt-based ORR catalysts with excellent performance, and hopefully can provide useful guidance for colleagues in the electrocatalysis community.

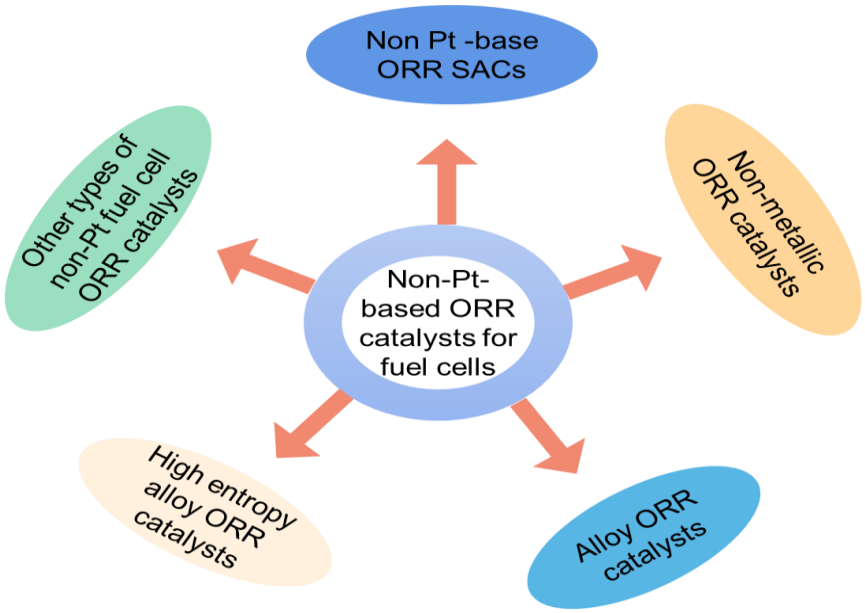


**Figure 1.** Outline of the major topics covered in this paper.

## 2. Non-Pt-Based ORR SACs

### *2.1. Single Metal Active Site ORR SACs*

The study of single-atom catalysts for ORR originated in 1964 when Jasinski et al. [31] discovered that metal phthalocyanines are capable of forming metal M-N4 centers that can catalyze ORR. This work brought inexpensive transition metal-based SCAs for ORR into the limelight and has attracted a great deal of attention from researchers. Based on this study, researchers have invested effort in recent years to immobilize metal-N complexes (mainly Fe-N) and improve their catalytic performance. Because metal macrocycles such as porphyrins and phthalocyanines are catalytically active for ORR, their basic M-N4 structure is considered the active center in heterogeneous environments. One of the most studied is the metal-organic backbone (MOF) class as pre-cursor ORR catalysts. Its most significant advantage is the ability to modulate the morphology and porosity of the carbon-based material, exposing more active sites. In 1989, Ernest Yeager et al. used a mixture of polyacrylonitrile, inorganic salt/cobalt salt, and carbon black as precursors to prepare Co/N/C type ORR catalysts with high catalytic activity by heat treatment at 800 °C in an argon atmosphere [32]. This study demonstrated for the first time that the involvement of macrocyclic compounds is not required, showing that precursors consisting of nitrogen, carbon, and transition metals can be used to prepare M/N/C-type non-precious metal catalysts with excellent ORR activity by high-temperature heat treatment in an inert atmosphere. Horst Jahnke et al. in 1976 and Vladimir S. Bagotzky et al. in 1977 successively published research showing that the activity and stability of the ORR of the products can be significantly improved by heat treatment of transition metal macrocyclic compounds in an atmosphere of inert air at temperatures of 800–900 °C [33,34]. These two works pioneered a new method for synthesizing carbon-based non-noble metal-based catalysts by thermal treatment. In 2011, Zhang et al. developed the concept of single-atom catalysis, which kicked off the research on single-atom nanomaterials [35]. In the ORR reaction, their p-orbital electrons react with the d-orbital of the active center of the catalyst between the oxygen and the intermediate product, causing oxygen uptake and electron migration [36]. This is a strong indication that the selection of suitable metal atomic centers is the most straightforward and effective way to improve the activity of SACs in catalysis.

With the continuous improvement of preparation and characterization techniques over the years, single-atom catalysts have broad applications and market prospects.

Common primary synthesis methods for SACs include pyrolysis [37], co-precipitation [38], atomic layer deposition [39], impregnation [40], chemical reduction [41], and high-energy ball milling [42]. To date, many advanced characterization techniques, such as X-ray photoelectron spectroscopy, atomic-level electron ttomography (AET) techniques, HAADF-STEM, XAFS, (XPS), and Musburger spectroscopy, as well as the development of theoretical calculations, have been irreplaceable for the discovery, development, and optimization of single-atom catalysts as well as the understanding of their catalytic mechanisms.

Although commercial Pt/C is the most efficient catalyst for ORR catalysts, it is expensive to fabricate and its resistance to toxicity is extremely weak. Therefore, in the past decades, scientists have never given up on developing a catalyst with low fabrication cost and high efficiency to replace commercial fuel cell Pt/C catalysts. Conventional non-precious metal-based single-atom catalysts (SACs) are of wide interest in the field of catalysis because of their advantages of up to 100% atomic utilization, flexible ligand structure (easy adjustment), good selectivity, stability, and excellent re-activity [43]. Transition metal N-doped carbon-based catalysts (M-N-C), one of the single-atom catalysts (SACs), are considered a candidate for platinum and have attracted much attention because of their good ORR catalytic activity and relative stability to ORR in acidic media. The reasons for the superior electrocatalytic activity of M-N-C are as follows: (1) doped nitrogen-carbon carriers can greatly stabilize and disperse the transition metals, improving the catalytic performance of ORR [44]; and (2) interaction between nitrogen-doped carbon carriers and non-precious metals can significantly increase the density of active sites and promote catalytic behavior [45]. It has been suggested that the ORR catalytic activity of M-N-C materials follows the pattern Fe > Co > Mn in both acidic and basic electrolytes. M-N-C may have a tunable electronic structure and unsaturated coordination environment, and has strong inter-action between individual metal atoms and the carrier, allowing excellent performance to be achieved [46]. M-N-C has the maximum efficiency of metal atom utilization and exhibits high activity and selectivity. The unique coordination environment and metal centers serve as a transition between the homogeneous phase and multi-phase catalysis, ensuring excellent activity and selectivity in various catalytic reactions. These catalysts are described in detail in the following section.

#### 2.1.1. Fe-Based SACs

With the potential advantages of low toxicity, high abundance, low cost, and magnetic properties, the application of iron in the catalytic industry can improve the efficiency of catalyst recycling and reduce production costs. Traditional precursors for Fe-N-C materials, such as polypyrrole [47] and dicyandiamide [48], suffer from cumbersome and expensive fabrication, which limits the commercialization of Fe-based SACs. To solve this problem, an increasing number of researchers are focusing their research and development efforts on the earth's abundant and low-cost bio-mass-derived carbon. To this purpose, Zhang et al. [49] synthesized novel atomically dispersed Fe-N-CSACs by encapsulating $FeCl_3$ on the porphyrin surface and pyrolyzing the catalytic material, in which Fe is mainly present in the form of $FeN_3S_1$ coordination structure, and half-wave potential of the catalyst in an alkaline environment (0.1 mol/L KOH) is 0.84 V (vs. RHE), showing good ORR catalytic activity. Compared with the noble metal catalyst Pt/C + $RuO_2$, the rechargeable Zn-Air cell composed of this electrocatalyst has a higher power density. This design strategy can expand the utilization of electrocatalysts synthesized from abundant biomass materials, and the effect of S doping on the structure–catalytic activity relationship was systematically investigated as well.

Although Fe-SACs electrocatalysts have become an ideal candidate for commercial Pt/C catalysts for fuel cell ORR, their true catalytic active sites have not been well studied and remain under intense controversy. The electrocatalytic community needs to thoroughly clarify the effect of different types of coordination nitrogen (including

pyridine nitrogen and pyrrole nitrogen) on catalytic performance. Moreover, understanding the pH dependence of the activity of Fe-NC catalysts is an urgent issue. Because of this research gap, Xu et al. [50] comprehensively investigated the ORR activity catalyzed by thirteen different N-liganded Fe-$N_xC$ configurations through simulations based on a constant potential implicit solvent model. Their results demonstrated that the ORR catalytic activity of pyrrole Fe-$N_xC$ is stronger than that of pyridine, with pyrrole $FeN_4C$ having the highest activity in acidic media. The activity of pyridine and pyrrole Fe-NxC usually decreases with the decrease in the amount of ligand N. Mean-while, the conversion of in situ active centers to *O-$FeN_4C$ and *OH-$FeN_4C$ clarifies the source of the higher activity of FeNC in alkaline media. Their work provides valuable guidance for the development of more efficient and stable Fe-based SCAs for ORR. For example, Zhang et al. [51] synthesized Fe SAC-MOF-5 catalysts with high ORR activity in 0.5 M $H_2SO_4$, and the active center was identified as pyridine $FeN_4$. Jiang et al. [52] prepared pyridine-type monoatomic $FeN_4C$ catalysts by pyrolysis reaction based on the good electrocatalytic performance of $SiO_2$@MOF composites under suitable acidic or basic environments. The research results presented above summarize the effects of different types of coordination nitrogen (including pyridine nitrogen and pyrrole nitrogen) on catalytic performance. These works provide a theoretical basis for the design of new efficient and stable Fe-based ORR catalysts.

It is well known that nitrogen-coordinated Fe monoatomic Fe-$N_x$SAs anchored on the carbon support are one of the most effective electrocatalysts for oxygen reduction reaction (ORR); however, it is challenging to enhance the activity of the catalyst by regulating the adsorption environment of Fe-Nx sites. Based on this, Wang et al. reported in a theoretical demonstration that doping nitrogen in carbon carriers can optimize the adsorption of ORR intermediates on Fe-$N_4$ sites by adopting an appropriate approach to anchor Fe-$N_4$ sites in N-rich carbon carriers with abundant tubular channels to synthesize Fe-SAs@NCTCs, with applications in ORR [53]. HR-TEM images showed no formation of metal-containing nanoparticles or clusters in Fe-SAs@NCTCs (Figure 2a). Furthermore, the corresponding energy dispersive X-ray (EDX) images showed a uniform distribution of Fe, N, and C on the prepared catalysts (Figure 2b), and demonstrated the presence of monatomic Fe. AC-HAADF-STEM images showed a high density of Fe unit substructures uniformly distributed in Fe-SAs@NCTCs (Figure 2c). Nitrogen adsorption/desorption isotherms at different pyrolysis temperatures showed abundant micropores and mesoporosity in the Fe-SAs@NCTCs of this catalyst, which fully demonstrated the presence of abundant laminar pores in the carbon walls. Figure 2d shows that the oxidation valence state of Fe is about 2+. The characterization of EXAFS with the related calculation results (Figure 2e–h), indicates that Fe-SAs@NCTCs are mainly coordinated with four N atoms to generate Fe-$N_4$ conformation and anchored in a carbon carrier with active Fe-SAs providing maximized Fe-$N_4$ active sites and electrochemical activity. The graded porous structure with tubular channels provide excellent fast mass transfer during the ORR process; therefore, Fe-SAs@NCTCs exhibit excellent ORR performance that exceeds the performance of Pt/C-based alternatives. The strategy of enhancing catalyst activity by modulating the adsorption environment of Fe-Nx sites provides a good guide for designing hierarchical porous structures and changing the coordination structure of active sites to design single-atom catalysts with high ORR activity.

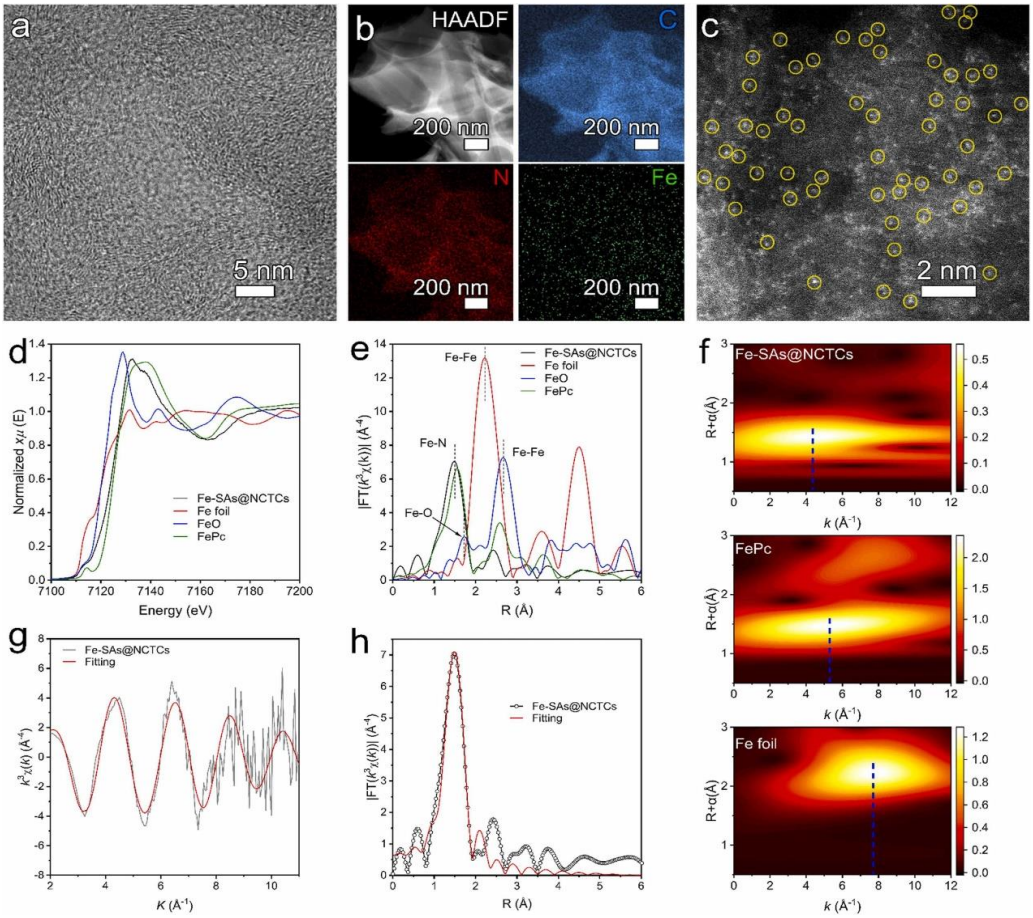


**Figure 2.** (**a**) HR−TEM, (**b**) EDX elemental mapping image, and (**c**) AC−HAADF−STEM image of Fe−SAs@NCTCs. (**d**) The Fe−K-edge XANES spectra and (**e**) Fourier transform of the Fe−SAs@NCTCs, Fe foil, FeO, and FePc in the Fe−K−edge EXAFS spectra. (**f**) WT−EXAFS plots of Fe−SAs@NCTCs, FePc, and Fe foil, respectively. (**g**,**h**) First−shell (Fe−N) fits to the FT−EXAFS spectra of Fe−SAs@NCTCs in K and R space, respectively. (Copyright 2022, Elsevier) (Reprinted with permission from [53]. Copyright 2022, Elsevier).

Currently, the lack of sufficient catalytic activity and long-term durability are two major issues that need to be addressed for Fe-based SCAs, and these catalysts cannot fully replace Pt catalysts for PEMFC applications. The performance of Fe-N-C catalysts can be enhanced by increasing the density of the active site ($FeN_4$) in the 3D structure [54,55]. Furthermore, the conventional preparation process of Fe-based SCAs has the limitation of potentially leading to heterogeneous morphologies, i.e., the presence of many nitrogens- and iron-related byproducts in the catalysts that mask the true active sites. This hinders further understanding of the structure–property relationships of Fe-based SCA catalysts.

To improve the limitations of Fe-N-C catalysts, Zhang et al. [56] obtained a single-atom iron catalyst without metal agglomeration (Fe-N-C) by doping iron ions into the ZIF lattice in a special way in order to form Fe-ZnZIF precursors, followed by one-step thermal activation; the ORR half-wave potential reached 0.85 V (vs. RHE) under acidic conditions, slightly lower than the 0.88 V of Pt/C. The AAT experiment showed that the stability of the catalyst was much better than Pt/C; in addition, the yield of $H_2O_2$ in the ORR process was less than 1%, indicating that the catalytic reaction was a four-electron reduction process. Figure 3a shows that the N4 complex tetrahedral $FeN_4$ structure may be present in the precursor. The combination of HAADF-STEM images (Figure 3c,d) and electron energy loss spectrometer (EELS) combined with microscopy analysis results (Figure 3d inset) demonstrate that these individual single atom sites were Fe. The highly

porous carbon phase dominates in each granule and does not form metal polymers. This catalyst represents one of the best ORR catalysts in acids thanks to the formation of $FeN_4$ in porous carbon carriers with a high density of uniform distribution. This work provides a new idea for scholars to develop novel Fe-based SACs by synthesizing Fe-doped ZIF nanocrystal precursors to modulate the size of catalyst particles.

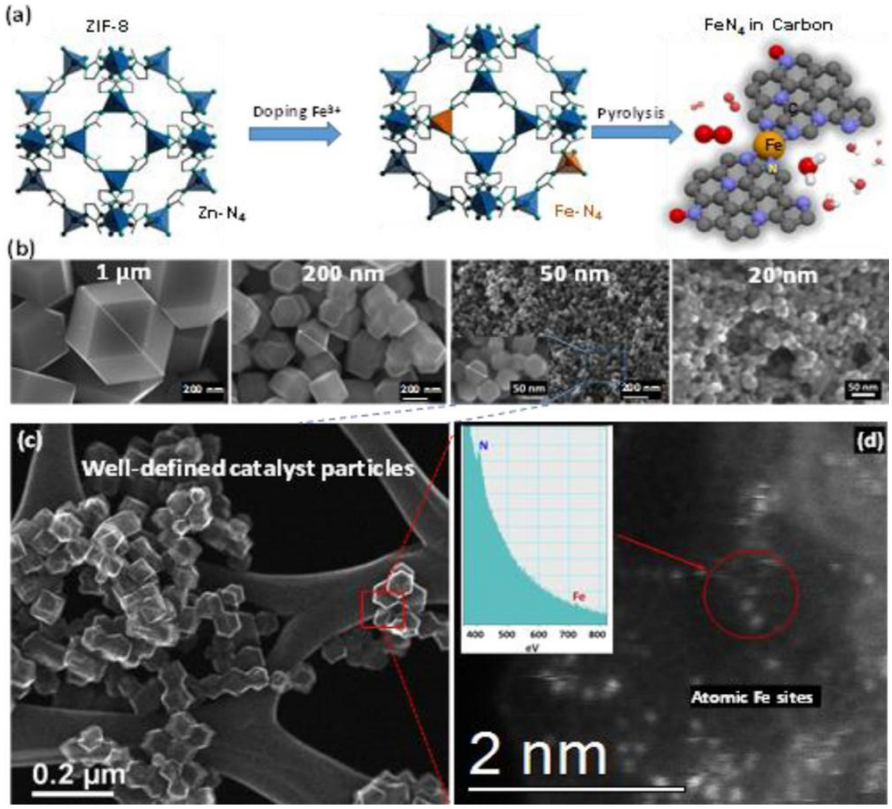


**Figure 3.** (**a**) Schematic representation of the synthesis process of Fe-doped ZIF catalysts. (**b**) Precisely controlled Fe-ZIF catalysts with sizes ranging from 20 to 1000 nm. (**c**,**d**) HAADF-STEM images of the highest performing Fe-doped ZIF catalyst (50 nm) and EELS analysis results (inset of (**d**)). (Reprinted with permission from [56]. Copyright 2017, American Chemical Society).

Although it has been suggested that increasing the loading of active metals can improve the toxicity resistance and stability of Fe-based SCAs to some extent, for typical carbon-supported Fe-N-C electrocatalysts the catalyst size has to reach the nanometer level, and it remains challenging to increase the density of FeNx active sites by simply increasing the number of metal salts [57]. In addition, certain FeNx active sites are not sufficiently exposed to the surface during pyrolysis, making it difficult for oxy-gen to access them [58]. An effective approach is to synthesize Fe-Ne-C electrocatalysts with abundant mesopores to improve the utilization of FeNx active sites.

In light of this, Gu et al. [59] recently developed unique Fe-based SCAs (Fe-Nx/N/$Ti_3C_2$), which they derived by loading $Ti_3C_2$ MXene onto MOF using a special method. TEM images show the wrinkled nanosheet morphology of Fe-Nx/N/$Ti_3C_2$, indicating the absence of iron-based crystalline phases. The relevant experimental and characterization results demonstrate that C, N, O, and Fe are homogeneously spread on the skeleton of the catalyst. X-ray photoelectron spectroscopy (XPS) results of this catalyst indicate that Fe-Nx-C is the predominant form of iron, and reveal a strong coupling effect between Fe-Nx-C and $Ti_3C_2$ MXene, which can improve the binding strength of ORR-related intermediates on the catalyst surface and regulates the d-band center of the iron. This explains the excellent ORR activity of the catalyst [60]. The electrochemical test results showed that the onset potential ($E_{onset}$) of Fe-Nx/N/$Ti_3C_2$ could reach 1.04 V (vs. RHE), its half-wave potential ($E_{1/2}$) could reach 0.92 (vs. RHE), and its limit current density

($J_L$) reached an amazing 0.1 mA/cm², which indicates that its electrocatalytic performance is better than that of commercial Pt/C catalysts (Figure 4A). From Figure 4B, it can be seen that it has $J_k$ = 35.8 mA $cm^{-2}$, which is better than other reference samples. The Tafel slope value of 96.2 (mV $dec^{-1}$) for Fe-Nx/N/$Ti_3C_2$ is the lowest among all the samples (Figure 4C). The ORR on Fe-Nx/N/$Ti_3C_2$ derived from the RRDE test proceeds through a four-electron reduction pathway with few byproducts (Figure 4D). The test results in Figure 4E show that the catalyst is highly stable, and when the electrochemical performance of Fe-Nx/N/$Ti_3C_2$ is compared with recently reported catalysts it is clear from the data, as shown in Figure 4F, that Fe-Nx/N/$Ti_3C$ is superior to many other ORR electrocatalysts [61–68].

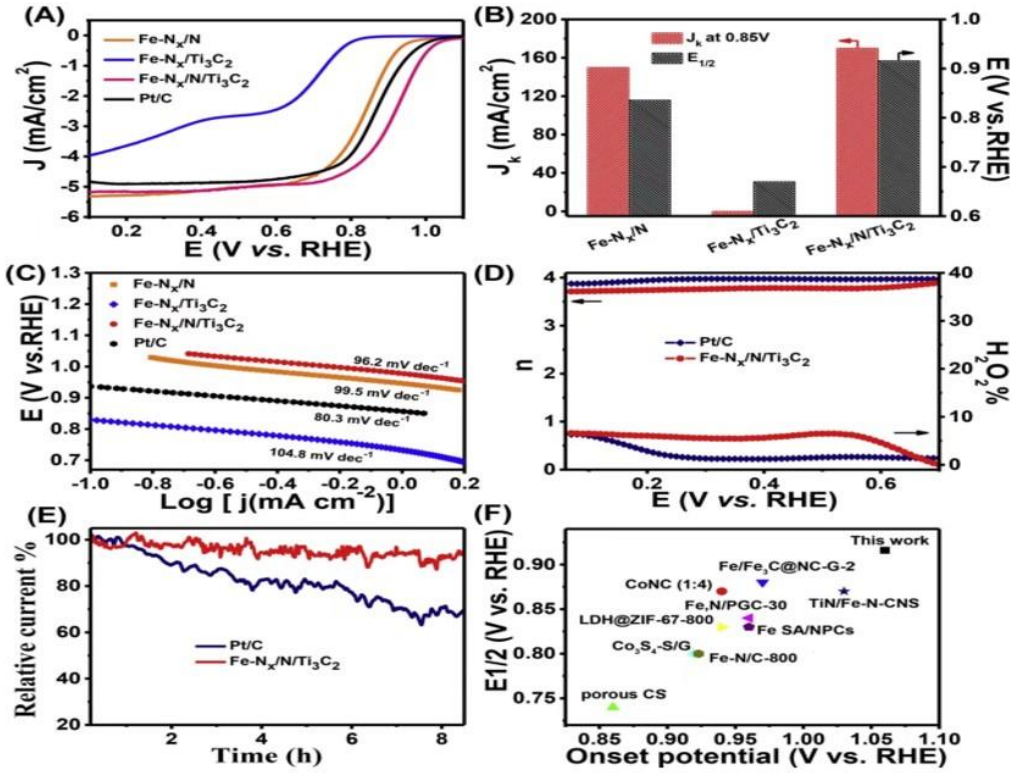


**Figure 4.** (**A**) ORR activity of the catalysts in an alkaline environment with 0.1 M KOH, rotation speed: 1600 rpm; (**B**) $E_{1/2}$ and $J_k$ values measured at 85 V; (**C**) Tafel plots of the catalysts; (**D**) n and peroxide yields of Fe−Nx/N/$Ti_3C_2$ and the commercially available Pt/C; (**E**) Fe−Nx/N/$Ti_3C_2$ and the commercially available Pt/C for i-t time-measured reactions; (**F**) comparison of Eonset and $E_{1/2}$ of Fe−Nx/N/$Ti_3C_2$ with reported ORR catalysts. (Reprinted with permission from [59]. Copyright 2022, Elsevier).

In another approach, the metal loading of the catalyst can be increased through sulfate ion-induced concave surface porous S and N co-doped carbon, which can limit the formation of $FeC_x$ nanoclusters, enhancing the intrinsic activity and density of the active sites of the catalyst to an extent and increasing the contact area of the active sites with the ORR intermediates. This approach can increase both the metal loading and the catalyst stability. In light of this, Mu and He et al. [69] designed an effective Fe/$S_2$-NC oxygen reduction electrocatalyst that confines a large number of $FeC_x$ nanoclusters with Fe-$N_4$ sites located in a concave porous S and N co-doped carbon matrix. The reason lies in the reaction of sulfate ions with carbon derived from ZIF-8 at high temperatures, which leads to the contraction of the carbon skeleton and then the formation of concave structures with a large number of macropores and mesopores. This concave architecture doped with S provides a larger area of contact with the electrolyte, facilitating the exposure of active sites and accelerating remote mass transfer. Thus, Fe/S-NC loaded with a certain amount

of nanoclusters of CSC, Fe-$N_4$, and $FeC_x$ exhibited good ORR activity and stability. When in an alkaline electrolyte, Fe/$S_2$-NC can reach an $E_{1/2}$ of 0.91 V, which far exceeds the value corresponding to commercial Pt/C catalysts ($E_{1/2}$ = 0.85 V), while in an acidic electrolyte, its $E_{1/2}$ is about 0.784 V, which is nearly equal to that of commercial Pt/C ($E_{1/2}$ = 0.812 V). This in situ S-doping with sulfate ions and direct hole formation opens new directions for the development and improvement of cost-effective Fe-based SCAs.

Furthermore, many factors should be considered in addition to the influence of the stability and durability of Fe-based SCAs on the catalytic activity of ORR. For example, M-N-C catalysts prepared from different precursors may show different electrocatalytic properties under complex conditions; that is, Fe-N-C catalysts doped with different iron salts produce different ORR electrocatalytic properties. Analysis shows that doping with different iron salts leads to differences in the distribution density of the formed Fe-$N_4$ active sites, and they may form inactive $Fe_3C$ structures that mask the active sites and reduce their contact area for reaction with the intermediates. Further studies have shown that the size of the iron source molecule and the degree of hydrolysis of the precursor are relevant [70]. The above results illustrate that the overall catalytic activity of the catalyst is related to the chemistry of the metal precursor, the type of carbon matrix, and the electrolyte environment, in addition to the active metal center.

#### 2.1.2. Cu-Based SACs

Copper has become a hot spot for catalytic research because it is a non-precious metal that can effectively solve the energy scarcity problem faced by noble metals. Based on its special electronic structure (no valence electrons in the third orbital), copper is different from all other elements in terms of its physical and chemical properties [71,72]. For example, the combination of uniformly dispersed Cu sites and nitrogen-doped carbon materials allows Cu-N-C SACs to exhibit excellent performance in many catalytic fields. However, the tuning of the coordination environment, the influence of the carrier material, and the dynamic evolution of the catalytic process are not known, which limits the application of Cu-N-CSAC.

To solve this problem, Jiang et al. [73] proposed an atomic interface strategy for designing single-atom copper catalysts and reported a new Cu-SA/SNC catalyst with a special carbon carrier consisting of copper atoms immobilized in a sulfur- and nitrogen-doped carbon carrier. The atomically dispersed Cu was directly observed by HAADF-STEM, the presence of monoatomic Cu in Cu-SA/SNC was confirmed based on HAADF-STEM images, and the absence of Cu-Cu signal in the EXAFS spectrum, and the resulting catalysts showed strong ORR activity due to the strong association between the Cu atoms and the carrier. The $E_{1/2}$ of Cu-SA/SNC in an alkaline environment (0.1 mol/L KOH) reached 0.893 V (vs. RHE), which surpassed that of commercial Pt/C catalysts. The atomic structure model of the catalyst is Cu-$N_4$-$C_8S_2$, based on the results of X-ray absorption spectroscopy (XAS), and the active site of the catalyst is the lower valence Cu(+1) in the Cu-$N_4$-$C_8S_2$ coordination structure per X-ray absorption fine structure (XAFS) analysis and DFT calculations. Furthermore, Cui et al. [74] synthesized Cu-SACs by pyrolysis of copper phthalocyanine with an $E_{1/2}$ of 0.81 V (vs. RHE) for ORR in an alkaline environment (0.1 mol/L KOH), which has high durability. Density flooding theory calculations indicate that the OOH* to O* conversion process determines the catalytic rate of Cu SACs. Qu et al. [75] prepared Cu-SACs using a zeolite imidazolium ester backbone material (ZIF-8) as a precursor with a half-wave potential of 0.895 V (vs. RHE) in an alkaline environment (0.1 mol/L KOH); ORR activity was better than commercial Pt-based catalysts. The excellent ORR catalytic behavior was due to the ammonia molecule acting as an intermediary to drag out and immobilize the copper atoms of the volatile zinc node of ZIF-8 during the high-temperature treatment. This work provides a new strategy for transition metal-based ORR SACs, highlighting the great potential of SACs to be promoted in the industry. The above studies are typical of the research results, both of which are discussed in detail later

in the text in our discussion of the influence of the ligand environment and the carrier material on the catalytic process.

In the Cu-N-C SAC catalytic system, it remains unclear how the N coordination affects the ORR activity of the Cu-$N_x$ site. This highlights the importance of studying the mechanism of interaction between the coordinated structure and catalytic performance of Cu-N-C at the atomic scale, which is important for the rational development of single-atom catalysts with high electrocatalytic activity. For this reason, Wang [76] proposed a unique synthetic strategy of tuning the coordination number of individual Cu atoms by using thiourea as an "in situ reductant" in the synthesis of Cu-NGS to obtain atomically dispersed Cu-$N_x$ structures (Figure 5a).

The $E_{1/2}$ of the synthesized catalyst in the alkaline electrolyte (0.1 mol/L KOH) reached 0.81 V (vs. RHE), which is almost identical to the value corresponding to the commercial Pt/C catalyst. The Cu-NG and Cu-NGS X-ray powder diffraction analysis showed highly dispersed Cu species on the carbon framework without any nanoparticles or clusters. The HAADF-STEM image (in Figure 5b) shows that the brighter spots shown in the figure are single-atom copper isolated from the carbon framework. Energy dispersive spectroscopy elemental mapping analysis of STEM images further confirms the uniform dispersion of C, N, Cu, and S throughout the Cu-NGS sample (Figure 5c), while the N K-edge X-ray absorption near edge spectroscopy (XANES) results and N 1s XPS peaks directly confirm the presence of a Cu-$N_x$ coordination structure and its coordinated effect on ORR activity. The results of X-ray absorption and XPS analysis directly demonstrate that the proportion of ligand-unsaturated CuI-$N_2$ sites increases with the addition of thiourea and that the oxygen reduction reaction catalytic activity of this catalyst increases significantly with the increase of CuI-$N_2$ proportion, which proves that CuI-$N_2$ is the real active site of ORR. The CuI-$N_2$ site was calculated from first principles to successfully reduce the free energy of each ORR reaction step through the fast $4e^-$ ORR pathway. The results of this study indicate that a good option is to improve the catalytic activity of ORR by precisely designing the coordination configuration of M-N-C catalysts, which creates more possibilities for further commercial applications of fuel cells.

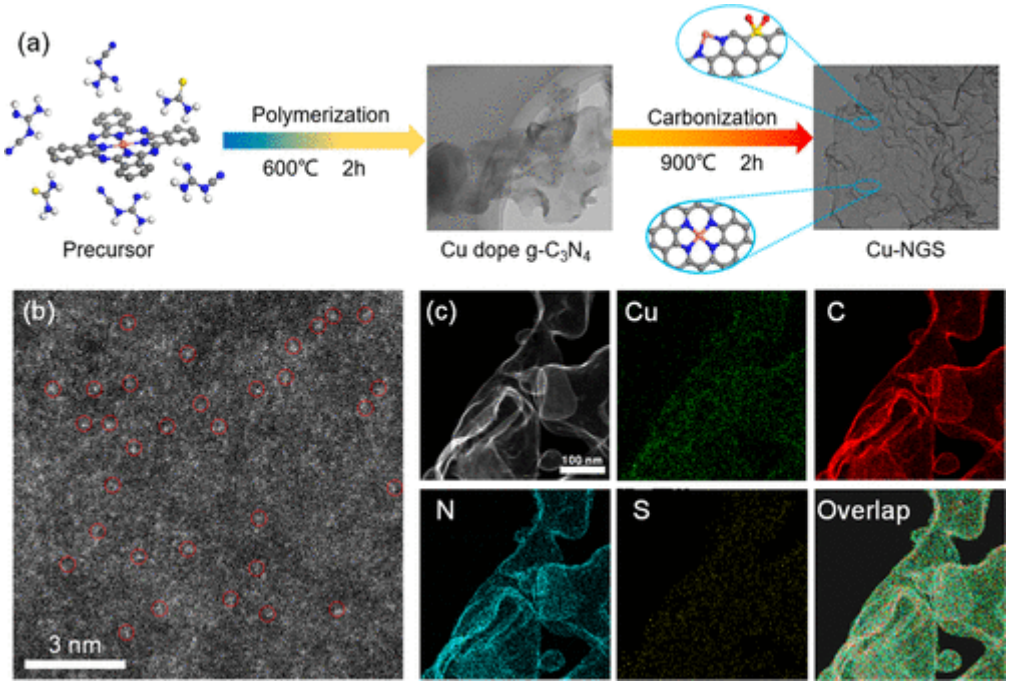


**Figure 5.** (**a**) The synthesis schematic of the atomically dispersible Cu-Nx site catalyst. The blue, yellow, pink, red, gray, and white spheres represent N, Cu, S, O, C, and H atoms, respectively. (**b**) Atom solution HAADF-STEM imaging of Cu-NGS. Single Cu atoms are highlighted by the red

circles. (**c**) STEM-EDS elemental mapping of Cu-NGS. (Reprinted with permission from [76]. Copyright 2019, American Chemical Society).

Recent studies have shown that the undesirable adsorption reaction of the active site with ORR intermediates can severely reduce the ORR kinetic activity, and it is important to develop strategies to solve this problem. The atomic interface modulation method was developed as an effective method to effectively control the catalytic activity of the whole SCAS, which changes the adsorption strength of the active site on the ORR intermediates by adjusting the interfacial configuration and coordination structure of the central metal atom, which in turn reduces the potential barrier and further improves the catalytic activity [77,78]. To consider this, Shang et al. [79] designed an asymmetric interfacial structure with metal atom centers and used this to successfully synthesize graded porous carbon-based Cu-based SCAs (S-Cu-ISA/SNC) for ORR. The designed S-Cu-ISA/SNC has an $E_{1/2}$ of 0.918 V (vs. RHE) in the alkaline electrolytes, which responds to the superior ORR catalytic performance of the catalyst. The correlation assay results showed that the atomic interface configuration of the Cu site in S-Cu-ISA/SNC is an asymmetrically distributed Cu-$S_1N_3$ fraction. The prepared catalysts showed good stability after long-term ORR stability tests with no significant current decay. Based on the EXAFS characterization results, relevant EXAFS fit data, simulations, and relevant calculations in XANES (Figure 6d–f), it was demonstrated that the excellent ORR activity can be attributed to the formation of the asymmetric Cu-S1N3 atomic interface in this catalyst, as well as that the low-valent Cu(+1)-containing structure is the active center of the ORR. In addition, this work provides a feasible pathway for the rational design and performance modification of other SACs.

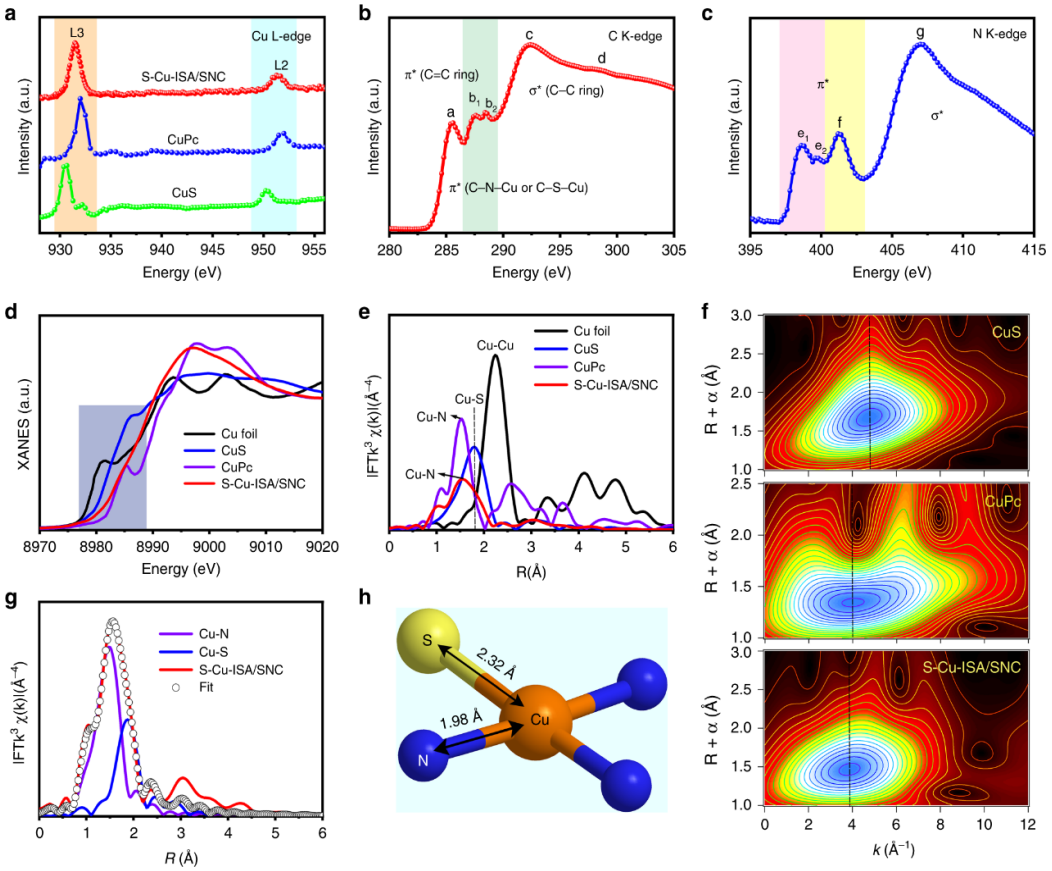


**Figure 6.** (**a**) Cu L-edge XANES spectrum of S-Cu-ISA/SNC, CuS, and CuPc. (**b**) C K-edge in the XANES spectrum of S-Cu-ISA/SNC. (**c**) N K-edge in the XANES spectrum of S-Cu-ISA/SNC. (**d**) Experimental Cu K-edge in XANES spectra of S-Cu-ISA/SNC and references (Cu foil, CuS, and CuPc). (**e**) The FT $k^3$-weighted Cu K-edge EXAFS Spectrum of S-Cu-ISA/SNC (**f**) WT-EXAFS graphs

of S-Cu-ISA/SNC, CuS, and CuPc, respectively. (**g**) FT-EXAFS fit curves of S-Cu-ISA/SNC on the Cu K-edge. (**h**) Diagram of the atomic interfacial model of S-Cu-ISA/SNC. (Reprinted with permission from [79]. Copyright © 2023, Springer Nature).

#### 2.1.3. Mn-Based SACs

In addition to using a variety of highly active Fe-based SCAs and Co-based SCAs to catalyze the ORR process, Li et al. [80] found that the $MnN_4$ active center has similar excellent ORR activity as the $FeN_4$ active site, which was concluded from DFT calculations. In addition, previous studies found that the doping of Mn promoted the graphitization of the carbon-loaded catalyst during the carbonization reaction, improving the overall stability of the catalyst [81]. On the other hand, the Fenton reaction of Mn ions is relatively small due to the weak reaction of Mn and $H_2O_2$. However, unlike Fe and Co ions, in the ZIF-8 precursors manganese ions are difficult to exchange with the pristine Zn to form coordination sites. In addition, manganese atoms tend to form inactive metal compounds during high-temperature treatment. Therefore, the formation of a certain number of MnN4 sites is affected, resulting in the inability of this catalyst to catalyze ORR. To solve this problem, Wu's group [80] developed a two-step method to synthesize Mn-based SCAs by doping and adsorption to increase the number of $MnN_4$ active sites First, as, in the conventional one-step chemical doping method, Mn-doped ZIF-8 precursors were prepared by partial exchange of $Zn^{2+}$ with $Mn^{3+}$ in ZIF-8. High-temperature pyrolysis followed by acid treatment and then a second high-temperature treatment resulted in porous carbon-containing a certain amount of Mn and N, which were co-doped and used as the host for the next step. In step 2, additional manganese and nitrogen sources were adsorbed into the resulting 3D porous carbon hosts. Then, a third heat treatment was used to increase the number of $MnN_4$ active sites. The atomic structure of the $MnN_4$ active site of the Mn-based SCAs was calculated by DFT, and its presence was demonstrated by XAS and EELS. The $E_{1/2}$ of the catalyst was up to 0.80 V (vs. RHE) in an acidic environment (0.5 mol/L $H_2SO_4$) and had good stability and neutrophilic resistance; after 30,000 CV cycles, the loss of $E_{1/2}$ was only a small 17 mV. In addition, the stability of the 20Mn-NC-second catalyst is better than that of the 20Fe-NC-second catalyst. The enhanced stability of the Mn-N-C catalyst is mainly due to the improved stability of the carbon carrier in the two-step synthesis and the stabilization of the $MnN_4$ ligand structure anchored on it.

In addition, the effect of the Fenton reaction on Mn-based SCAs is weaker than that of the Fenton reaction on Fe-/Co-based SCAs [82]. For this reason, Bai et al. [83] embedded manganese into nitrogen-doped graphene carriers using a high-temperature annealing strategy, and after acid leaching treatment, Mn@NG was obtained. Their $E_{onset}$ and $E_{1/2}$ in alkaline conditions (0.1 mol/L KOH) were 0.97 and 0.82 V (vs. RHE), respectively. The ORR activity of this catalyst was nearly equal to the commercial Pt/C ORR activity. The elemental mapping of Mn@NG based on EDS and STEM demonstrated that C, O, N, and Mn were uniformly distributed within the nitrogen-doped graphene framework. XANE analysis demonstrated that the valence state of Mn in Mn@NG was close to 2+. The EXAFS pattern of Mn@NG showed that no Mn-Mn bond was formed in Mn@NG, proving that the Mn in the prepared catalyst existed in the form of single atoms. This strategy can be applied to the preparation of other metal and nitrogen co-doped catalytic materials to facilitate the development of heterogeneous catalysis and electrocatalysis, among others.

It has been demonstrated that the intrinsic electrocatalytic activity of Mn-based catalysts can be significantly improved by modulating the local coordination environment of O and N atoms adjacent to Mn atoms in Mn-N-C catalysts. Yang et al. [77] prepared Mn single-atom catalysts by high-temperature treatment of Mn-doped MOFs. Structural analysis revealed that Mn formed Mn-$N_xO_y$ ligands with both O and N atoms, and the obtained Mn/C-NO reached an $E_{1/2}$ of 0.86 V (vs. RHE) under alkaline conditions (0.1 mol/L KOH). The ORR catalytic activity of the bionic electrocatalyst under alkaline conditions was very good, even outperforming the electrocatalytic activity of commercial Pt-based catalysts. The synthetic process is shown in Figure 7. According to the relevant

characterization results, excellent ORR activity was associated with the abundant Mn cofactor in the graphene carrier. This study offers new perspectives for the design of single-atom catalysts other than M-N-C by considering the geometry engineering aspects of the ligand atoms.

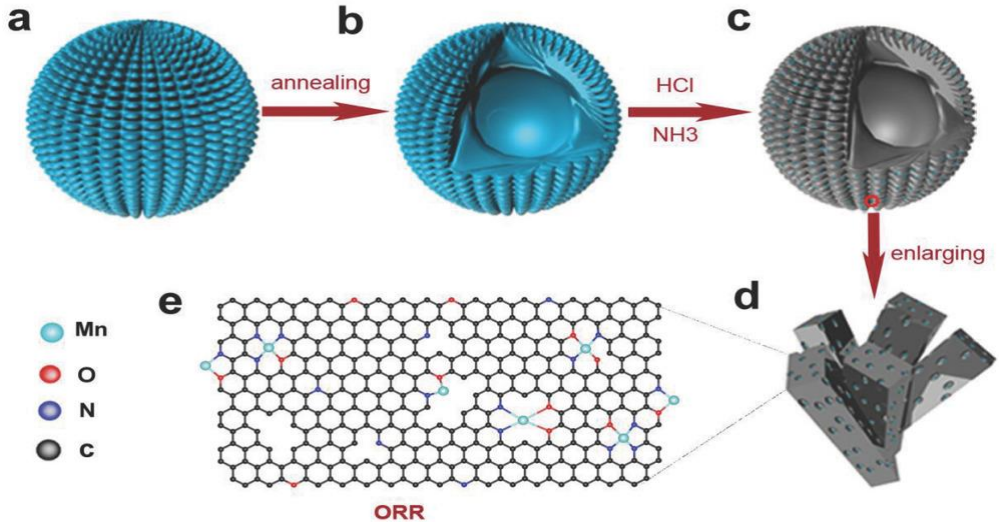


**Figure 7.** The synthesis process of the catalyst is shown schematically. (**a**) Precursor of Mn-BTC with a sphere-like morphology. (**b**) Ultrafine MnO nanocrystals embedded homogeneously in porous carbon framework with hollow sphere framework (MnO/C) are obtained after annealing process under $N_2$. (**c**) Mn/C-NO are obtained after HCl acid etching process and $NH_3$ activation treatments. (**d**) Enlarged edge area illustrating the hollow sphere carbon framework is composed of porous nanorods. (**e**) Detailed structure of Mn/C-NO where Mn residues embedded in 3D graphene framework predominantly existing as single atoms coordinated with O and N atoms. (Reprinted with permission from [77]. Copyright 2018, John Wiley and Sons).

In addition, Zhu et al. [84] synthesized MnNPC-900 by loading nitrogen and phosphorus-conjugated Mn atoms on a porous carbon carrier, where the Mn in this catalyst existed in such a coordination structure as $MnN_xP_y$. Under alkaline conditions (0.1 mol/L KOH), the $E_{onset}$ of this catalyst was 0.97 V and its $E_{1/2}$ was 0.84 V (for RHE). The above results indicate that the Mn-based SCAs have excellent ORR activity and stability. All these results indicate that transition metal Mn-based SCAs have a very high potential for development.

#### 2.1.4. Zn-Based SACs

The transition metal sources for M-N-C type single-atom ORR catalysts are mainly limited to Fe, Co, Ni, etc. It is currently believed that these transition metal ions (e.g., $Fe^{2+}$, $Fe^{3+}$, and intermediate valence of transition metals) and certain incompletely coordinated ions reduce the stability of the electrode and electrolyte film during the ORR process. In contrast to Fe, Co, Ni, etc., the d-orbitals of Zn elements are filled ($3d^{10}4S^2$), which makes it difficult to form oxidized ions in higher valence states [85]. Therefore, a Zn-N-C catalyst is theoretically considered to be harmless to the electrode and electrolyte membrane. In the course of catalytic ORR, related studies have then pointed out that the $Zn\text{-}N_4$ coordination structure is more stable than the $Fe\text{-}N_4$ coordination structure, and this finding has promoted the practical application and development of new efficient and stable single-atom catalysts (ZnSACs) [86].

Song et al. [87] prepared single-atom Zn catalysts dispersed in the Zn-N4 coordination form with a Zn loading of only 0.3 wt% due to the high volatility of the Zn precursor during high-temperature thermolysis. Therefore, it is necessary to find ways to increase the Zn loading when developing Zn-based SCAs in the future. To address this challenge, Li et al. [86] increased the loading of monatomic Zn in the catalyst by

controlling the gasification rate of the Zn precursor to 9.33 wt% (2.06 at%) loading. Both high-resolution transition electron microscopy (HRTEM) and XRD characterization results confirmed the absence of any visible Zn-based particles or clusters in the Zn-N-C-1 catalyst. Aberration-corrected atomic resolution HAADF-STEM measurements clearly show that the single Zn atoms are scattered uniformly in the Zn-N-C-1 sample at a very high density. The above results indicate that the catalyst has a single-atom distribution of the Zn.

In addition, the $E_{1/2}$ of Zn-N-C-1 in acidic conditions (0.1 mol/L $HClO_4$) is 0.746 V (compared with RHE), which is equivalent to that of Fe NC ($E_{1/2}$ = 0.743 V). In alkaline conditions, its $E_{1/2}$ reaches 0.873 V, which is higher than commercial Pt/C ($E_{1/2}$ = 0.858 V). The Zn K-edge XANES spectrum (Figure. 8a) indicates that Zn-N-C-1 may have a valence of +2. The EXAFS spectral image in Figure 8b shows that Zn-N-C-1 exhibits similar Zn-N coordination and that Zn elements are scattered atomically in the Zn-N-C-1 catalyst. The best fit based on the obtained EXAFS data indicates that the dominant coordination mode of the Zn atom in Zn-N-C-1 is Zn-$N_4$ rather than the Zn-Zn/Zn-$N_2$ coordination structure (Figure 8c,d). This result indicates that the Zn species in the Zn-NC-1 catalyst are structured in Zn-$N_4$ coordination. The results of this work expand the range of ORR family members.

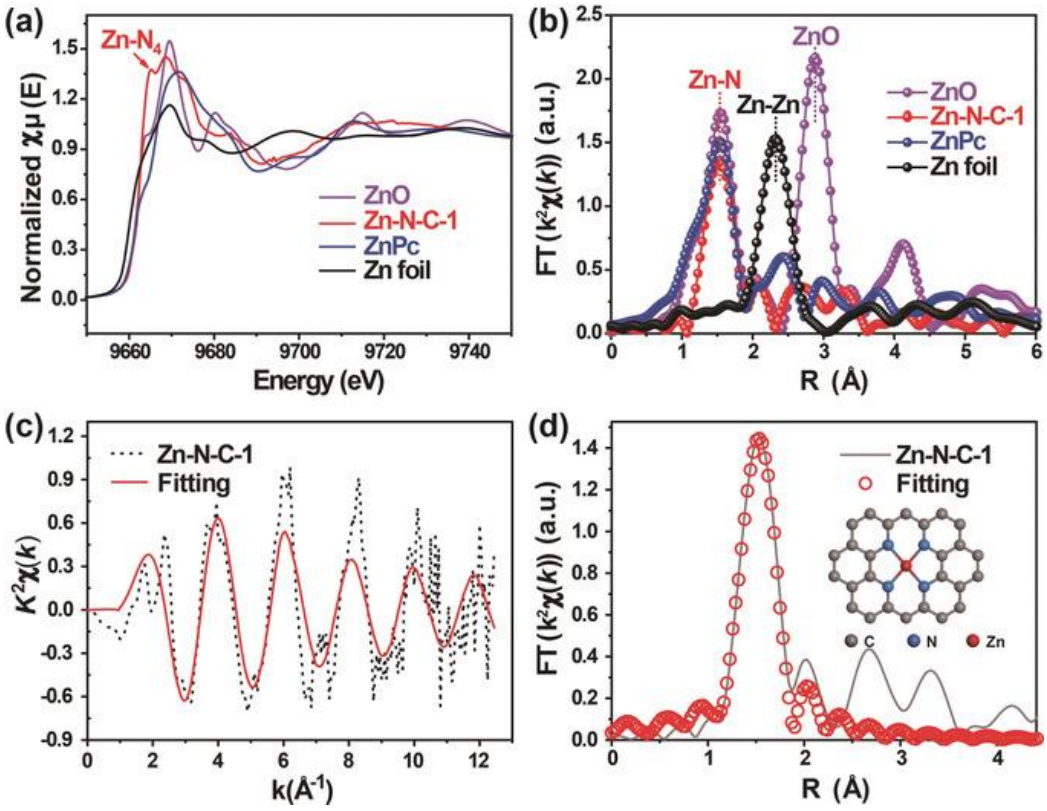


**Figure 8.** (**a**) XANES spectra of the Zn K-edges of Zn-N-C-1, ZnO, ZnPc, and Zn foil. (**b**) Fourier transforms (FTs) of the $k^2$-weighted χ(k) functions of Zn K-edge EXAFS spectra. (**c**,**d**) Corresponding EXAFS spectra fit in k- and R-space, respectively; insets show the model of the Zn coordination environment. (Reprinted with permission from [86]. Copyright 2019, John Wiley and Sons).

### 2.1.5. Co-Based SACs

Although Fe-based SCA catalysts exhibit remarkable ORR catalytic activity, their poor stability is the main drawback limiting their practical application. The Fenton reaction of Fe tends to oxidize the carbon matrix and destroy the Fe-N-C active center [88]. Co-N-C catalysts with weak Fenton reactions seem to be ideal alternatives. However, the conventional Co-N-C catalysts are prone to generating unwanted $H_2O_2$ via the two-

electron transfer pathway in acidic media. Relevant experimental results indicate that the Co-N-C catalyst has more than 90% selectivity for $H_2O_2$ in acidic media, suggesting that this catalyst has good catalytic activity that is slightly higher than other M-N-C catalysts [89]. Therefore, central metal atoms other than Fe and Co have been considered for practical applications. For example, an Mn-N-C catalyst synthesized by an innovative polyaniline hydrogel approach could inhibit the Fenton reaction and two-electron transfer pathway and improve the stability of Mn-C-SAC. However, the barely satisfactory ORR electrocatalytic activity remains a bottleneck limiting its practical application [90].

Currently, most of the Co-based SCAs catalysts exhibit excellent ORR performance in alkaline conditions. However, their low ORR activity in acidic media may be attributed to the formation of inactive cobalt aggregates; therefore, for high-performance cobalt catalysts for PEMFC applications, a new approach is required to improve the density of the loaded metal active centers and to disperse them uniformly. To this end, Wu et al. [91] prepared Co-N-C catalysts by one-step pyrolysis of cobalt-doped ZIF-8 under a nitrogen atmosphere at 1100 °C to obtain nano-carbon-based Co catalysts (denoted as nCo-NC-1100), where n is the atomic percentage of Co relative to the total metal. It is widely believed that the N-ligated Co structure is the oxygen reduction active site [92]. In this work, the authors observed this N-ligated Co activity based on HAADF-STEM images combined with electron energy loss spectroscopy (EELS) and demonstrated the existence of coordination of single-atom Co with N. The 20Co-NC-1100 catalyst was assembled into a membrane electrode device as a fuel cell cathode with a catalyst loading of 4.0 mg/cm$^2$. The stability of the 20Co-NC-1100 catalyst was improved, although the fuel cell performance degraded at a higher voltage/potential of 0.7 V at 100 h of continuous operation. This work suggests that increasing the density of atomic active sites is an effective way to improve the catalytic activity of ORR.

#### 2.1.6. Other Conventional Transition Metal-Based SACs

Tungsten is a transition metal in group 6 of the periodic table, and can form different oxidation states with coordination numbers ranging from 3 to 6. Pure tungsten has a strong binding effect on oxygen, and it is difficult to remove the adsorbed O* and OH* from the thermodynamic point of view; thus, there are few ORR catalysts for W-based SCAs. When tungsten metal is loaded onto a nitrogen-doped carbon carrier by certain means, the coordination environment and conditions of W can be changed such that tungsten W-N-C has better thermodynamic properties for ORR intermediates, making this catalyst have good ORR catalytic performance. Chen et al. [93] prepared tungsten SACs with ORR catalytic activity by controlling the synthesis temperature. The W-N-C catalyst with W-N coordination number 5 (W-$N_5$) exhibited significant ORR catalytic activity in a basic environment (0.1 mol/L KOH) with an $E_{onset}$ of 1.01 V (vs. RHE) and an $E_{1/2}$ of 0.88 V, which outperformed the Pt-based catalysts; in an acidic environment (0.1 mol/L $HClO_4$), the starting potential reached 0.87 V and the $E_{1/2}$ reached 0.77 V. The mass activity was up to 0.63 A/mg when measured at 0.9 V (vs. RHE), which is six times higher than that of conventional Pt-based catalysts. The W-$N_3$ and W-$N_4$ configurations exhibited poor ORR activity in both acidic and basic electrolyte environments.

To resolve the instability caused by the Fenton reaction, Luo et al. [94] prepared atomically dispersed cadmium SACs (Cr/N/C-950) in the form of Cr-$N_4$ by pyrolyzing the ZIF backbone of adsorbed cadmium ions using cadmium as the central metal atom. The half-wave potential was 0.773 V (vs. RHE) in an acidic environment (0.1 mol/L $HClO_4$), and the decay of Cr/N/C-950 half-wave potential (15 mV) was lower than that of Fe/N/C-950 catalyst (31 mV) after 20,000 potential cycles, showing good electrochemical stability. It is generally believed that the main group metals, such as Mg and Al, do not possess ORR catalytic activity; however, the intrinsic activity of the catalytic sites is strongly related to their electronic states, and can be adjusted by changing the coordination number of the metal sites [95]. Therefore, ORR catalytic activity of the Mg site can be achieved by changing the coordination environment.

Liu et al. [96] reported ORR-active Mg-SACs by DFT simulations and experimental studies of graphene-based N-ligand metal cofactors centered on the main group metals, Mg, Ca, and Al. The XANES results showed that the catalysts consisted of heteroatom-doped carbon. According to the results of XPS analysis, it is clear that most of the Mg is bonded to nitrogen atoms and that the valence state of Mg is between the metallic state (0) and the oxidation state (+2), without the formation of Mg-O bonds. The relevant ORR activity tests showed an $E_{onset}$ and $E_{1/2}$ of 1.03 and 0.91 V (vs. RHE), respectively, in an alkaline environment (0.1 mol/L KOH). The ORR activity of Mg-N-C in the acidic electrolyte (0.1 mol/L $HClO_4$) was close to that of commercial Pt/C, with an $E_{1/2}$ up to 0.79 V. The DFT simulation results show that the $MN_1C$ ligand is morphologically unstable, the ORR activity of $MN_3C$ is poor, and there is no catalytic activity for ORR. The Mg-N-C ligand has no catalytic activity for ORR. Therefore, the DFT and XANES results for Mg-N-C suggest that the most likely highly active part of Mg-N-C is the $MN_2C$ morphological ligand, and the catalytic performance of the main group Mg can be regulated by the coordination of the two N atoms, which in turn affects its ORR catalytic activity. This work demonstrates that the catalytic performance of metallic Mg can be changed by changing its local N coordination with two N atoms, which originates from the modulation of the p-band filling and then affects the catalytic performance of the ORR.

The SACs mentioned above usually consist of a single transition metal atom forming a coordination structure (active site) with a C or N atom, which is then immobilized in an N-doped carbon carrier [97]. In recent years, scientists have worked on various means to improve catalytic activity, for example, by studying how the active metal center and the coordination atoms or coordination environment within the system affect the adsorption or binding energy of the SAC to the reaction intermediate. Scholars have combined their results over the years to propose various strategies to modulate the active sites of SACs, such as controlling the number of in-plane coordination sites [98], doping heteroatoms in carbon carriers (e.g., B, P, or S) [99–101], and the design of multi-metallic active centers (e.g., Fe-Pt, Fe-Ni, Cu-Zn) [102]. However, as the most ideal substitute for commercial Pt/C, the non-noble metal SACs developed thus far have only a few metals (such as Fe, Co, Mn, or Zn) [103]. Therefore, it is necessary to extend SACs with metals other than Fe, Co, Ni, etc. For this purpose, Wang [104] and colleagues recently reported a five-ligand zirconium-based SAC with a nontrivial axial O ligand (denoted as O-Zr-N-C) for ORR. The significantly better ORR performance of O-Zr-N-C compared to the conventional Pt-based catalyst can be explained by the fact that the O ligand of this catalyst reduces the d-band center of zirconium, imparting a stable local coordination structure to the zirconium site and a certain adsorption capacity to the oxygen reduction reaction intermediates. Its $E_{1/2}$ is 0.91 V (vs. RHE), and it has excellent durability. In addition, the zirconium site has excellent resistance to aggregation and is capable of synthesizing zirconium-based SACs with high loading (9.1 wt%) under certain circumstances. The RDE evaluation results indicate that the optimal activity of O-Zr-N-C is related to its highest half-wave potential ($E_{1/2}$). The overall ORR performance of recently reported transition metal-based SACs is summarized according to references, demonstrating that O-Zr-N-C outperforms these state-of-the-art SACs (e.g., Fe, Co, Mn, and Zn-based SACs) concerning different parameters. This study shows that in addition to the in-plane coordination structure adjustment, controlling the axial coordination structure may be a new design approach for effective SAC in ORR and other electrocatalytic reactions, and a possible means to expand the family members of SACs.

Furthermore, Investigating where the active catalysts come from is critical but also challenging to develop efficient catalysts. Here, Yang [105] reports a strategy for synthesizing chromium nitride nanocatalytic materials (CrNNPs) by encapsulating special nanoparticles in hollow CrN@H–Cr–$N_x$–C, which is very practical. The catalyst exhibits excellent electrocatalytic activity under acidic conditions. The experimental results show that the coexistence of atomically dispersed $CrN_x$ sites and sufficient CrNNPs is crucial for the excellent performance of PEMFC. DFT studies have confirmed

that CrNNPs can increase the ORR activity of H–Cr–$N_x$–C. The results of this study open up a new way for the preparation of low-cost, highly active and durable ORR catalysts for ORR.

Summary and Outlook

SACs have received a great deal of attention in the world of catalytic reactions due to their excellent catalytic selectivity and activity, maximum atomic utilization, and versatile ligand structure alteration. However, there remain many unanswered issues. First, the loading of metal elements in SACs is usually small, which makes their current densities small and consequently unavailable for industrial production. To obtain highly dispersed and high-density SACs, it is imperative to develop and optimize the synthesis process. Based on this, there is a need to develop ORR electrocatalysts to the sub-nanometer and even atomic level to improve their catalytic activity, selectivity, and usage efficiency. Therefore, for realistic fuel cell applications, the development of increasingly scattered high metal loading (or high metal concentration) electrocatalysts is crucial. Second, under alkaline conditions the majority of SACs have superior ORR than the marketed Pt/C. However, there are gaps in ORR performance under acidic conditions; therefore, more studies are needed to determine how changes in the structure and ORR activity of SACs are related. At present, most studies have been carried out theoretically; however, in the actual reaction process the adsorption–desorption interaction between intermediates and solvent molecules leads to dynamic changes in the structure. In addition, the preparation of SACs with high activity and stability needs to be accompanied by the development of low-cost and high-scale SACs, which is highly relevant to the practical application of SACs. Thus far, the synthesis methods of most SACs are tedious and time-consuming. Therefore, the development of a simple and inexpensive large-scale production process for SACs is key to the industrialization of SACs. Carbon-loaded ORR electrocatalysts (including nanoparticles and atomic-level structures) face the problems of carrier carbon corrosion and catalyst instability in practical applications. Therefore, to accelerate the development of ORR electrocatalysts for application in fuel cells, a ceramic carrier material with or without high electrochemical and thermal stability, such as conductive metal oxides, carbides, and borides, needs to be developed in future research.

The problem of the positioning of monoatomic metal on the carrier remains a mystery. There has to be enough free space on the skeleton, as well as improved efficiency in the use of memory management. As the reactivity of transition metals increases, it becomes more difficult to synthesize SACs. Because different electronic structures cause new interactions, more effort needs to be put into the interaction between the transition metal and the carrier. Therefore, it is necessary to further understand SACs in order to accurately develop more advanced synthesis methods and single-atom carriers. However, due to their higher activity, transition metal elements yield more structures during more reactions, providing favorable conditions for new synthetic pathways. In general, combining catalyst carriers with transition metals by different methods requires different devices and steps. This may increase costs, and the resulting material may be unstable and inactive in various cases. However, the development of bifunctional or multifunctional SACs can avoid unfavorable phase transitions between different catalytic processes due to intermolecular interactions, as phase transitions occurring in different reaction processes are effectively prevented. In this way, stability can be maintained, further reducing production costs and increasing the efficiency of monomer and carrier utilization. Although many questions remain to be explored in depth, recent studies have provided fundamental knowledge that addresses synthesis and performance while providing excellent properties and factors that affect synthesis and performance.

Catalysts (including SAC, DAC, and SCC) with high M-N-C metal loading (M = Fe, Co, Ni, etc.) have ORR properties very similar to those of Pt-based catalysts; however, they have great difficulties in acidic environments. In particular, their corrosion resistance

decreases under acidic conditions. Therefore, the application of high-density non-noble metal-based M-N-C (especially Fe-$N_4$SAC) in fuel cells is very difficult due to its instability and possible Fenton oxidation. Based on the above limitations of M-N-C catalysts, the following means can be adopted as solutions in future research: (1) currently, the central metal atom of most high-density atom-dispersed metal catalysts is only coordinated to the N atom in the carbon matrix. Enhancement of M-N-C intrinsic activity or introduction of other heteroatoms (e.g., S, O, P, F, etc.) or bimetallic atoms in M-N-C catalysts can better regulate the electronic structure of metal active sites; (2) the exposure and mass transfer of active sites can be increased by constructing equilibrium porous structures; (3) with respect to DFT calculations, most are currently based on idealized models, which cannot accurately reflect the real catalytic mechanism or experimental factors such as pH, electrolyte, catalyst, and surface/interface between electrolyte and $O_2$; (4) in the actual electrochemical reaction, the local structure of the metal active center undergoes a dynamic process; therefore, the structure-activity relationship of SACs/DACs should be studied more accurately by techniques such as in situ characterization and theoretical calculations; (5) at present, the research on DACs is in its infancy, and controlling the number of metal atoms is a great challenge. There is an urgent need to develop advanced preparation techniques to control the number and type of metals; (6) there is a need to find new catalysts with high activity, high stability, and high four-electron selectivity. Therefore, the rational design of the dimer and trimer as well as larger metal clusters is an important way to solve SA-C-S defects.

### *2.2. Multimetallic Active Site ORR SACs*

The variety of SACs is very diverse, and the state of the metal species on the carrier can be monoatomic, diatomic, small clusters, etc. [106]. Although single-metal active site SACs have been extensively studied and are highly active against ORR, their performance in relevant performance tests lags behind the top of the M-N-C volcano diagram, and monometallic site atomic catalysts have drawbacks: (1) because only one specific active site acts, it is difficult to break the scalar relationship between intermediates; (2) because of the low loading of single metal active site catalysts, single atomic site catalysts are often deactivated and easily covered by intermediates; (3) single metal site catalysts are unable to rapidly drive some specific reaction transfer processes, such as those containing multiple electron transfer reaction steps.

To solve these problems, one approach is to try to generate more active sites in the catalyst, for example, by introducing other kinds of metal active sites to the monometallic active site catalyst in order to make the surface electron transition frequency of the catalyst faster [107]. This approach overcomes these deficiencies by modulating the surface electronic environment of the catalyst, and has great potential for enhancing the activity of the catalyst [108]. At the same time, diatomic systems composed of metals and nonmetals have seen their research area expanded [109–111]; furthermore, they can be improved by properly tuning the intermediate metal atoms and the coordination environment (e.g., doping N, O, S, P, etc. into the neighboring coordination structure), as discussed in detail above. Based on this, a new type of multi-metallic active site ORR SACs has been developed.

#### 2.2.1. Dual Metal Active Site ORR SACs

In certain cases, monatomic catalysts cannot meet the requirements of industrial production for catalyst performance. Bi-metallic active site single-atom catalysts are a special type of single-atom catalysts that have emerged in recent years to increase the number of single-atom active sites and enhance the stability of loaded single atoms [112]. Diatomic catalysts (DACs) have the advantages of single-atom catalysts (SACs) (e.g., highest atom utilization, high activity, and selectivity) and overcome the disadvantages of SACs (e.g., low loading and isolated active sites), and as such have received increasing attention; in addition, they provide synergistic functions based on different molecules and

their interfaces to significantly improve the catalytic activity of the catalyst [109,110,113]. In particular, bimetallic monoatomic catalysts such as Fe-$N_4$/Ni-$N_4$ have higher catalytic activity than single atoms [114]. Representative research results are described in detail in the following section.

Bimetallic nanocatalysts (BNs) require precise control and comprehension of the degree of order, which is difficult yet essential for producing improved materials for oxygen reduction processes (ORR). Chen [115] synthesized AuCuBNs with different degrees of ordering and used in situ Raman spectroscopy to assess the effect of ordering on ORR at the molecular level. The change from disorder to order increased the activity of AuCuBNs by more than a factor of two, enabling the highly ordered Au-Cu BNs to exceed the benchmark Pt/C. The crucial intermediate's (*OH) direct Raman spectroscopic data demonstrated that the active sites were the binding locations for the active sites of Au and Cu. Additionally, two distinct *OH species were seen on ordered and disordered structures, respectively, with the ordered location being more advantageous for ORR due to its reduced affinity for *OH. This research advances our understanding of the crucial function that orderliness plays for BNs, and makes it possible to build better catalysts. In addition, the use of modulation of metal single-atom coordination structures and heteroatom doping to prepare novel catalysts is envisioned.

Mixing transition metal atoms leads to different catalytic properties and helps to obtain the best ORR electrocatalyst [113]. Previous research has demonstrated that adding B, S, or P to carbon can boost the charge density of $FeN_4$ sites [116]. Recent related studies have pointed out that the integration of another transition metal, such as Co, Ni, or Mn, can improve the ORR activity of Fe-N-C catalysts through bimetallic synergy [117]. Based on this, Zhang [118] synthesized nitrogen-doped bimetallic silicon carbide-graphite composites (N-$Fe_2$MoC-GC) at 1300 °C. N-$Fe_2$MoC-GC showed excellent ORR activity and stability, largely overcoming the lack of stability of conventional metal catalysts. The synthesized N-$Fe_2$MoC-GC had a high degree of graphitization even after N doping, and there was a high degree of electron transfer between N and $Fe_2$MoC. All the above factors indicate that ORR has good activity and stability, better oxygen reduction reaction (ORR) activity than commercial Pt/C, ultra-high stability, and excellent resistance to methanol and CO. It ranks as one of the most active and stable noble metal-free catalysts reported thus far. In addition, N-$Fe_2$MoC-GC maintains high power density even at low relative humidity or high operating temperature. The positive charges on Fe and Mo atoms caused by the electron transfer from $Fe_2$MoC to N are believed to be responsible for the excellent ORR activity. The inherent electrochemical stability of $Fe_2$MoC, the graphite substrate, and the strong interaction between the catalyst components caused by the electron transfer are responsible for its ultra-high stability. The relevant characterization results demonstrate the apparent coexistence of graphite (002) and $Fe_2$MoC (305) lattices and the successful formation of $Fe_2$MoC and graphite crystals, as well as the key role of iron for the graphitization of the carbon source (D314 resin) (Figure 9a–d).

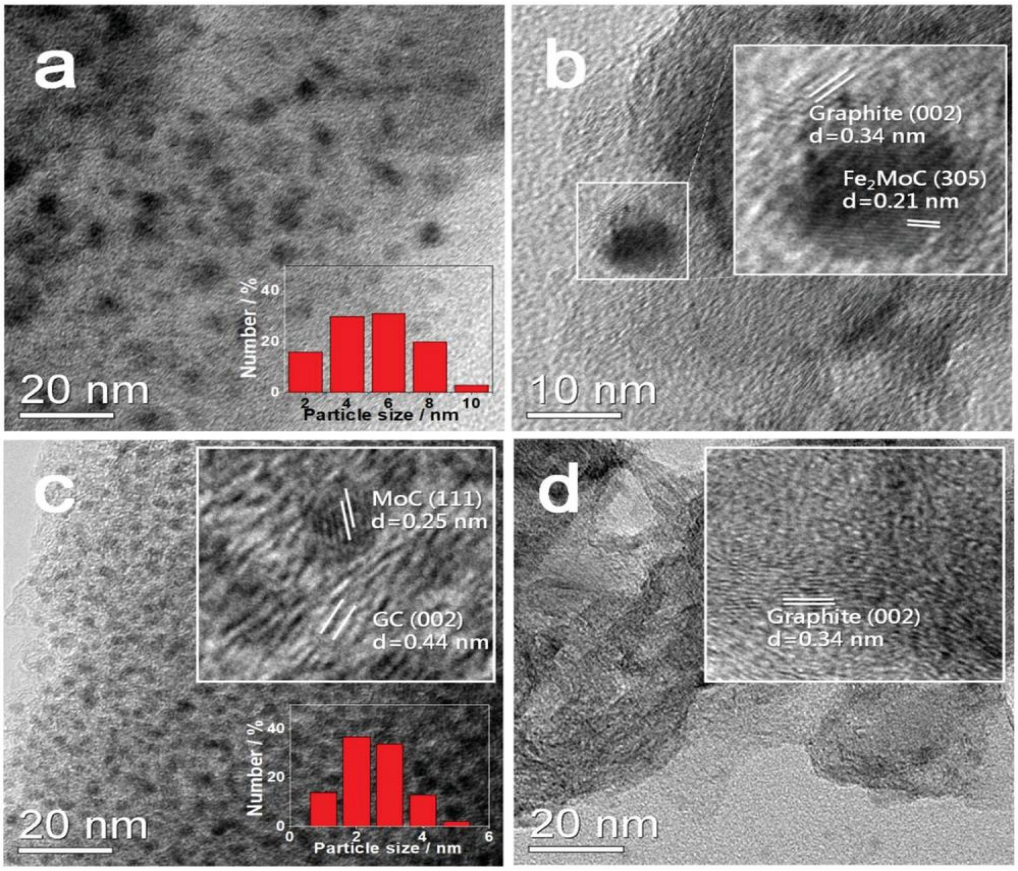


**Figure 9.** (**a**) TEM image of the prepared catalyst; (**b**) enlarged TEM image of the prepared catalyst; (**c**) TEM image of N-MoC-GC; (**d**) TEM image of N-GC. The bottom inset of the figure shows the corresponding $Fe_2MoC$ and MoC particle size distributions. The insert at the top of the figure is the correspondence HRTEM image, where the crystal lattice is labeled. (Reprinted with permission from [118]. Copyright 2022, John Wiley and Sons).

In addition, Wang [119] reported a novel Mn-Fe-N/S@mC bimetallic catalyst consisting of atomically uniformly dispersed Fe-$N_4$ sites and trace amounts of Mn-$N_2S_2$ sites immobilized on an ordered mesoporous graphitic carbon skeleton. The synthesis of this bimetallic catalyst was achieved by chemical transformation of their own synthesized $Mn_{0.43}Fe_{2.57}O_4$ nanocrystals with bimetallic sites and graphitic frameworks derived from the nanocrystal cores and associated capping ligands, respectively. The results in Figure 10a indicate that the Fe species in Mn-Fe-N/S@mC are dominated by atomically dispersed Fe-$N_4$ sites. The quantitative EXAFS curve fitting data in Figure 10b confirm the structure of Fe-$N_4$ formed by the coordination of Fe with four N atoms. Based on the analytical results in Figure 10c, it is known that Mn is coordinated with both N and S. The EXAFS fit data according to Figure 10d further confirmed that the Mn-$N_2S_2$ site is the main junction and site of Mn among Mn-Fe-N/S@mC. The above results demonstrate the absence of the formation of Fe-Fe-N/S@mC and Mn-Mn-N/S@mC structures in Mn-Fe-N/S@mC. Furthermore, Mn-Fe-N/S@mC exhibited excellent catalytic activity in alkaline media, which was superior to the conventional Pt/C and most of the previously reported non-precious metal catalysts. It is noteworthy that the synergistic effect of Fe and Mn increases the ORR catalytic activity by a factor of about 5. Density flooding theory calculations were performed to demonstrate the role of Mn doping in enhancing the activity of Fe-$N_4$ sites, revealing that the synergistic interaction between the bimetallic sites reduces the *OH reduction energy barrier in the oxygen reduction pathway. The integration of Mn effectively reduces the energy barrier of Fe-$N_4$ sites in the four-electron oxygen reduction pathway, significantly increasing the ORR activity. This study by Wang

provides an opportunity to develop a new idea for the development of efficient bimetallic single-atom ORR catalysts.

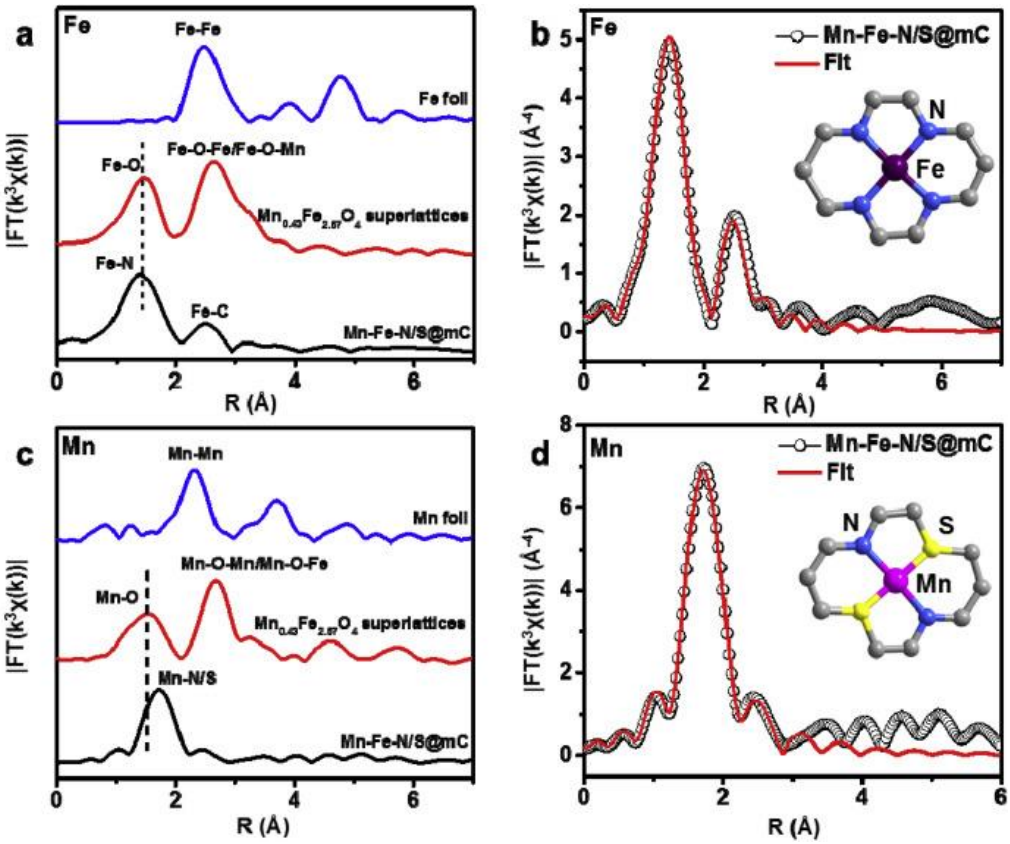


**Figure 10.** Fourier transform EXAFS curves of (**a**) Fe and (**c**) $k^3$-weighted Mn for the prepared catalysts. the EXAFS curves of $Mn_{0.43}Fe_{2.57}O_4$ super crystals are included for comparative purposes. The corresponding K−edge EXAFS fittings of (**b**) Fe-N/S@mC for Mn-Fe-N/S@mC and (**d**) Mn. The insets show the constructions of Fe-N4 and Mn-$N_2S_2$ sites. (Reprinted with permission from [119]. Copyright 2019, Elsevier).

In addition, Lin's study showed that all iron, molybdenum, and nitrogen species in (Fe, Mo)-N/C catalysts form more active centers to promote ORR activity [120]. Mixing transition metal atoms leads to different catalytic properties and helps to obtain the best ORR electrocatalyst [121]. The tireless efforts of researchers have led to a significant improvement in the activity and stability of non-Pt catalysts; the high potential range during fuel cell start-up and shutdown (i.e., 1.0 to 1.5 V, vs RHE) causes severe corrosion of the carbon carrier, resulting in reduced surface area and metal shedding; while metal stripping and metal dissolution are the main factors leading to decreased activity during stable operation [122].

To overcome the above-mentioned problems, it is necessary to introduce other single atoms to create heteronuclear diatoms that can improve the conversion efficiency of the catalyst. This method has great potential to overcome the above-mentioned defects and to improve ORR activity by improving the electronic environment and geometry. ORR catalysts combining metals and nonmetals have rarely been reported in the past. Combining these two types of atoms can provide different roles in catalytic reactions. Selenium atoms have been shown to significantly improve the electron transport efficiency of two-dimensional materials [123].

Taking this into account, Yao et al. [124] prepared atomically dispersed iron and selenium diatomic catalysts ($Fe_1Se_1$-NC) anchored on nitrogen-doped carbon by a ball milling strategy. The Fe/Se diatomic catalysts exhibited a significant synergistic

enhancement effect compared to the single-component $Fe_1$-NC and $Se_1$-NC catalysts. The $Fe_1Se_1$-NC catalyst showed optimal ORR activity, with an onset potential ($E_{onset}$) of 1.0 V (vs. RHE), which is better than Pt/C (0.98 V). The results of K-edge EXAFS spectroscopy of Se shown in Figure 11A indicated that Se in the material was present as a single atom on the carrier surface. Fitting the EXAFS data of Se in the $Fe_1Se_1$-NC catalyst, Figure 11B shows that Se is attached to carbon (C-Se-C) in the form of a diastereomer. The analysis in Figure 11C shows that the iron atom is positively charged and its oxidation state is located between the two. The results of the Fe (EXAFS) spectra (Figure 11D) demonstrate that $Fe_1Se_1$-NC and $Fe_1$-NC are mainly present in the form of single-atom dispersions without the formation of Fe nanoparticles or clusters. Figure 11E,F shows that the coordination number of Fe atoms in $Fe_1Se_1$ NC and Fe1NC is about 5, and the bond lengths are about 2.02 Å and 2.0 Å, respectively. This work demonstrates for the first time that the prepared metal (Fe) and non-metal (Se) diatomic sites have a significant enhancement on the ORR, which provides a new idea for the design of more efficient multi-metal single-atom catalysts.

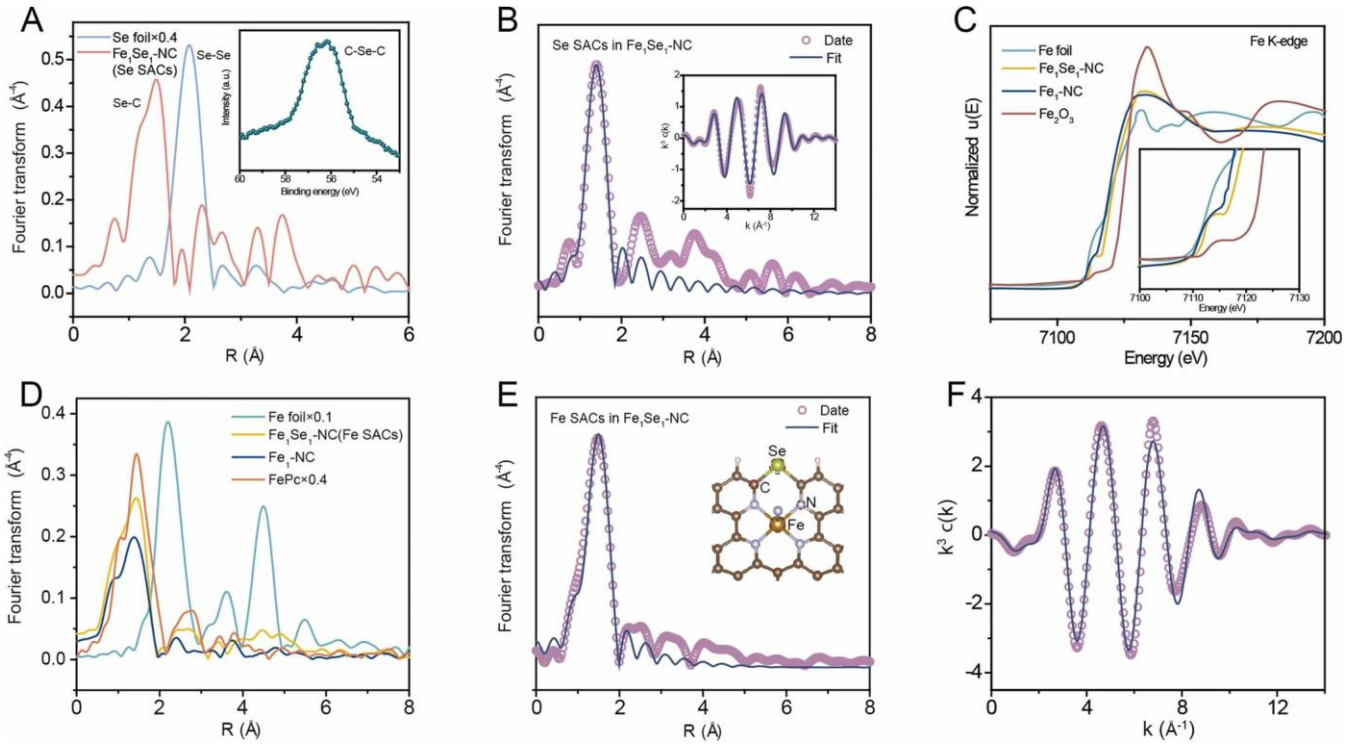


**Figure 11.** Multispectral characterization of the catalyst: (**A**) EXAFS spectrum of Se K edge in $Fe_1Se_1$-NC; (**B**) EXAFS fitting curve in R space and K space of Se monoatomic in $Fe_1Se_1$-NC catalyst; (**C**) K−edge XANES spectra of Fe in $Fe_1Se_1$-NC and $Fe_1$-NC; (**D**) EXAFS spectrum of Fe K edge in R space; Fitting Curve of Monoatomic Fe in R Space and K Space in (**E**,**F**), $Fe_1Se_1$-NC Catalysts. (Reprinted with permission from [124]. Copyright 2022, Elsevier).

Moreover, there are many diatomic catalysts with excellent properties; for example, in 2017, Li et al. developed an Fe-Co diatomic site based on the ORR of nitride porous carbon [125]. Later, researchers found that AuCo and FeMn diatomic catalysts have higher ORR activity than single metal catalysts [126,127].

It has been shown that the calcination of MOF precursors can uniformly disperse the transition metals and doped nonmetallic elements on the carbon skeleton; thus, tightly connected and uniformly distributed transition metal/carbon composite catalysts can be easily prepared with the help of MOFs as precursors [128]. In addition, MOF-derived metal/carbon composite catalysts can inherit the morphology and porous structure of

MOFs, which facilitates the exposure of active sites, electron transfer, and mass transport during electrocatalysis [129].

Based on this, Zhou and Xie [130] et al. reported that a series of Co nanoparticles and highly dispersed Fe loaded on N-doped porous carbon substrate were prepared by the "double solvent" method using in situ doped metal–organic frameworks (MOFs, ZIF-8) as precursors, namely, CoNP@FeNC Electrocatalyst. Experimental testing found that the prepared CoNP@FeNC-0.05 catalyst showed excellent oxygen reduction reaction (ORR) and oxygen evolution reaction (OER) performance in an alkaline medium. In addition, compared with commercial Pt/C+$RuO_2$, CoNP@FeNC-0.05 as the positive catalyst of a Zn air battery, the rechargeable Zn air battery showed higher peak power density and better cycle stability. Based on the characterization of the structure according to the performance test and structure, CoNP@FeNC-0.05 Fe-N sites and Co nanoparticles with medium and uniform dispersion contributed to the excellent performance of electrocatalytic ORR/OER. In addition, the porous structure, large specific surface area, and unique 3D carbon network of CoNP@FeNC-0.05 were conducive to improving ORR/OER performance. This work provides a valuable reference for the rational design and construction of a single catalyst with different active centers for oxygen electrocatalysis and paves the way for the practical application of rechargeable Zn air batteries.

Considering that the structure of bimetallic NP-modified NC catalysts is related to their energy band properties as well as to the type and number of active metals, the study of NP-modified NC catalysts has received increasing attention in recent years. The introduction of complementary bimetals allows for more precise tuning of the electronic structure and provides multiple atomic interfaces for the adsorption of oxy-adsorbents, accelerating the ORR reaction pathway and significantly improving electrocatalytic activity and selectivity [131–134]. For example, Jiang et al. reported the synthesis of FeCo alloy NPs embedded in N and P co-doped carbon-coated nitrogen-doped carbon nanotubes (NPCs)/FeCo@NCNTs) for effective bifunctional catalysis [135]. Although many research results have been published, the simple synthesis of NP-type NC catalysts and the relationship between their properties as relates to their resolved electronic structures remains a great challenge.

#### 2.2.2. Other Types of Multi-Metal Active Site ORR SACs

At present, although SACs with mono- or bimetallic sites have been frequently reported, the synthesis and precise regulation of SACs with multi-metallic sites remain difficult and rarely reported, and the understanding of the related ORR catalytic mechanisms is yet to be studied in depth.

Recently, Wang [136] reported a ternary catalyst ($Co_2$/Fe-N@CHC) consisting of Co-Co and Fe sites loaded with atomically dispersed N-ligands on a hollow carbon cage grown with carbon nanotubes. Density flooding theory (DFT) calculations revealed that such ternary single-atom $Co_2$/Fe-N10 sites have higher intrinsic ORR electrocatalytic activity than $Co_2$-$N_6$ and Fe-$N_4$ sites alone. The specific reason for this is that the introduction of the $Co_2$-$N_6$ site increases the filling of the Fe antibonding orbital charge in the Fe-$N_4$ site, which reduces the binding energy of the oxygen-containing intermediate (OH) to the active site in the decisive step of the ORR reaction process, thereby reducing the free energy barrier. Experimentally, $Co_2$/Fe-N@CHC exhibits excellent ORR activity and stability under alkaline conditions, with a half-wave potential ($E_{1/2}$) of 0.915 V (vs. RHE), which is superior to binary catalysts ($Co_2$-N@CHC), monolithic catalysts (Fe-N@CHC), and commercial Pt/C. Under acidic conditions, $Co_2$/Fe-N@CHC has better ORR performance than $Co_2$-N@CHC and Fe-N@CHC. The ternary catalyst shows higher power density and better cycling stability than Pt/C when used in zinc vacancy batteries.

Encouragingly, recent studies have demonstrated that bimetallic compounds (FeNi, FeCo, FeCu, etc.) seem to be endowed with extremely effective OER and ORR active sites after the introduction of another active metal, showing a significant increase in OER and ORR activity compared to single-element compounds. This is probably due to the

synergistic effect of the two components and the increase in electrical conductivity at the same time thanks to the synergistic effect between the different metal positions.

Summary and Outlook

The excellent catalytic performance of multi-metal active site ORR SACs is mainly determined by four major factors: (1) these ORR SACs have high atomic utilization along with good selectivity and corrosion resistance, which are strongly related to their atomic dispersion properties based on the synergistic interaction between multiple metal active centers (multiple metal centers with effectively tuned d band center interactions), in turn promoting their catalytic activity; (2) the ability of such catalysts to anchor different single-atom metal active centers, leading to the rational design of catalytic materials with greater activity and stability. Polymetallic active site ORR SACs provide more metal sites thanks to a more complex and flexible specific coordination space, though their complex surface chemistry is understudied [137–141]; (3) in addition to having the functionality of SACs, DACs typically have a higher metal loading density and a more flexible active site configuration, resulting in excellent electrocatalytic activity [142]; (4) the catalysts benefit from their highly exposed polymetallic active centers and fine structure, and their electrocatalytic activity and excellent durability are superior to those of the latest catalysts.

Although the catalytic performance of polymetallic active site ORR SACs is excellent, there are many aspects that need to be improved and enhanced, such as: (1) the research on such catalytic materials in the catalytic community is at an early stage, and more experimental and theoretical exploration is needed to further guide the rational design of polyatomic active centers; (2) due to the huge design space of polymetallic active site ORR SACs, development costs are high for both experimental and computational studies; (3) how to design polymetallic catalytic materials in a rational, efficient, and stable manner is a challenging topic, as there is no solid synthesis technique with bimetallics as the catalytic core, and the structural characteristics of polymetallic active centers have not been studied deeply enough to accurately study their coordination environments; and (4) at present, there is little direct knowledge about the target active sites of catalytic reactions in operation. These aforementioned problems complicate the synthesis process, and these issues must be taken into account before success can be achieved. This review provides a new vision for future generations to innovatively design polymetallic catalytic materials based on this synthesis.

### *2.3. Noble Metal-Based ORR SACs*

Although the reserves of noble metals are relatively small, this does not affect their ORR catalytic performance in any way. According to the U.S. Department of Energy 2020 specifications, the stability of platinum group metal catalysts should meet the condition of less than 40% decay rate of mass to activity at 0.9 V potential after 30,000 cycles. According to the current literature, a large proportion of catalysts have difficulty achieving this target. A key factor in designing efficient ORR electrocatalysts is determining how to control the binding energy of reaction intermediates on the surface. The volcano diagram of ORR activity distribution can show the relationship between the binding energy of various metal elements and oxygen atoms, with elements located on the sides of the volcano diagram having poor ORR activity and those near the top having better activity. The noble metals are located at the top of the volcano diagram, meaning that the noble metal-based catalysts theoretically have the highest ORR activity [143,144]. Several of the more representative precious metal catalysts are described below.

Zhang et al. [145] prepared RuSACs on nitrogen-doped graphene; Ru-N/G showed good ORR activity in an acidic environment (0.1 mol/L $HClO_4$), with starting and half-wave potentials of 0.89 V and 0.75 V (vs. RHE), respectively. Theoretical calculations using DFT demonstrated that the ORR active site of Ru-N/G-750 is not Ru-$N_4$, and is rather an Ru-oxo-$N_4$ structure. These research results provide a good idea for the design of high-performance ORR electrocatalysts in acidic media in the future. Furthermore, Xiao et al.

[146] synthesized RuSACs (Ru-SSC) by pyrolysis of MOF materials in an acidic environment (0.1 mol/L $HClO_4$) with a starting potential of 0.92 V (vs. RHE) and a half-wave potential of 0.824 V, which is similar to the corresponding data for commercial Pt/C shown in Figure 12a. The dynamic current density of Ru-SSC is 1.5 times higher than that of commercial Pt, while the dynamic current density of Ru-SSC is 1.5 times higher than that of commercial Pt/C and 2.7 times higher than that of Fe-SSC. Figure 12b shows that the Tafel slope value of Ru-SSC (54.2 mV $dec^{-1}$) is much lower than that of Pt/C (67.2 mV $dec^{-1}$), which indicates faster ORR kinetics for Ru SSC. In addition, the average value of kinetic current density $J_k$ for Ru-SSC at 0.8v potential is 11.95 mA $cm^{-2}$, and Figure 12c indicates that the $J_k$ of Ru-SSC is even higher than that of Pt/C (4.7 mA $cm^{-2}$) and Fe-SSC (average value of 3.23 mA $cm^{-2}$). From the TOF test results in Figure 12d, it can be seen that the turnover frequency (TOF) of Ru SSC is 4.99 $e^{-1}$ site-1 $s^{-1}$, which far exceeds that of the monatomic MSACs (M = Fe, Co, and Mn). From the data in Figure 12e, the electron transfer number can be calculated as 4, indicating an effective four-electron transfer process. From Figure 12f, the hydrogen peroxide yield is lower than 1.8%. The probe experiment of the Fenton reaction activity of Ru-SSC by UV-VIS absorption spectroscopy is shown in Figure 12g; it can be seen that the generation of reactive oxygen species is inhibited on Ru-SSC, meaning that the catalyst is less disturbed by the Fenton reaction. Figure 12i shows that the half-wave potential of Ru-SSC has a negative shift of only 18 mV after 20,000 potential cycles, which shows superior stability compared to Fe-SSC (32 mV). Density flooding theory (DFT) calculations show that the OH* ligand adsorbed on the Ru-$N_4$ site adjusts the d-orbital electronic structure of Ru, which optimizes the adsorption-to-sorption behavior of the oxygen-containing intermediates on the Ru site and thereby improves the ORR activity of the catalyst. This work discovered a linear relationship between the Bader charge at the metal center, the adsorption energy of ORR intermediates, and the ORR overpotential through theoretical calculations and experiments, which can hopefully guide the rational design of new ORR efficient catalysts without considering the metal element, laying a strong theoretical foundation.

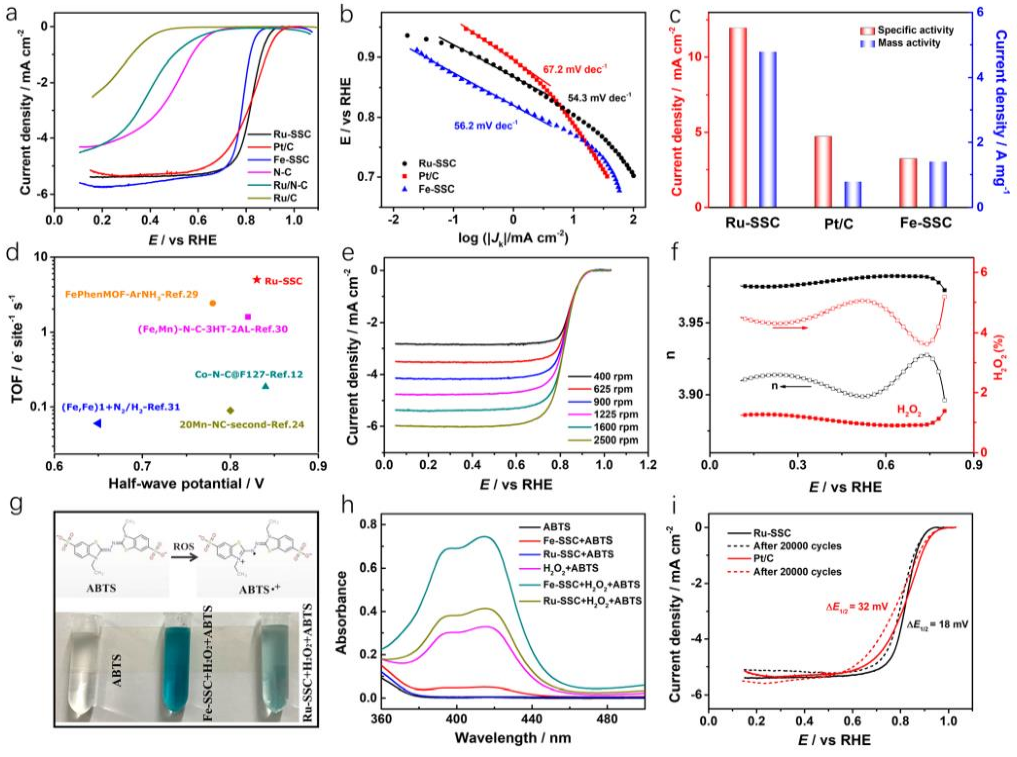


**Figure 12.** (**a**) ORR polarization curves of the synthesized catalysts at a scanning speed of 5 mV $s^{-1}$ at 1600 rpm; (**b**) Tafel slopes of Ru-SSC, Pt/C, and Fe-SSC; (**c**) comparison of specific and mass

activities of Ru-SSC, Pt/C, and Fe-SSC; (**d**) TOF (at 0. 8V vs RHE) as well as Ru-E1/2 values for SSC and other recently reported SSCs; (**e**) LSV curves for Ru-SAC with different rotation rates; (**f**) $H_2O_2$ production and the calculated electronic transfer numbers of Ru-SSC (solid squares) and Fe-SSC (hollow squares); (**g**) reactions of ROS and ABTS (top) and a photograph showing the color change of the solution after the Fenton reaction (bottom); (**h**) UV−Vis absorbance spectra of 0.1 M $HClO_4$ solution including only the following: abts; Ru-SSC and abts; $H_2O_2$ and abts; Fe-SSC and abts; Ru-SSC, $H_2O_2$ and abts; Fe-SSC, $H_2O_2$, and abts after 7 min of reaction. (**i**) Potential cycling stability test before and after ORR the polarization diagram. (Reprinted with permission from [146]. Copyright 2019, American Chemical Society).

To thoroughly understand the relationship between the interactions between noble metal atoms and ligand anions, it is necessary to investigate the principles of active site coordination of noble metal SACs in PEMFC applications. For this reason, Liu et al. [147] doped numerous noble metal atoms (Ir, Pt, Pd, etc.) into zeolite imidazolium salt skeletons (ZIF), which were then pyrolyzed to obtain noble metal SACs with M-$N_4$ active sites. The metal loading of IrSACs was 4.5 wt%. IrSACs showed higher ORR activity than the nanoparticle catalyst Ir/C in an acidic environment (0.1 mol/L $HClO_4$), with starting and half-wave potentials of 0.923 and 0.831 V (vs. RHE), respectively. Electrochemical tests and DFT calculations revealed that the ORR activity of the synthesized catalysts depends on the compatibility of the electronegativity of the ligand anion with the affinity of the metal site surface for $OH^*$. For IrSACs, the strong electronegativity of $N_4$ can reduce the over-adsorption of $OH^*$ on the surface of Ir single atoms; thus, the ORR activity of Ir SACs is higher than that of their nanoparticle counterparts. This work provides a theoretical basis for the design of noble metal SACs for acidic ORR and PEMFC applications.

Outlook and Summary

Although noble metals have relatively high electrocatalytic activity, their expensive nature and resource scarcity are major influences limiting the commercialization of energy conversion devices such as zinc–air batteries. In addition, precious metals as electrocatalyst materials suffer from low toxicity resistance and low stability. To solve this problem, this paper summarizes two major solutions. (1) Future researchers can consider physical confinement, which is an effective strategy to improve the stability of catalysts. Without affecting the catalytic activity of precious metal catalysts, the physical confinement layer can inhibit the sintering of catalysts and reduce agglomeration, shedding, and dissolution of catalysts during the reaction process, thereby enhancing catalyst lifetime. Therefore, it is necessary to focus more attention on the design of domain-limited redox electrocatalysts by "immobilizing" the noble metal catalysts, both to inhibit their dissolution in strong acid environments and to limit their movement and shedding on the carrier, in order to maintain their maximum activity and improve their stability. This kind of catalyst can generally be carried out at a low temperature, which solves the problem of catalyst particle aggregation at high temperatures and can greatly reduce energy consumption in the process of catalyst production, providing convenience for large-scale production. The key issue is how to encapsulate the precious metal catalysts to make effective use of precious metals. (2) Future researchers could consider the following aspects to further improve the efficiency of using non-Pt noble metals: (i) crystal plane modulation, which can achieve optimal performance by selectively exposing specific crystal planes; (ii) electronic structure modulation, which can achieve modulation of the Pt/Pd electronic structure by introducing a second element for alloying; (iii) morphology modulation, which can reduce the need for noble metals through constructing (iii) morphology control, which can reduce the required amount of precious metals and maximize the exposure of active sites by constructing morphologies with specific dimensions. In addition, it is difficult to ignore the problems of particle shedding and agglomeration due to metal dissolution. These aspects are among the main considerations for future research on noble metal catalysts.

## 3. Non-Metallic ORR Catalysts

Researchers have long been striving toward the goal of developing a new, efficient, durable, and inexpensive ORR catalyst to reduce or even replace the use of Pt. Although TM-N-C (TM = Fe, Co, etc.) materials are widely considered a promising alternative to Pt/C catalysts due to their excellent ORR electrocatalytic performance, and non-Pt catalysts have been developed with ORR catalytic performance, they have many drawbacks, such as poor stability during application and environmental pollution [148]. In addition, views about their corresponding active sites are controversial. Thus far, there are two different views: most researchers insist that the TM-N fraction is the active site, while others believe that the metal-free N-C fraction itself can catalyze ORR processes efficiently [149,150]. It was not until 2006 that Ozkane et al. found that TM species were not necessarily required for the ORR catalytic process, as they demonstrated that nitrogen-doped carbon with metal contamination of less than 1 ppm could catalyze ORR in acidic electrolytes [151]. Next, Dai's team reported that the ORR performance of N-doped carbon nanotube arrays in alkaline media was comparable to that of commercial Pt/C [152], making metal-free ORR catalysts (MFORC) an important candidate to replace commercial Pt/C.

For these reasons, the research on metal-free ORR catalysts has attracted a great deal of attention. The main components of metal-free catalysts are usually various carbon-based materials, among which the most widely used are graphite, graphene, carbon nanotubes, and ordered mesoporous carbon. The doping of carbon materials with heteroatoms (e.g., B, N, S, Se, P, F, etc.) intrinsically changes carbon-based catalysts, resulting in excellent catalytic performance [153]. However, the catalytic mechanism of carbon-based catalysts doped with different heteroatoms is very complicated, and no accurate conclusion has been reached. Recently, Zhang et al. determined by DFT calculations that the spin density is more important for the catalytic active site than the atomic charge density. Professor Zhang's theory can be applied to explain the enhanced catalytic effect of S and Se doping on ORR reactions. Thus, the detailed mechanism of doping of different heteroatoms needs to be further investigated [154]. Non-metallic catalysts have been studied for various heteroatom-doped carbon nanomaterials, mainly including boron-doped [155], nitrogen-doped [152], phosphorus-doped [156], sulfur-doped [157], and polyatomic doping such as double-doping [158] or triple-doping [159]. It has been shown that carbon materials doped with or without transition metal complexes show significant oxygen reduction catalytic activity [160]. Nitrogen atom doping is the most common heteroatom-doped carbon-based catalyst. In N-C-based catalysts, the nitrogen atom structure is the main factor affecting the catalytic performance of nitrogen-doped carbon nanomaterials. In the following section, the doping of different atoms is discussed in detail.

### *3.1. N-Doped Catalysts*

The related literature indicates that carbon materials doped with or without transition metal complexes show significant oxygen reduction catalytic activity [160–163]. The ORR modification of $sp^2$ carbon by N doping has two advantages: (1) the atomic radii of N and C are similar, which avoids lattice mismatch to an extent; and (2) N has one more electron than C, which facilitates the electron-requiring ORR reactions. Therefore, N should be an effective element for doping $sp^2$ carbon as an ORR electrocatalyst [152,161]. With a few exceptions, N-single-doped carbon performs better than most other single-doped carbons with non-metallic elements prepared by similar methods [164]. Therefore, N-doping is the most widely studied carbon-based metal-free electrocatalyst [165]. The most typical example consists of N-doped vertically grown carbon nanotubes, first synthesized by Dai et al. [152] in 2009, in which the high electronegativity of N results in a positive charge from the surrounding C atoms. The modified C atoms enhance the adsorption of oxygen and readily attract electrons from the anode to promote the ORR

reaction. Typical N-doped non-metallic catalysts are described in detail in the following section.

Jeon et al. [166] prepared N-doped nonmetallic ORR catalysts by direct immobilization of $N_2$ at the edges of graphene nanosheets (GnPs) using a ball-milled graphite method. The synthesized catalysts have a large number of pyridine and pyrazole rings at the edges, and have excellent catalytic properties for ORR. At the edge position of graphene, the dangling bonds are more reactive than the covalent bonds on the basal plane. Therefore, the combined effect of doping elements and their doped edge positions can induce synergistic effects to further enhance the ORR activity. This synthetic strategy is a simple, low-cost, and eco-friendly approach that provides a new way of thinking for the development of preparative environmentally friendly catalysts. In addition, Radoslav et al. [167] successfully synthesized N-doped ordered mesoporous graphite array materials from N, N′-bis(2,6-xylene)perylene-3,4,9,10-tetracarboxylic diimide using ordered mesoporous silica SBA-15 as a template, and showed that the materials annealed at 900 °C were the electrocatalysts with the strongest ORR electrocatalytic activity. Parvez et al. [168] reported an N-doped graphene catalyst with higher catalytic performance than commercial Pt/C catalysts for oxygen reduction in alkaline electrolytes. The authors concluded that the electrocatalytic activity depended on the graphitic -N content, while pyridine-N had no significant effect on the ORR performance. He et al. [169] used polydopamine-modified mixed cellulose ester filter membranes and KOH activation to synthesize 3D layered porous N-doped carbon materials with ORR (NC-A) activity close to that of Pt/C. Due to the high specific surface area of NC-A (2191 $m^2 \cdot g^{-1}$) resulting in more exposure to ORR catalysis, the high specific surface area is more advantageous than pyrrole N and pyridine N functional groups. On the other hand, pyridine-N species in carbon-based materials have been proposed as active sites for ORR in alkaline media [170]. Tucci et al. [171] proposed that high ORR electrocatalytic activity of nitrogen-doped carbon nanotubes compared to Pt/C is mainly reflected in the superiority of pyridine N in terms of onset potential ($E_{Onset}$) and limiting current density ($J_L$). Furthermore, Yasuda et al. [172] proposed that the 4e- process of oxygen reduction in N-doped graphene catalysts is due to the presence of pyridine-N, whereas graphite N is in the transfer pathway of ORR process 2e-, suggesting that pyridine-N is a more efficient site for oxygen reduction activity. By correlating ORR catalytic performance with the chemical composition of the N-doped carbon samples, the order of catalytic activity of the different N species was revealed as pyridine-N > pyrrole-N > graphite-N > oxide-N > C(carbon).

To date, a large amount of research has been devoted to the development of non-precious metal catalysts, including carbon-based catalysts and transition metal-based catalysts. However, transition metal-based catalysts always suffer from low electrical conductivity and metal dissolution, leading to degradation and contamination [173]. Therefore, it is particularly important to explore metal-free, highly active, cheap, and stable carbon-based electrocatalysts. Following the discovery of nitrogen (N)-doped carbon nanotubes (CNTs), carbon nanomaterials doped with metal-free heteroatoms (N, B, O, F, P, S, etc.) have been widely investigated for their excellent catalytic properties for ORR, and doping can effectively change the intrinsic electronic properties of the carbon matrix due to the different atomic sizes and electronegativity of the doped heteroatoms [150]. For example, in 2009, Lai-Ming Dai et al. found that nitrogen-doped carbon nanotube vertical arrays (CNTs) outperformed Pt in ORR catalysis and had excellent stability in alkaline media [152]. Using DFT calculations combined with experimental data, it was found that the improved ORR catalytic performance of nitrogen-doped carbon catalysts could be attributed to the doping-induced charge redistribution, resulting in a change in the chemisorption mode of $O_2$ from end-to-end adsorption on undoped CNT surfaces (Pauling model) to shoulder adsorption on nitrogen-doped CNT surfaces (Yeager model). Nitrogen doping induces charge transfer, and parallel adsorption of $O_2$ can effectively lower the ORR potential and weaken the O-O bond, ] promoting smooth ORR

on the nitrogen-doped CNT electrode. Subsequently, the field of metal-free catalysis has been developing rapidly.

### *3.2. B-Doped Catalysts*

The introduction of B atoms results in lower electronegativity of hole-type carriers than carbon, while the positively charged B atoms promote effective chemisorption of negatively charged oxygen atoms. The use of boron–carbon (BC) nanomaterials is considered an effective strategy to enhance electrocatalytic activity. It has been demonstrated that boron–carbon (BC) nanomaterials have high ORR catalytic properties. Mu et al. [174] prepared catalysts for BClCNTs by chemically tailoring 2D boron carbide ($B_4C$) with $Cl_2$. While the B atoms in $B_4C$ were partially extracted with $Cl_2$, the residual B and C atoms were combined with Cl atoms to self-organize into nanotube microstructures. An electron acceptor (B) and donor (Cl) co-doped into the C nanomaterials in the whole system can synergistically activate π-electrons in the $sp^2$ carbon for the oxygen reduction reaction (ORR). Simultaneous doping of graphene is an effective way to improve electrochemical activity. This is attributed to the fast electron transfer kinetics between the graphene backbone and the redox probes/analytes used for electrochemical studies. For example, Chung et al. [175] synthesized novel all-carbon-based composites consisting of B-doped graphene quantum dots anchored on graphene hydrogels (GH-BGQD) using a facile one-step hydrothermal method. GH-BGQD materials are 3D structures with high porosity and large specific surface area, and can enhance mass migration and ion diffusion of electrolytes. As a result, the prepared GH-BGQD composites show the highest onset potential (0.93 V) and highest ultimate current density (5.74 $mAcm^{-2}$) compared to for-doped materials. DFT calculations show that boron and nitrogen doping can modulate the energy band gap, spin density, and charge density while promoting the onset potential through synergistic electron transfer interactions between the doped atoms and the surrounding carbon atoms ORR [176]. In 2011, it was reported that co-doping metal-free based catalysts with different heteroatoms is an effective method to further improve the ORR electrocatalytic activity, and boron and nitrogen co-doped graphene exhibited better ORR electrocatalytic activity than the commercially available Pt/C [177]. These findings could pave the way for the commercialization of heteroatom-doped carbon nanotubes for large-scale applications.

### *3.3. Polyatomic Doped Catalysts*

The doping of heteroatoms is not limited to the doping of individual atoms, whether electron-rich N and O or electron-deficient B (electronegativity of 3.04, 3.44, and 2.04, respectively [178]), whose electronegativity affects the charge density of carbon atoms in the $sp^2$ lattice. Modified carbon atoms can promote the formation of oxygen adsorption sites. Carbon nanomaterials doped with binary or multiple heteroatoms have been investigated for their unique electronic structures, coexisting active centers, synergistic effects, and lower activation potentials, which can further enhance catalytic activity. For example, carbon nanomaterials doped with both N and boron (B) are expected to be promising co-doping catalysts due to the higher and lower electronegativity of N and B, respectively, compared to carbon.

For example, Wei [179] et al. prepared porous nitrogen (N) and boron (B) co-doped carbon nanotubes (NBCNT) by a controlled solid-phase method using tubular polypyrrole (PPy) and sodium tetraphenyl boron $(C_6H_5)_4BNa$, where $(C_6H_5)_4BNa$ acts as a B source as well as a pore-forming material that can help to modulate the N conformation and expose more active sites. NBCNT-10's high ORR activity is mainly due to the introduction of an appropriate amount of $(C_6H_5)_4BNa$, which is characterized by (1) the introduction of $(C_6H_4)_4BNa$ as a B source to form N, B co-doped carbon-based catalysts, with the synergistic effect between the two heteroatom dopants able to effectively modulate the electronic properties and surface polarity of the electrocatalyst, and (2) $(C_6H_5)_4BNa$ adsorbed on PPy nanotubes, which can create pores and defects in the tube

walls while effectively increasing the residual N content and modulating the N conformation in the catalyst, leading to more exposure of the active center. All of these are beneficial for improving ORR performance [180].

From the test results shown in Figure 13a, the oxygen reduction peak potential of NBCNT-10 is 0.78 V, which is higher than other boron-doped samples. Figure 13b shows the LSV curves of NBCNT samples and commercial Pt/C (20%). nBCNT-10 (LCD = 5.52 mA $cm^{-2}$, $E_{onset}$ = 0.958 V, $E_{1/2}$ = 0.82 V) is comparable to commercial Pt/C (LCD = 5.65 mA $cm^{-2}$, $E_{onset}$ = 0.984 V, $E_{1/2}$ = 0.84 V), and Figure 13c shows that NBCNT-10 has the lowest Tafel slope (87 mV $dec^{-1}$) among all samples, further demonstrating the excellent ORR kinetics of this catalyst. Figure 13d shows the LSV curves of NBCNT-10 at different rotational speeds from 400 to 2000 rpm. Combining the data calculated in Figure 13d and its inset, the average electron transfer number (n) of the NBCNT-10 catalyst is about 3.9, indicating that the catalytic behavior is an effective pathway for 4e- ORR. From the analysis in Figure 13e, it is clear that the catalyst is more methanol-tolerant than Pt/C, indicating that the prepared catalyst is extremely resistant to contamination. The data shown in Figure 13f indicate that the NBCNT-10 catalyst has better durability in alkaline electrolytes than Pt/C. The above results indicate that the catalyst has good ORR catalytic activity.

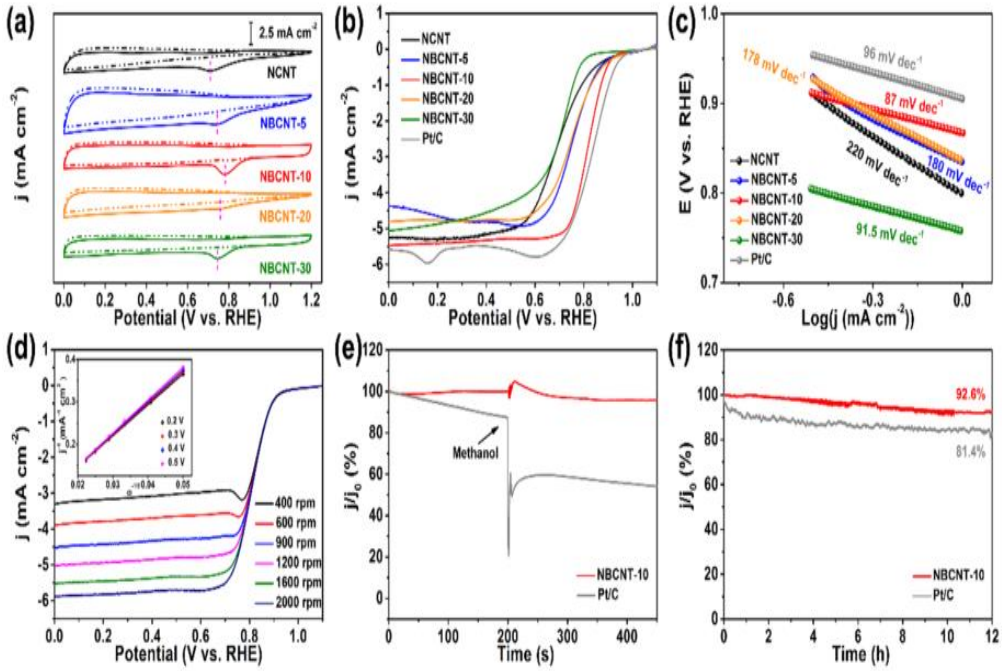


**Figure 13.** Catalytic performance of ORR in 0.1 M KOH electrolyte. (**a**) CV curves of different electrocatalysts in $N_2$-saturated (dashed curve) and $O_2$-saturated (solid line) alkaline electrolytes. (**b**) LSV curves for a fixed speed of 1600 rpm and a voltage of 10 mV $s^{-1}$ (**c**) Tafel plots for NCNT, NBCNT-5, NBCNT-10, NBCNT-20, NBCNT-30, and commercially available Pt/C catalysts obtained by applying mass transfer correction to the corresponding LSV curves. (**d**) LSV curves and K-L plots for NBCNT-10 at various rpm from 400 rpm to 2000 rpm (inset). (**e**) Methanol tolerance of NBCNT-10 and Pt/C. (**f**) i-t chronoamperometry response. (Reprinted with permission from [179]. Copyright 2021, Elsevier).

Furthermore, Higgins et al. [181] reported that N and S co-doped graphene/nanotube composites (GC-NLS) exhibited better electrochemical ORR activity than graphene-only or N and S co-doped CNTs. Triple doping showed excellent oxygen reduction activity, as reported by Meng et al. [182]. N-, O-, and S-triple-doped polypyrrole-based nanoporous carbon exhibited good ORR activity (onset potential of about 0.96 V), with a half-wave

potential value of 0.74 V. In addition, it was found that the ORR activity of N, P, and B co-doped porous nanocarbon was better in terms of current density and onset potential than single-doped or double-doped catalysts [183].

In addition, S- and N-doped carbon is one of the most important co-blended carbon materials. Many studies have shown that S- and N-doped carbon materials have ORR activities comparable to Pt/C. For example, Yan [184] used dopamine hydrochloride and 2-mercaptoethanol as nitrogen and sulfur sources; solid core-mesoporous-shell-silica microspheres (SCMSSs) were used as templates and doped with N by the template method with solid mesoporous shell-layer silica (SCMSS) to form the porous S-N-C mesoporous structure of the catalyst. The formation of mesoporous structures facilitates the exposure of sulfur and nitrogen in the carbon matrix. This porous-S-N-C is even better than commercial Pt/C, showing potential economic value. This new method to increase the doping and exposure of N and S atoms is expected to be applied to the preparation of other high-content heteroatom-doped materials. The relevant electrochemical tests for ORR activity have shown that porous S-N-C in $N_2$ and $O_2$ saturated 0.1 mol $L^{-1}$ KOH solution with peak ORR potential (+0.91 V) > Pt/C (+0.89 V) and porous S-N-C ($E_{1/2}$ = 0.835 V) > Pt/C ($E_{1/2}$ = 0.8 16 V), which confirms that porous materials have higher ORR catalytic activity due to more dense active sites, more exposure, and better mass transfer. Furthermore, the ORR efficiency of S-modified materials (porous S-N-C and S-N-C) is much higher than the corresponding sulfur-free materials (porous N-C and N-C), demonstrating the promotion of S species with respect to N-C materials.

However, although nitrogen (N) and sulfur (S) co-doping of ordered mesoporous carbon (OMC) has shown good performance as a platinum-free catalyst for the oxygen reduction reaction (ORR), the complex and expensive synthesis method has seriously hindered its development and application. In light of this, Hua et al. [185] successfully prepared SN-OMC catalysts by combining hard template and high-temperature pyrolysis methods using inexpensive saccharin as a single-source molecular precursor and SBA-15 as a hard template. It was found that the prepared SN-OMC catalysts had comparable ORR electrocatalytic activity to the commonly used commercial Pt/C (20 wt.%), mainly for the four-electron (4e) ORR pathway, and better stability than methanol in alkaline media, mainly due to the synergistic effect from the highly ordered mesoporous structure and the double nitrogen-sulfur doping. Based on the results of the relevant CV curves, it was shown that SN-OMC exhibited better electrocatalytic activity along with more aggressive onset reduction potential (−0.005 V) and limiting current density (−4.2 mA $cm^{-2}$) than the values of SN-C (−0.185 V, −2.7 mA $cm^{-2}$). This may be attributed to the synergistic effect of the highly ordered mesoporous structure and the double nitrogen-sulfur doping. More importantly, the ORR activity of SN-OMC in alkaline media was comparable to that of commercial Pt/C. These results suggest that SN-OMC could be a promising alternative to Pt-free ORR catalysts, with good activity, excellent durability, and good methanol tolerance in alkaline media. Carbon-based metal-free catalysts are usually carbon materials doped with single or multiple non-metallic elements (B, N, F, P, S, etc.) and mainly include pristine carbon materials (carbon nanotubes, acetylene black, graphene, etc.) and derived carbon materials processed from carbohydrates [186–190] and various biomass carbon precursors [191–193]. In recent years, metal-organic backbones (MOFs) for the preparation of nanoporous carbon have received much attention. Usually, the methods for the preparation of carbon-doped materials include pyrolysis, templating, and acid-catalyzed dehydration. Currently, reduced nitrogen or sulfur precursors are used as reagents for doping atoms. Jutao Jin et al. obtained N,-S co-doped porous exfoliated carbon nanosheets by one-step pyrolysis of glucose/melamine sulfate, which exhibited excellent catalytic activity for ORR [194]. Yi and Li et al. synthesized N, -S co-doped three-dimensional reduced graphene oxide as an oxygen reduction catalyst by a soft-template-assisted method [195]. Min Seok Lee et al. prepared imine-rich doped graphene electrocatalysts for ORR from the acid-catalyzed dehydration reaction of graphene oxide and aniline derivatives [196]. Nitrogen-doped mesoporous carbon ORR electrocatalysts

with high catalytic activity and excellent capacitive properties were prepared by activating pre-carbonized milk powder with potassium hydroxide according to Jia et al. [197]. These results are relatively excellent ORR catalysts, and broaden the avenues for the development of nonmetallic catalysts.

### *3.4. Other Types of Non-Metal Catalysts*

In general, the preparation of conventional doped carbon materials requires a long reaction time and high energy consumption, and it is necessary to develop new doping methods for the preparation of doped carbon materials to shorten the production time and to achieve multifunctionality of catalytic activity. To this end, Zhou [198] developed a deflagration method for the preparation of nonmetallic catalysts which uses Vulcan XC/72 carbon black, sublimated sulfur, potassium nitrate, urea, and ammonium nitrate as raw materials for the rapid synthesis of ORR catalysts (D-NSOCs) co-doped with nitrogen and sulfur. The prepared D-NSOC electrocatalysts exhibited good bifunctional catalytic activity for ORR and OER, and the potential difference (ΔE) between the corresponding potential and the half-wave potential ($E_{1/2}$) was 0.77 V when the OER current density reached 10 mA $cm^{-2}$, which is slightly better than the corresponding potential difference for commercial Pt/C + $IrO_2$ (ΔE = 0.78 V). This method of deflagration synthesis is usually applied to other carbon material catalysts as well. It allows the doping of nitrogen and sulfur elements into carbon materials to achieve the functionalization of oxygen on the surface of carbon materials quite simply.

Moreover, carbon nanocages without any apparent dopant have shown good ORR performance under alkaline conditions [199], which DFT calculations have shown to be inseparable from pentagonal and zigzag edge defects. In this context, a novel ORR catalyst based on graphene quantum dots supported by graphene nanoribbons was developed by a one-step reduction reaction, achieving better ORR performance compared to Pt/C. This good electrocatalytic performance was attributed to the presence of a large number of surface and edge defects on the graphite quantum dot alkene and nanoribbons, respectively, and the effective charge transfer between the closely contacted graphene quantum dots and nanoribbons [200]. Studies on the defect-induced ORR catalytic activity remain at an early stage, and further mechanistic studies are needed.

### *3.5. Summary and Outlook*

In summary, despite considerable efforts towards the synthesis of N, B co-doped carbon-based catalysts, exploring simple, low-cost, and controllable synthetic strategies for efficient metal-free electrocatalysts remains a great challenge. Because metal-free catalysts usually exhibit limited activity and poor stability, especially in acidic media, despite the rich results achieved by metal-free catalysts in recent years problems in their development have been revealed at the same time, such as the specific difficulty of distinguishing the contributions from heteroatoms, vacancies, or Stone-Wales defects due to the heteroatom doping, which often introduces defects and/or vacancies. In addition, high precision control and detection of the atomic-level position, structure, and chemical composition of CACs are difficult to achieve. Therefore, a combination of synthesis, characterization, modeling, and theoretical calculations is necessary to elucidate the fundamental issues controlling the catalytic process and to trace the kinetic evolution of the substances during the reaction.

## 4. Alloy ORR Catalysts

As the most critical technology for fuel cells, the performance of the oxygen reduction reaction (ORR) is closely related to electrocatalysts. However, although Pt-based catalysts remain one of the most effective catalytic materials for ORR, they are expensive to fabricate. Alloying the active metal is one of the most effective means to reduce catalyst fabrication cost; the most suitable candidates to replace Pt are transition metal alloy

materials and other noble metal alloy materials. The electrocatalytic properties of alloys are influenced by the interactions between several elements, which induce different atomic configurations [201]. Therefore, alloy-based catalysts have become a popular research topic.

### *4.1. Bimetallic Alloy-Based Catalysts*

Metal-organic backbones (MOFs) contain a variety of organic functional groups and metal centers, which can be transformed into porous carbon frameworks and carriers of active metal species after special treatments such as carbonization and are very promising carriers for the synthesis of M/NC hybrids [202,203]. In addition, palladium (Pd) is an important metal catalyst used in various industrial reactions [204]. It has higher carbon monoxide (CO) tolerance and catalytic activity than Pt-based catalysts when used as a fuel cell cathode catalyst [205]. Therefore, alloying it with other metals might be a good strategy for replacing Pt/C catalysts. For this reason, Xu [206] embedded a Pd-Co binary alloy ($Pd_xCo$) into a bimetallic organic backbone (BMOF)-derived polyhedral carbon carrier to form a catalyst for ORR. The results showed that the BMOF-derived $Pd_3Co$ had the best ORR activity at 300~400 °C, with a half-wave potential ($E_{1/2}$) of 0.977 V (vs. RHE) and a mass activity of 0.86 mA/μgPd in 1 M KOH, both of which are better than commercial Pd/C electrocatalysts. The improved performance and stability are attributed to the homogeneous distribution of Pd and Co elements and the N-doped carbon (Co-N-C) structure containing Co. In anion-exchange membrane fuel cell (AFC) tests, cells with BMOF-derived $Pd_3Co$ cathodes achieved a peak power density of 1.1 W/cm$^2$ at an ultra-low partial discharge loading of 0.04 mg Pd/cm$^2$. This strategy provides promising insights for the rational design and synthesis of highly active and durable ORR electrocatalysts for alkaline fuel cells.

In addition, Zhu [207] synthesized FeCo alloy NPs nitrogen-doped mesoporous carbon catalytic materials using a simple two-step strategy (including ligand-driven self-assembly of MOF composites and high-temperature carbonization process); the synthesis process and related characterization are shown in Figure 14. The catalyst exhibited superior ORR activity and durability attributable to its highly exposed bimetallic active sites and well-designed structure. X-ray absorption fine structure spectroscopy and density flooding theory calculations indicated that the excellent catalytic performance originated from the electronic structure modulation of the co-active sites by Fe atoms, which resulted in the optimal binding energy of the catalyst to the oxygen reduction reaction intermediates. The material (MIL-101@ZIF-67 composite) is an excellent ORR electrocatalyst. The experimental results show that the material has a large half-wave potential, high durability, and strong tolerance to methanol, and the research results provide a valuable guide to studying the relationship between the structure and performance of transition metal-based ORR alloy catalysts.

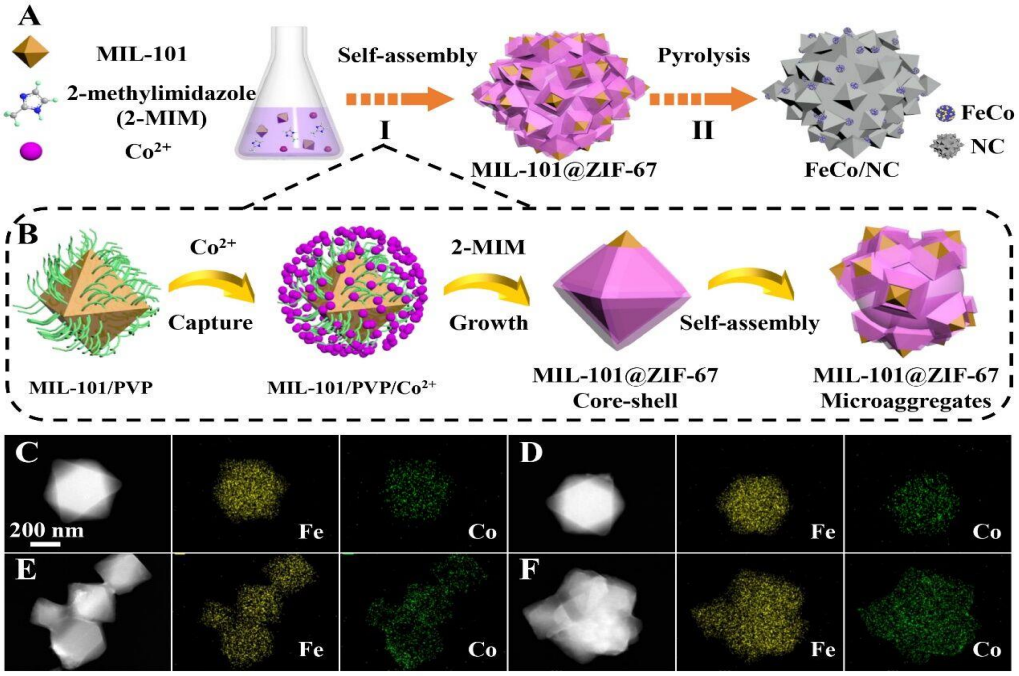


**Figure 14.** (**A**) Diagram of FeCo/NC catalyst synthesis. (**B**) Schematic diagram of the ligand-induced self-assembly process. (**C**) TEM images of the intermediates after (**C**) 2 min, (**D**) 5 min, (**E**) 10 min, and (**F**) 20 min. (Reprinted with permission from [207]. Copyright 2022, John Wiley and Sons).

To solve the problems of low active site utilization and deactivation due to the overconsumption of active sites on the surface of conventional catalysts, it is necessary to develop catalytic materials with multidimensional structures, especially those combining 1D nanotubes with 2D nanosheets/layers, which can accelerate the mass/electron transfer rate and make it easier to expose the active sites of the catalyst, in turn facilitating the stabilization of each reaction step involving ORR [208,209]. Lei [210] synthesized $Fe_1Co_2$ alloy nanoparticles (NP) embedded in nitrogen-doped carbon nanotubes/carbon nanosheets (CNTs/CNS) (denoted as $Fe_1Co_2$-NC) by pyrolysis of Fe-chitosan, cobalt-chitosan chelates, and urea in situ. The results show that the interaction between Fe and Co can effectively modulate the electronic structure of Fe and Co, where the ionic state of Co and Fe are partially oxidized, contributing to the intrinsic catalytic activity. Meanwhile, the CNT/CNS multidimensional porous carbon framework contributes to the adequate exposure of the active site and smooth mass/electron transport. As a result, the obtained $Fe_1Co_2$-NC catalyst shows a high half-wave potential (compared to RHE) of 0.88 V for ORR, making it an ultra-low potential difference (0.706 V) comparable to Pt/C+$RuO_2$ (0.69 V). In addition, a large amount of research work has been devoted to the design of efficient and durable bifunctional electrocatalysts in recent years. Transition metal oxides with a spinel structure (denoted as $A_xB_{3-x}O_4$ (A, B = Co, Zn, Ni, etc.)) have attracted great attention in the ZAB system because of their low price, easy synthesis, tunable morphology, high doping ability, electrochemical activity, and stability [211–213]. Moreover, the coexistence of metal cations (redox couples) with different ORR/OER activities in the same interconnected structure confers mixed transition metal oxides a unique ability to promote the progression of redox reactions [214–216]. In this regard, the addition of Ni [217], Zn [218], and Mn [219] with cobalt-based spinel oxides has been shown to enhance ORR and OER performance.

### *4.2. Trimetallic Alloys*

The formation of alloys of different active transition metals in electrocatalytic reactions can effectively improve catalyst activity and stability [220–223], and alloying of

non-precious metals can help to further reduce the required amount of precious metals [224–226]. Compared with well-studied bimetallic alloys, trimetallic alloys, although possessing a more complex alloy lattice, higher reactivity, and stability, are more complex to synthesize, and the additional metal composition can further modulate the catalyst activity [203,227].

It has been widely reported in the literature that carbon-coated transition metal alloys can be used as ORR catalysts [228,229]. Based on the synergistic effect between alloy particles and N-doped carbon surfaces [230,231], these carbon-coated catalysts have excellent ORR catalytic properties. Inspired by this, Wang [232] developed a ternary transition metal alloy nanoparticle anchored on nitrogen-doped carbon nanotubes (N-CNT) as an ORR catalytic material by a simple sol-gel method, which can be denoted as $Fe_2Co_2Ni_2$/N-CNT. Relevant characterization and theoretical calculations indicate that the surface oxidized Fe-Co-Ni alloy anchored on N-doped carbon nanotubes is an effective catalyst for ORR. The $E_{Onset}$ of this catalyst is 0.811 V (vs. RHE), its $E_{1/2}$ is 0.749 V (vs. RHE), and its ultimate current density $J_L$ is 5.28 mA $cm^{-2}$. Its ORR performance is close to and/or better than that of most previously reported Pt/C catalysts, and the stability and methanol resistance of $Fe_2Co_2Ni_2$/N-CNTs are much better than those of Pt/C catalysts. The stability and methanol resistance of $Fe_2Co_2Ni_2$/N-CNTs are far superior to those of Pt/C catalysts. The excellent ORR catalytic activity of $Fe_2Co_2Ni_2$/N-CNTs can be attributed to three aspects: (1) the synergistic interaction between the three metals (Fe, Co, and Ni) in this catalyst; (2) the interaction between the ternary metal and the carbon composite interactions accelerate the catalyst surface charge transfer rate, better anchoring of $Fe_2Co_2Ni_2$ nanoparticles and preventing their detachment and aggregation; (3) the thin oxide layer on $Fe_2Co_2Ni^2$ nanoparticles can provide more catalytic active sites, which is beneficial for better adsorption of ORR intermediates. This strategy of synthesizing new alloy catalysts with the oxide layer of alloy particles as catalytic active sites provides a good example and idea for the design of new non-Pt-based ORR catalysts. Wang's research results indicate that catalysts based on ternary transition metal alloy nanoparticles anchored on carbon materials have great potential for fuel cell development.

### *4.3. Other Types of Alloy Catalysts*

The good ORR performance of alloy-like catalysts is inseparable from the synergistic, ligand, and strain effects of the individual metals in the alloy [233,234], which affect the number of specific active sites and the local composition of the active sites. Wang and coworkers developed porous tetrametallic Pt-Cu-Bi-Mn nanosheets with enhanced catalytic activity due to the increase in band vacancies caused by the introduction of the transition metal Mn, with stronger ORR catalytic performance and catalytic stability than ternary Pt-Cu-Bi alloys [235]. These results considerably broaden the family members of alloy catalysts, and provide additional synthetic strategies.

However, it remains challenging to control the synthesis of nanostructured multi-alloys containing five or more elements due to each element's different physical and chemical properties. A special class of SASCs, such as single-atom alloys (SAAs), can be fabricated based on metallic carriers by taking advantage of metals. Single-atom alloys (SAAs) formed by doping transition metal atoms on the surface of covalent host metals exhibit unique catalytic properties [219,220]. SAA typically binds CO more weakly than pure PGM materials, and therefore exhibits greater CO tolerance [236,237].

Based on this, Michail Stamatakis [238] studied SAA composed of Ni, Pd, Pt, Co, and Rh doped into Ag and Au bodies with the help of DFT. The results of their DFT calculations are shown in Figure 15. The calculations show that the PdAu SAA exhibits a slightly lower overpotential compared to Pt(111). Its KMC simulation experimental results show that it is more tolerant to CO poisoning. Furthermore, the experimental results show that it prefers the four-electron ORR pathway, while the density of active sites of PdAu SAA is lower than that of Pt(111). Based on the desirable ORR properties

described above, its catalytic performance is close to that of Pt/C. Although the use of Au and Ag to replace a large amount of Pt in the ORR catalyst is not cheap to prepare and reduces the number of active surface sites by a factor of 20 to 100, it enhances the catalyst's selectivity and resistance to poisoning, representing a feasible strategy for replacing the Pt/C catalyst. The above results indicate that PdAu SAA can be a catalytic material for the cathode of PEM fuel cells, providing a new solution for future electrochemical technologies.

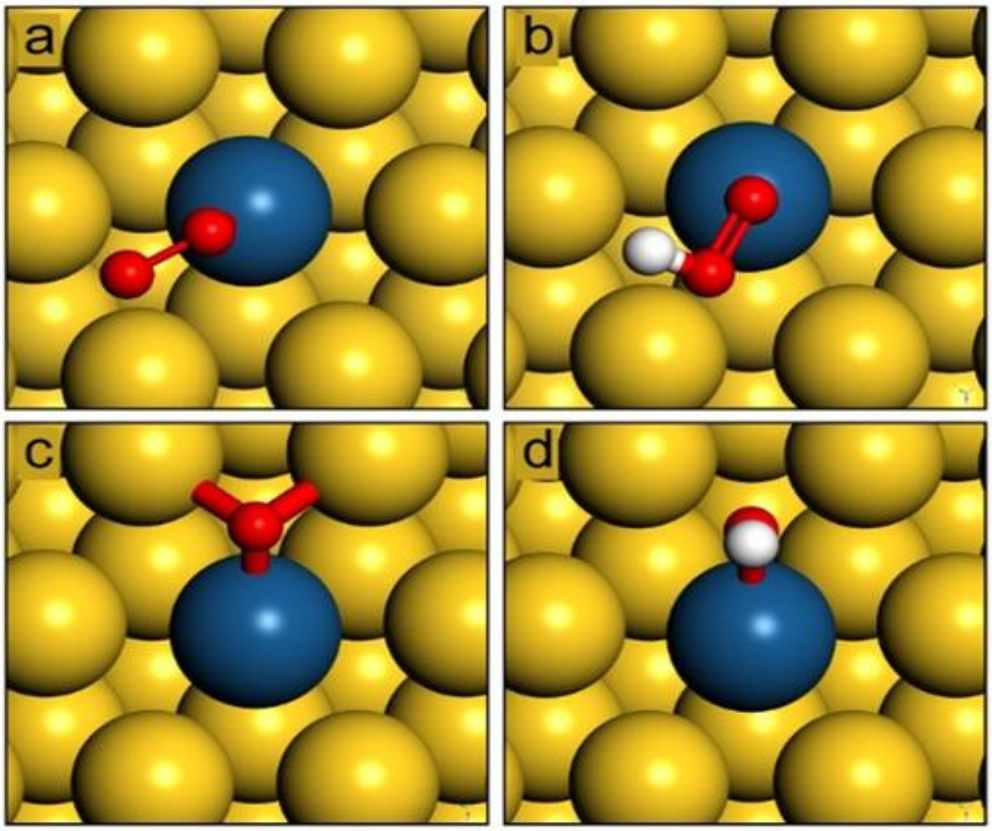


**Figure 15.** The most favorable adsorption geometries of (**a**) $O_2$*, (**b**) OOH*, (**c**) O*, and (**d**) OH* on PtAu(111) as calculated by DFT. The adsorption geometry on PtAu(111) is typical of all SAAs in this study. (Reprinted with permission from [238]. Copyright 2021, John Wiley and Sons).

### *4.4. Summary and Outlook*

Nanocatalysis materials formed by either transition metal alloying or noble metal alloying are one of the most important means of improving the catalytic activity of ORR to replace Pt. Transition metal alloys have unique physicochemical properties and low cost, and as such have received wide attention. These physicochemical properties can improve catalyst activity and stability and increase the number of active sites to significantly enhance ORR activity. For example, the introduction of low-cost transition metal elements such as iron (Fe), cobalt (Co), and nickel (Ni) can significantly reduce the total cost of catalysts, relieving the pressure of precious metal resource scarcity. This paves an important path for the reasonable construction of low-cost and high-performance platinum-free electrocatalysts. In addition, a large number of studies have shown that the catalytic effect of noble metal alloys or transition metal-precious metal alloy catalytic materials is excellent, and alloying 3d transition metals with noble metals can reduce the center of the d-band of metals and optimize the adsorption conditions of intermediates (e.g., $OH_{ads}$ or $CO_{ads}$), improving the ORR activity [239].

Although the performance of alloy-based catalysts is excellent, there are limitations. For example, many alloy-based catalysts have great room for improvement in terms of

toxicity resistance and preparation processes. For this reason, in addition to surface structure control of alloys, researchers should work on electronic modulation of catalysts in order to improve their electrocatalytic properties and enhance their toxicity resistance, and develop materials that can replace precious metals to minimize the use of precious metals and reduce production costs. In addition, it is important to develop a simple and green preparation strategy in order to further commercialize fuel cells.

## 5. High-Entropy Alloy ORR Catalysts

High entropy alloys with a single-phase solid solution structure, first proposed in 2004, are composed of five or more different elements [240]. As shown in Figure 16, HEAs differ from conventional alloys mainly by their high entropy effect, lattice distortion effect, slow diffusion effect, and "cocktail effect" [241]. In addition, due to their unique microstructure, excellent thermal stability, and catalytic activity for various reactions, they have attracted great interest in the development and application of electro/thermo-catalytic clean energy conversion. There is an intrinsic synergy among the components in HEAs that can regulate the electronic state of the resulting HEA, resulting in high catalytic activity [241–243]. Meanwhile, due to their higher entropy and slower diffusion, they have better heat resistance, chemical stability, and corrosion resistance, ensuring the stable operation of HEAs in harsh environments. Currently, the main methods for synthesizing high-entropy alloys are carbon thermal shock synthesis [244], mechanical alloying [245], sputtering deposition [246], power-controlled laser synthesis [247], solvothermal synthesis [248], ultrasonic treatment-assisted wet chemistry [249], the fast-moving bed pyrolysis (FMBP) method [250], casting and low-temperature grinding methods [251], etc.

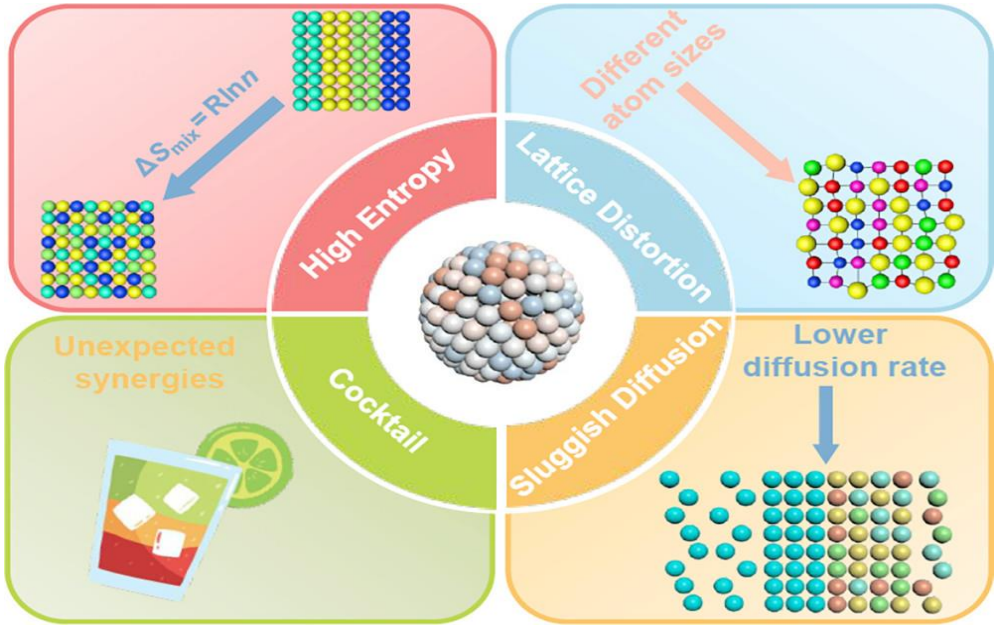


**Figure 16.** Schematic representation of the characteristics of HEA. (Reprinted with permission from [241]. Copyright 2020, American Chemical Society).

The controlled anchoring of multiple isolated metal atoms into a single carrier has great potential in many reactions, while the synthesis of catalysts with multiple single metal atoms remains a challenge and has been rarely reported in the literature. Furthermore, Beller et al. predicted the successful preparation of binary/polymetallic SACs as the next scientific breakthrough achievement for SACs, as they have tremendous potential applications in many reactions [252]. However, very little work has been done on the preparation and application of BSACs, while polymetallic alloy SACs are expected to exhibit more attractive properties and functionality. Nonetheless, there have been few

results reported in this area. This is mainly due to the huge barriers to the coexistence of various metals in atomic dispersions with significantly different chemical/physical properties. Therefore, it is difficult to stabilize multiple isolated metal atoms in a single support structure for different atomic and anchor locus types. As such, the development of a versatile and efficient method to control SACs with multi-metal centers is urgently needed, and while high-entropy alloys should emerge, these are challenging.

Recently, HEAs have been used as catalysts for electrocatalytic reactions, showing superior stability, catalytic selectivity, and activity compared to conventional alloys [253–256]. The interaction between pure Pt-based catalyst surfaces and oxygen-containing substances is too strong, limiting the number of oxygen adsorption sites and consequently their catalytic activity. Alloying with transition metals (e.g., Fe, Co, Ni) or other elements can improve the ORR activity. Polymetallic systems [233,257] combine the properties of each metal, and exhibit unprecedented properties through possible synergistic effects. The addition of non-precious metals changes the atomic structure of Pt, which is more favorable for the adsorption and dissociation of $O_2$ and accelerates O-O bond breakage. Positions and elements in high entropy alloys can be screened by theoretical calculations (machine learning) to ensure that the best composition finds the best activity.

The catalysis of high entropy alloys (HEA) applied to ORR has become a hot research topic. HEAs consist of a mixture of elements in a solid solution, forming an ordered crystal structure and randomly distributed constituent elements. The surface of an HEA provides many active sites, and thus has extraordinary catalytic properties. As there are many combinations of randomly distributed constituent elements, it is necessary to develop a method to optimize the elemental composition of HEAs.

Recently, Thomas A.A. Batchelor [258] performed calculations of *OH and *O adsorption energies on the IrPdPtRhRu surface using the density generalization function (DFT) to build a database of adsorption energies and a constructive function model (volcano plot) (Figure 17A–C) to evaluate their ORR activity. These constituent elements (IrPdPtRhRu) were chosen because of their similar atomic radii and lower heat of formation, which make them likely to form stable HEAs; furthermore, the standard electrode potentials of all these elements are high, which in turn reduces the possibility of alloy oxidation. Later, using a simple machine learning algorithm (ML), the residual adsorption energy was predicted and good agreement was found between the calculated and predicted values. Based on this, appropriate expressions for predicting catalytic activity were used to optimize the HEA composition. The composition of highly active ORR electrocatalysts can be predicted by constructing active sites near the peak of the surface volcano map, based on which $Ir_{10.2}Pd_{32.0}Pt_{9.30}Rh_{19.6}Ru_{28.9}$ HEAs were designed. The catalysts exhibit even lower overpotentials compared to Pt/C. Because HEAs have sites that promote specific catalytic activity, HEAs can be used as a platform for the design of ORR catalytic materials. The absorbing material is correlated with the local atomic environment around the atom bound by the adsorption energy and used as a model for the calculation of the absorption energy. In short, by combining different elements, it is possible to find a cheaper and more active ORR catalyst.

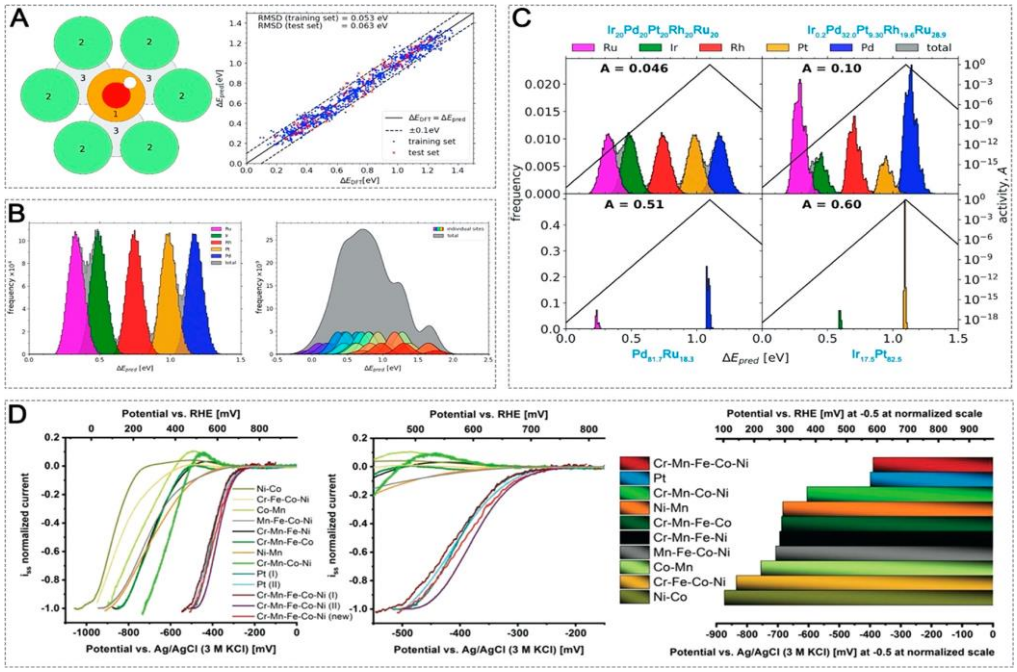


**Figure 17.** (**A**) OH* adsorbed on HEA. Each colored area represents an adjacent shell with a set of five parameters; the OH* adsorption model was trained on 871 specimens (blue dots) and tested on 76 specimens (red crosses). (**B**) OH*, and O* adsorption on the HEA model. (**C**) The activity of the redesigned IrPdPtRhRu HEA composition [40]. (**A**–**C**) Reproduced with permission from reference [40]. (**D**) Comparison of the intrinsic activity of different catalysts for ORR. (Reprinted with permission from [241]. Copyright 2020, American Chemical Society).

The random configuration of HEAs with a high degree of disorder due to the huge chemical space can increase the mixing entropy of the HEA system, which facilitates the formation of stable single-phase solid solutions rather than metal polymers. The ability of HEAs to form stable solid solutions is closely related to the atomic radius, enthalpy of the configuration formation, and mixing entropy of the HEA constituents. According to the Hume–Rothery law, stability evaluation can be performed by assessing the difference between the atomic radius and the enthalpy of the formation–entropy ratio [259–261]. The absorption energy of the reaction intermediates is usually a good description of the catalytic activity from Sabatier's rule [262]. Therefore, a volcano curve between the intermediate product adsorption energy and the catalytic activity of the ORR can be established, which facilitates understanding of the activity variation at millions of possible active sites on the HEA surface. Moreover, the formation of a stable single solid solution of a high-entropy alloy would be necessary in order to be consistent with the Hume–Rothery rule.

The effects of ligand effects (spatial arrangement of different elements) and coordination effects (different crystallographic surfaces and defects) on the catalytic performance of HEAs can be investigated using neural network models and density flooding theory (DFT) [263]. These two effects can lead to significant changes in the active site. Lu predicted the OH* adsorption energy on IrPdPtRhRu HEA catalysts with random elemental distribution and twelve unique ligand environments using a neural network model to describe the ORR (Figure 18a). As far as the ligand effect is concerned, it is clear from Figure 18b that the adsorption energy is determined by the contribution of different elements, where the two active central atoms bound to OH* are key in determining the adsorption energy. The frequency of OH* adsorption energy is continuous, indicating that the catalytic activity of HEA can be fine-tuned to the desired value[264]. In addition, the effect of changing the metal composition of the HEA catalyst on catalytic performance was investigated using a data-oriented artificial intelligence (ML)-based algorithm. A total of 10,000 equimolar HEA surfaces were generated in each ligand environment, and all of

the generated surfaces were predicted (see Figure 18c). On the surface of HEA (Figure 18d), the adsorption energy forms a continuous distribution. The study of the interrelationship between complex coordination conditions and catalytic performance can provide a basis for the design of efficient and effective HEA catalysts.

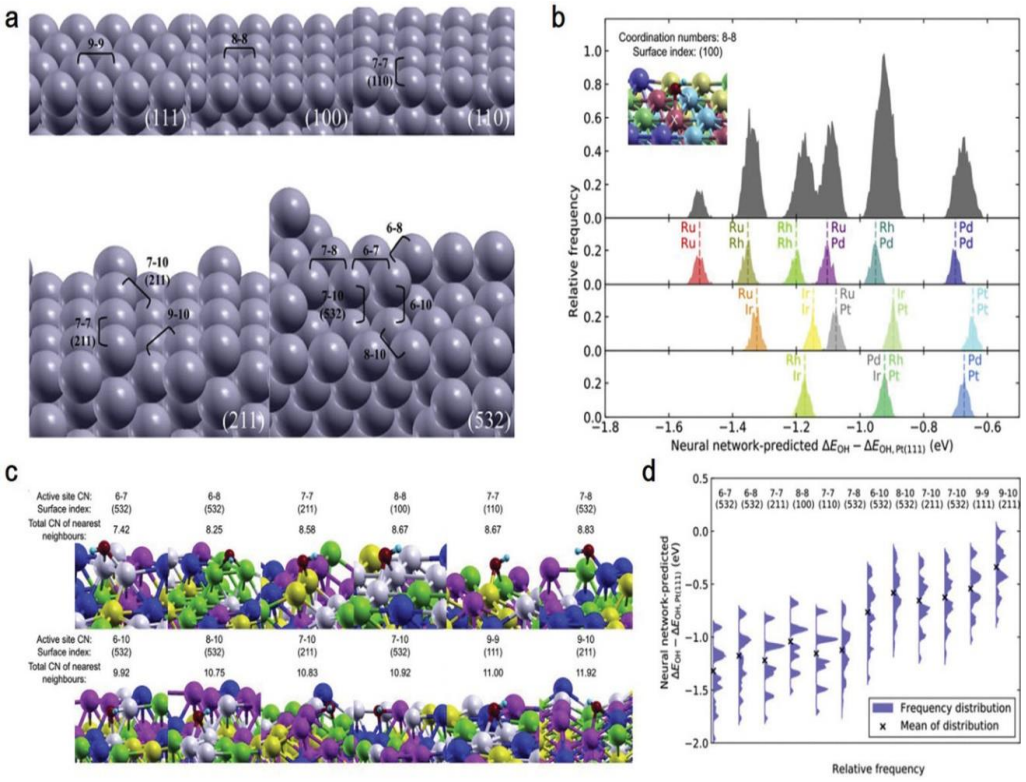


**Figure 18.** (**a**) Datasets of HEA surfaces and active sites were used for model training and evaluation. (**b**) The frequency distribution of OH* adsorption energies due to ligand effects for the [100] surface is shown as an example. (**c**) The different coordination environments are listed in increasing sequence of the total number of ligands in immediate proximity. (**d**) Frequency distributions of OH* adsorption energies for each ligand environment. (Reprinted with permission from [242]. Copyright 2021, John Wiley and Sons).

### *5.1. High-Entropy Alloy ORR Catalysts Containing Noble Metals*

Conventional synthesis methods focus on large-size HEAs rather than nanoscale HEAs [265–268]. In addition, the preparation of homogeneous nanostructured HEAs of small size (<10 nm) currently requires specific devices that can be rapidly heated and cooled as well as being resistant to high temperatures and with conductive substrates [244]. Therefore, there is a need to develop new strategies to prepare high-entropy alloy catalysts.

The preparation of nanoscale high-entropy alloy catalysts is a challenging task using conventional synthetic processes. In the conventional bottom-up process approach to the preparation of high-entropy alloy catalysts, the controlled combination of multiple immiscible metal elements into a single nanostructure has unlimited potential for development; however, it currently presents great difficulties. Moreover, the theory of dealloying points out that nanoporous noble metal catalysts such as Ir, Rh, Ru, Ag, Au, Pt, etc. can be obtained by dealloying [269]; thus, these noble metal elements can be easily added to Al-rich precursor alloys for the preparation of more complex np-HEAs. Inspired by this, Qiu [270] proposed a fast cooling dealloying strategy for aluminum-containing precursors to prepare ultrafine nanoporous high-entropy alloys (AlNiCuPdAuCoFe np-HEAs) with precisely controlled composition. The results exhibited ten times the Pt/C mass activity in ORR and maintained 92.5% of the initial activity after electrochemical

cycling. This excellent electrocatalytic performance can be attributed to inherent low diffusivity and the multi-principal element mixing effect. This top-down synthesis strategy offers the advantages of versatility, tuneability, and scalability for the synthesis of high-entropy alloys.

The enhanced catalytic performance promoted by order has been extensively studied in bimetallic and trimetallic electrocatalyst (e.g., PtCo, PtFe, and PdCuSn) systems [271–273]. However, the synthesis of structurally ordered HEA (OHEA) NPs and the evaluation of their effects on catalytic performance have not been achieved. Based on this, Zhu [274] constructed structurally ordered novel FeCoNiCuPd-HEANP on a 2D nitrogen-rich mesoporous carbon sandwich framework (OHEAmNC) by combining ligand-assisted interfacial assembly and $NH_3$ annealing. The characterization results showed that the synthesized materials have ultrathin 2D nanosheet structures and large mesopores (≈10 nm) with a structurally ordered L12 phase The HEA NPs are uniformly dispersed. Atomically resolved chemical analysis determined the location of each atomic position. In evaluating the oxygen reduction reaction, the OHEA mNC NP provided greatly enhanced catalytic performance, including large half-wave potential (0.90 eV) and high durability (0.01 V decay after 10,000 cycles) compared to disordered HEA and commercial Pt/C catalysts. This excellent performance is attributed to the improved mass transfer rate, increased electronic conductivity, and the presence of a stable chemically ordered HEA phase, as shown by both experimental results and theoretical calculations. This study presents a highly feasible approach to achieving structurally ordered HEA NPs with advanced mesoporous functionality in the field of electrochemistry. An ORR assay of the resulting material was performed, and the results showed good activity, with a large half-wave potential (0.90 eV), small Tafel curve value, and high durability (decay of 0.01 V after 10,000 cycles). From the experimental results and theoretical calculations, the resulting good performance is attributed to a well-designed spatial structure and the presence of a stable chemically ordered HEA phase, which provides fast mass transfer and regulates the active sites for adsorption and electron transfer of the reacting species during ORR.

In addition, it was found that excessive strain changes in HEAs can adversely affect catalytic performance. Constructing hollow structures improved ECSA, mitigated the effects of strain changes caused by heteroatoms, and modulated catalyst performance; however, with the often harsh fabrication conditions and complex composition of HEAs, the effective preparation of hollow HEAs remains a major challenge. Based on this, ZUO [275] synthesized a PdCuNiCo-HEA with a hollow nanosphere structure on $RGO_3$-CNT (PdCuMoNiCo-NHS/$RGO_3$-CNT) using a simple one-pot solvothermal method. The advantage of the developed catalyst, i.e., PdCuMoNiCo NHS for carbon hybridization, was demonstrated by its comparable ORR activity, while its long-term durability was much better than that of the commercial Pt/C. The hollow structure further amplifies the catalyst activity due to its various favorable properties, including a fully exposed active center, the shortened path length of the reactants, and increased utilization of noble metal atoms. Other metals (Ni, Co, and Mo) with different electronic structures and electronegativities were introduced into the hollow PdCu structure to form a stable HEA system, as it has been shown that forming an alloy with Cu, Co, Ni, and Mo with Pd can effectively optimize the lattice constant of Pd and improve the catalytic performance of ORR [276–278]. A schematic representation of the work of this catalyst in catalytic FAO and ORR is shown in Figure 19. The authors first synthesized PdCuMoNiCo HEAs with hollow spherical structures using a one-step solvothermal method with the help of glutamate. The hollow structure, intermetallic synergy, and slow diffusion effects of HEAs significantly improved the activity and stability of PdCuMoNiCo NHS/$RGO_3$-CNT in DFAFC against acidic ORR and FAO. Specifically, the relevant ORR performance test results show that the half-wave potential ($E_{1/2}$) of PdCuMoNiCo NHSs/$RGO_3$-CNT is 0.86 V and the ultimate current density ($J_L$) is 5.1 mA $cm^{-2}$, far exceeding that of commercial Pd/C ($E_{1/2}$ = 0.63 V, $J_L$ = 3.4 mA $cm^{-2}$), which is equivalent to conventional Pt/C catalysts

($E_{1/2}$ = 0.85 V, $J_L$ = 5.3 mA $cm^{-2}$). The mass activity (MA) of the catalyst is 0.882 A $mgPd^{-1}$, which far exceeds that of marketed Pt/C (MA = 0.630 A $mgPt^{-1}$), and both alloys are superior to their solid HEA counterparts and Pd-based binary, ternary, and tetrameric alloys. Thus, this work provides a viable strategy for the fabrication of hollow-structured HEAs that exhibit enhanced activity and stability towards both ORR and other reactions.

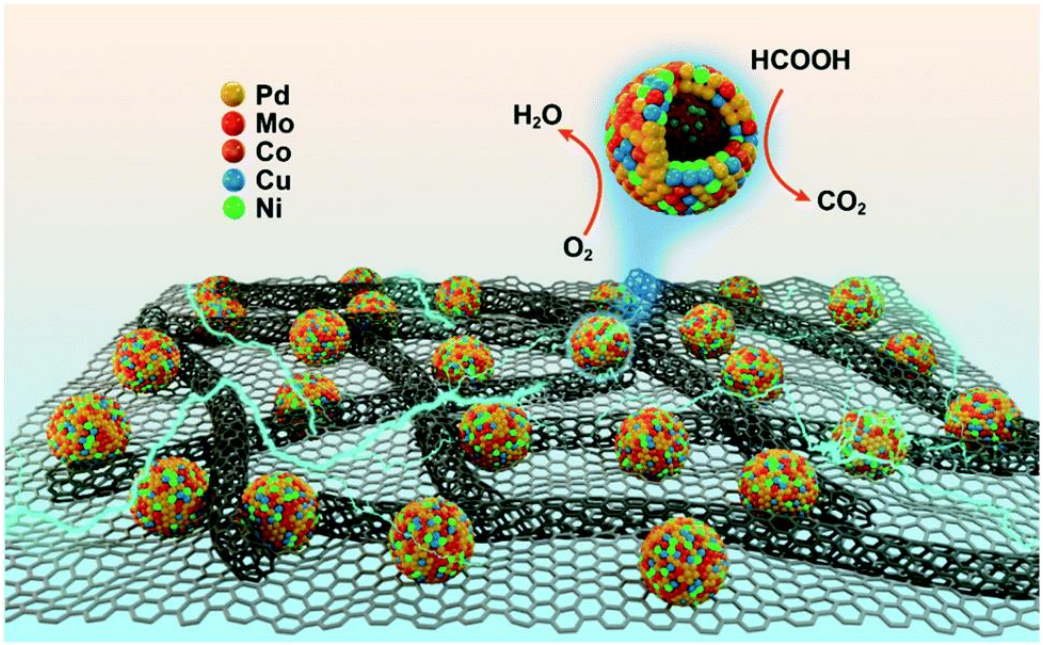


**Figure 19.** A schematic representation of the work of the catalyst in catalytic FAO and ORR. (Reprinted with permission from [275]. Copyright 2022, Royal Society of Chemistry).

*5.2. High-Entropy Alloy ORR Catalyst without Noble Metals*

As a new type of electrocatalytic material with unlimited catalyst design possibilities, multi-transition metal alloys are very promising option to replace noble metal-based catalytic materials. Based on this, Schuhmann et al. successfully developed a noble metal-free CrMnFeCoNi HEA NPS ORR catalyst with catalytic performance equivalent to that of commercial Pt/C catalysts (Figure 17D) [279]. Tests showed that the catalytic activity of the formed quaternary alloys decreased significantly with the reduction of one of the elements. For example, the lowest activity was observed in the absence of manganese, indicating that manganese can effectively promote the participation of the active site in the reaction. The experimental results show that in addition to the selection of suitable elements in the ground, the ratio of the catalyst performance has an influence on the reaction. Therefore, an excellent catalyst can be designed by simply changing the components and ratios, or even by using only non-precious metal components. In addition, the high entropy-induced single solid–solution phase leads to uniform distribution of all components, which has potential in the construction of more novel active sites for ORR and further improving catalytic performance. This study provides a novel idea for better design of non-precious metal catalysts.

Currently, conventional high-entropy alloy noncore–shell catalytic materials use vapor-phase deposition (coating method). Although high-entropy alloys synthesized by this method contain many components, these film materials are not consistent with the catalyst state, and many parameters and sizes cannot be tuned. Therefore, it is necessary to develop simple synthesis methods, such as a printing method to print different precursors onto the substrate, which can then be synthesized in one step at a high temperature. The advantage of this approach is that these printed materials are all in a more realistic internal state, a state in which the catalyst size, phase, and composition are all consistent. Thus, all the advantages of the different catalytic properties are attributed

to the design aspects of the composition. This has very significant implications for the development of high-entropy alloy ORR catalysts. Inspired by this, Tian [280] developed a versatile removable printing approach for the synthesis of high-entropy single-atom catalysts by transferring individual metal atoms from a printed template to a porous nitride-doped carbon carrier, a strategy that allows for the synthesis of high-entropy alloys consisting of up to eleven different combinations of metal elements. The strong ORR catalytic activity of the pentameric HESAC (FeCoNiCuMn) catalysts synthesized by this method should be derived from the abundance of active centers and the synergistic effect between different activity centers. The relevant characterization results showed that no metal agglomerates and/or microparticles were observed on the carbon carriers of the prepared HESACs. Energy dispersive spectroscopy (EDS) mapping images showed that the distribution of nitrogen and metals was homogeneous throughout the carbon carriers. The above results provide strong evidence for the successful synthesis of the proposed synthetic strategy from five to eleven elements of HESAC. The characterization results of the five-membered HESAC and the reference sample are based on XANES and EXAFS (shown in Figure 20). The results shown in Figure 20a,d,g,j,m demonstrate that the metal species (FeCoNiCuMn) of five-membered HESA present positive valence states. The EXAFS spectra (R-space) of Figure 20b,e,h,k,n were analyzed by Fourier transform spectroscopy, and based on the results of EXAFS fitting and the fitting parameters, it was concluded that the synthesized high-entropy metallic materials were each in an isolated state of dispersed metal atoms without forming aggregates, while the isolated five metal atoms coexisted with N atoms to form a typical M-N coordination structure. The atomic configuration of the five-membered HESAC (FeCoNiCuMn) was further investigated by metal (e.g., Fe, Co, Ni, Cu, Mn) K-edge wavelet transform (WT)-EXAFS and compared with the WT signal of the metal foil to further determine the separation characteristics of the metal species in the five-membered HESARC (FeCoNiCuMn), which proved that the catalyst did not form multi-metal polymers (as shown in Figure 20c,f,i,l,o). The ORR catalytic activity of the obtained HESAC catalyst was tested in $O_2$-saturated 0.1 M KOH solution and compared with Pt/C and carbon nitride carrier (also called NC) under the same conditions; the $E_{Onset}$, $E_{1/2}$, and $J_k$ of HESAC were 0.999 V, 0.887 V, and 3.114 mA $cm^{-2}$, respectively, which were higher than the corresponding values for Pt/C of 17 mV, 21 mV, and 1.151 mA $cm^{-2}$. The NC catalysts were prepared by the same procedure used for HESAC without a metal substrate. As expected, the ORR catalytic performance of pure NC was very poor, confirming that the good ORR catalytic behavior of the prepared HESAC is closely related to the synergistic interaction of the individual atomic metals.

In addition, the prepared HESAC catalysts have good durability, stability, and ORR performance. Using this method, HESACs ranging from five to ten metals were successfully synthesized. The proposed live-printing method broadens the ability to study HESACs and can combine the advantages of various metal elements with different intrinsic properties. The method has the following advantage of non-equilibrium treatment, which loads dispersed individual metal atoms onto the carrier by direct point-to-point loading, effectively preventing the ability to control the synthesis of high-entropy catalytic materials by regulating the temperature. This work broadens the family members of ORR catalysts and opens the way for the study of new multi-component high-efficiency high-entropy alloy catalysts.

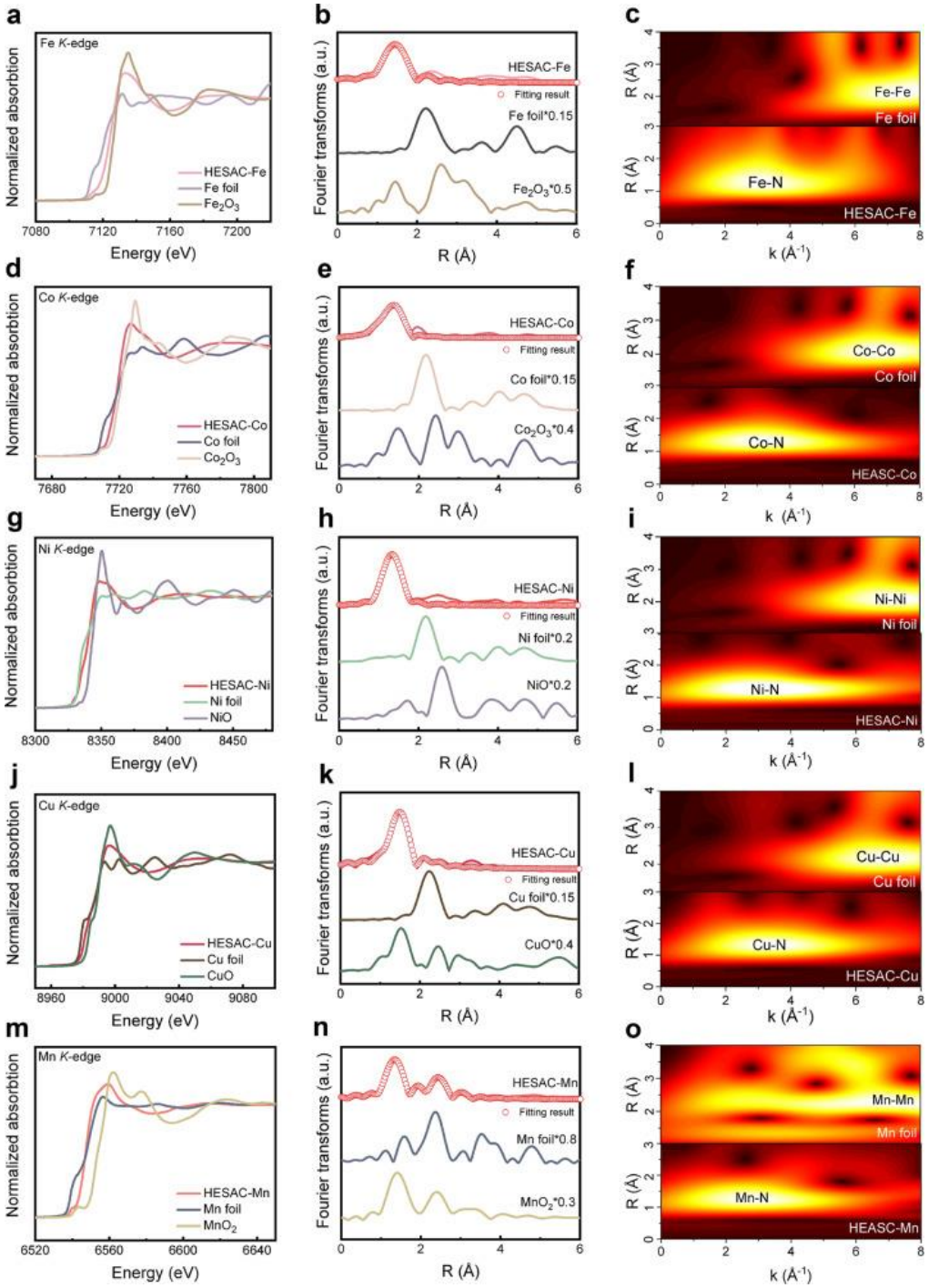


**Figure 20.** XANES and EXAFS data of the prepared binary high-entropy alloy (FeCoNiCuMn). (**a**,**d**,**g**,**j**,**m**) XANES spectra of (Fe K-edge), Co K-edge, Ni K-edge, Cu K-edge, and Mn K-edge of the binary high-entropy alloy. (**b**,**e**,**h**,**k**,**n**) and (**c**,**f**,**i**,**l**,**o**) WT of the EXAFS signals of the quaternary high-entropy alloy (FeCoNiCuMn) and the reference sample, respectively. (Reprinted with permission from [280]. Copyright 2022, Springer Nature Limited).

To combine five or more metallic elements with specific carriers in order to form efficient and stable high-entropy alloys, MOF with such carriers is a better way to synthesize multicomponent alloys or nanoparticles. In view of this, Hu [281] prepared a one-pot hydrothermal method to prepare a hollow high-entropy metal-organic backbone (MOF-74) composed of Mn, Fe, Co, Ni, Cu, and Zn, followed by a high-entropy nanocomposite. The catalyst preparation process is shown in Figure 20. The structure contains six different metallic elements; the biggest highlight of the process is that it does

not require any template and can be easily synthesized by a one-step hydrothermal method. This is the first report of porous hollow polymetallic MOF-74 known thus far. In addition, the obtained hollow porous MOF materials were heat treated in $Ar/H_2$ under different heat treatment conditions to obtain optimized porous hollow metal alloy/metal oxide nanocomposites, which are excellent ORR electrocatalysts. The synthesis process of MOF-74-H material and MOF-74-H-650 composite is shown schematically in Figure 21. According to the ICP analysis results, the elemental ratio of this sample can be interpreted as $Mn_1Fe_{1.24}Co_{1.27}Ni_{1.35}Cu_{1.27}Zn_{1.39}$. The relevant characterization tests confirm that the prepared MOF-74-H is a hollow porous structure. Its $E_{1/2}$ = 0.79 V for MOF-74-H-650 in alkaline ($O_2$-saturated 0.1 M KOH solution) electrolyte is much higher than the half-wave potential of the bimetallic MOF-derived CuNi/C ORR catalyst [282]. The best performance among the prepared samples was obtained for MOF-74-H-650. Moreover, the ORR performance of MOF-74-H-650 was superior to that of the high-entropy MOF-74-derived MOF-74-W-650 synthesized by the microwave technique. This is further confirmation that the unique hollow characteristics of the MOF-74-H-650 facilitate the provision of multiple internal voids/channels for the enhancement of electron transfer. It has been shown in the literature that the high inherent resistance of ZnO hinders the transmission of electrons from the glassy carbon electrode to the oxygen in solution during ORR [283]. Nevertheless, metal nanoparticles (Mn, Fe/Ni, Co, Cu) and metal alloys ($Cu_{0.18}Ni_{0.91}$, $Co_{0.52}Cu_{0.48}$) can dramatically improve the electrical conduction of ZnO formed in situ. Furthermore, the large specific surface area of the unique hollow structure can increase the adsorption of oxygen during ORR. The Mn nanoparticles formed in MOF-74-H-650 are essential for the stability of the catalyst, which contributes to its ORR activity. It should be pointed out that the overall ORR performance of the catalyst is equivalent to that of the tetrameric FeCoNiMn-based carbon nanocatalyst [81]. According to the Kentucky–Levich (K-L) curves of MOF-74-H-650 catalysts at different potential ranges from 0.3 to 0.5 V, it is apparent that the oxygen reduction process of MOF-74-H-650 follows the first-order kinetics [284]. The above data illustrate that the catalyst exhibits excellent ORR performance. It is evident from the experiments that its good ORR catalytic activity is attributed to the unique hollow structure of the catalytic material synthesized by the one-step hydrothermal method along with the synergistic effect of the high-entropy multi-element interactions between the in situ formed ZnO, metal, and alloy nanoparticles, which guarantees multiple internal cavities/channels and high electrical conduction for enhanced charge transport and electrocatalytic activity centers.

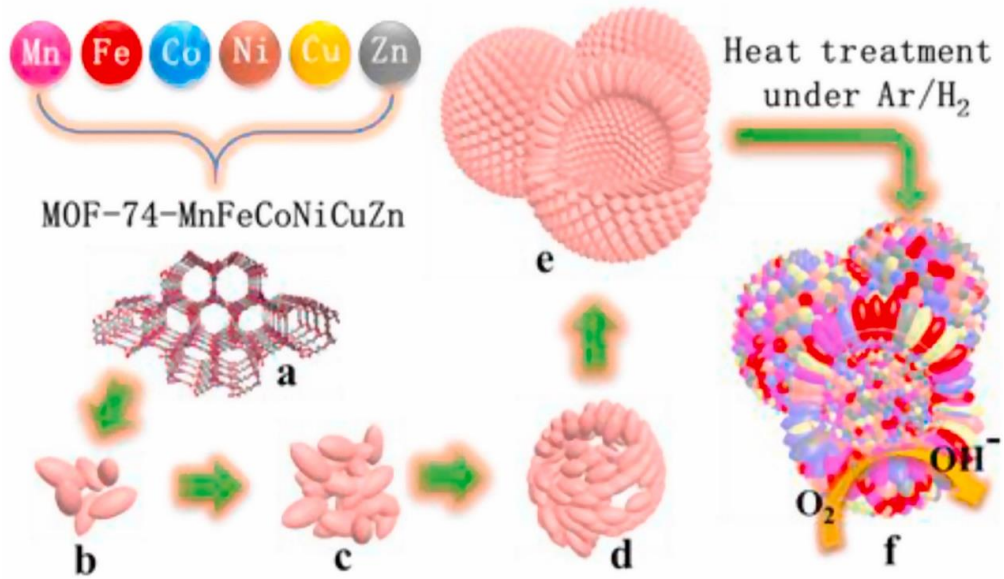


**Figure 21.** Schematic diagram of porous hollow high-entropy alloy catalyst production. (**a**) Crystal structure of MOF-74-H. (**b**) Small number of MOF particle aggregated. (**c**) Large number of MOF

particle aggregated. (**d**) Secondary nucleation. (**e**) Dissolution regrowth-formation of hollow multi-metal-organic framework. (**f**) Hollow metal/metal-alloy/metal-oxide (MOF-74-H-650) nanocomposite for ORR. (Reprinted with permission from [281]. Copyright 2021, Elsevier).

### *5.3. Summary and Outlook*

Three major aspects are mainly reflected in these studies. (1) Because the research on HEA is in its infancy, there are many problems with synthesis, testing methods, theoretical studies, and practice. For example, it is difficult to understand the origin of the properties of high-entropy alloys and such conformational relationships. (2) screening the optimal components from a library of millions of alloy candidates is a daunting task, and a new and rapid method for screening a large number of combinations needs to be developed to obtain the target properties required for catalytic applications. This can be achieved by artificial intelligence-based computation and "high throughput experiments", including machine learning (ML)-based methods and combinatorial methods to find the right choice for screening the best active ingredient by creating a catalytic "material library". Therefore, in the future scientists can use machine learning (ML) methods based on AI technology principles to assist in screening of the most catalytically active high-entropy metal components and the best locations. In particular, combining DFT with ML to develop high ORR performance catalysts can achieve good results. (3) Because HEA catalytic materials contain multiple components, it is very difficult to analyze and understand their complex catalytic systems. Finding the active positions in the chaotic arrangement of atoms is a challenge. At present, a large number of results have been obtained for single and diatomic systems, however, research on HEA systems is not comprehensive enough for. (4) The d-band theory used to predict the catalytic activity and absorption energy of the adsorbate of HEAs materials must be further refined, as most HEAs are strain lattices, which may result in changes in the degree of d-band overlap and cause the d-band center to not match the Fermi energy level. We believe that deeper development is necessary for the study of such materials. In the future, HEA catalytic materials can be systematically categorized and, different models can be studied independently. (5) Finally, the interaction between HEAs and complexes can influence the stability and activity of HEA catalysts, and this issue cannot be ignored. In conclusion, HEAs represent a vast and complex project with both opportunities and challenges.

## 6. Other Types of Non-Pt Fuel Cell ORR Catalysts

In addition to the above-mentioned SCA ORR catalysts, non-metallic ORR catalysts, and high-entropy alloy ORR catalysts, scientists have developed various forms of non-Pt ORR catalysts, such as transition metal compounds and other catalytic materials, to further enrich the ORR fuel cell catalyst family members. These uncommon catalysts are discussed in detail in the following section.

### *6.1. Transition Metal Oxide Catalysts*

Manganese oxides, as a low-cost and abundant green material, have high electrocatalytic activity in ORR. The relationship between the catalytic activity of ORR and the structure and composition of TMOs has been investigated, and as early as the 1990s Bockris and Utagawa determined the effect of the nature of transition metal cations on oxygen electrocatalysis [285]. This conclusion was extended to ORR transition metal oxide catalysts in later results when they studied OER on transition metal oxides with chalcogenide structure. In a recent study on the effect of crystal structure [286], the authors reported the order of ORR activity as $\alpha$-$MnO_2$ > amorphous Mn oxides > $\beta$-$MnO_2$ > $\delta$-$MnO_2$, and investigated its relationship with oxygen adsorption strength by a programmed warming desorption method.

Among the transition metal oxides, cobalt- and manganese-based oxides exhibit particularly good ORR activity in alkaline electrolytes. Previously, preparation of nitrogen-doped carbon materials loaded with CoO and $CO_3O_4$ nanoparticles by the

hydrothermal method has been reported, which could synergistically enhance the ORR activity [287,288]. XANES analysis showed that this catalyst formed M-C-N and M-C-O covalent bonds with electron transfer from nitrogen atoms to metal oxides first, enhancing the electrical conductivity of metal oxides and their corresponding electrochemical activity. Zhang [289] published a unique magnesium-modified three-dimensionally ordered mesoporous (3DOM) $Co_3O_4$ electrocatalyst as a cathode material for zinc–air batteries. The coordination with substituted magnesium atoms modulates the electronic structure and bond configuration of the cobalt sites, effectively enhancing the interaction with oxygen species, and thus the ORR/OER activity. The schematic synthesis of this catalyst is shown in Figure 22a, and scanning transmission electron microscopy (STEM) images of the catalyst indicate that the catalyst forms a highly ordered and homogeneous nanostructured framework with regular porosity and an average pore size of about 160 nm (Figure 22b). The corresponding energy dispersive X-ray spectroscopy (EDS) maps of 3DOM $Mg_xCo_{3-x}O_4$ (Figure 22c–f) clearly show the uniform distribution of Co and Mg elements in the catalyst backbone. Transition electron microscopy (TEM) (Figure 22g–i) shows the honeycomb structure and high crystallinity of 3DOM $MgxCo_{3-x}O_4$. Its superior ORR activity can be attributed to the substitution of $Co^{2+}$ with $Mg^{2+}$ to produce an abundant and more catalytically active octahedral site ($Co^{3+}$) in 3DOM-$MgxCo_{3-x}O_4$. The prepared catalysts maintained 99% and 98% of their initial ORR and OER currents, respectively, after 16 h under chrono-current measurement. Zinc–air batteries assembled with 3DOM-$Mg_xCo_{3-x}O_4$ exhibited a high-power density of 253 mW $cm^{-2}$ and a long-term cycling performance of more than 236 h, outperforming commercial noble metal-based catalysts in terms of performance and stability. XPS spectroscopic investigation of 3DOM $Mg_xCo_{3-x}O_4$ confirmed that the material consists of cobalt, magnesium, and O elements. The experimental results show that the area of $Co^{3+}$ in 3DOM $MgxCo_{3-x}O_4$ is much larger than in 3DOM $Co_3O_4$, implying that replacing $Co^{2+}$ with $Mg^{2+}$ at the tetrahedral position generates more $Co^{3+}$ to occupy the octahedral position, enhancing oxygen catalysis. This work provides a simple and promising design strategy for the development of robust bifunctional electrocatalysts for practical applications in zinc–air batteries. In addition, materials such as $NiFe_2O_4$, $CoFe_2O_4$, and $Fe_2O_3$ showed good ORR activity [290–292]. These studies suggest that metal oxides can catalyze ORR effectively.

It is believed that the formation of interfacial Co-O-C and Co-N-C bonds and the accompanying synergistic effects may be responsible for the increased activity of ORR and OER; however, although the ORR/OER performance of transition metal oxides is excellent, their behavior needs further improvement to make them highly economical and stable compared with noble metal catalysts and suitable for commercial applications. More importantly, more and more mesoporous materials have been reported as OER/ORR bifunctional catalysts because of their special structural features of narrow pore size distribution, high specific surface area, and well-ordered mesoporous structure, which meet the requirements of energy-related conversion, catalysis, adsorption, and sensing applications [143,293–295]. In addition, mesoporous electrocatalysts possess a large number of active surface sites, and the mesoporous network contributes to the mass transport of reactants and products in addition to improved catalytic performance [296].

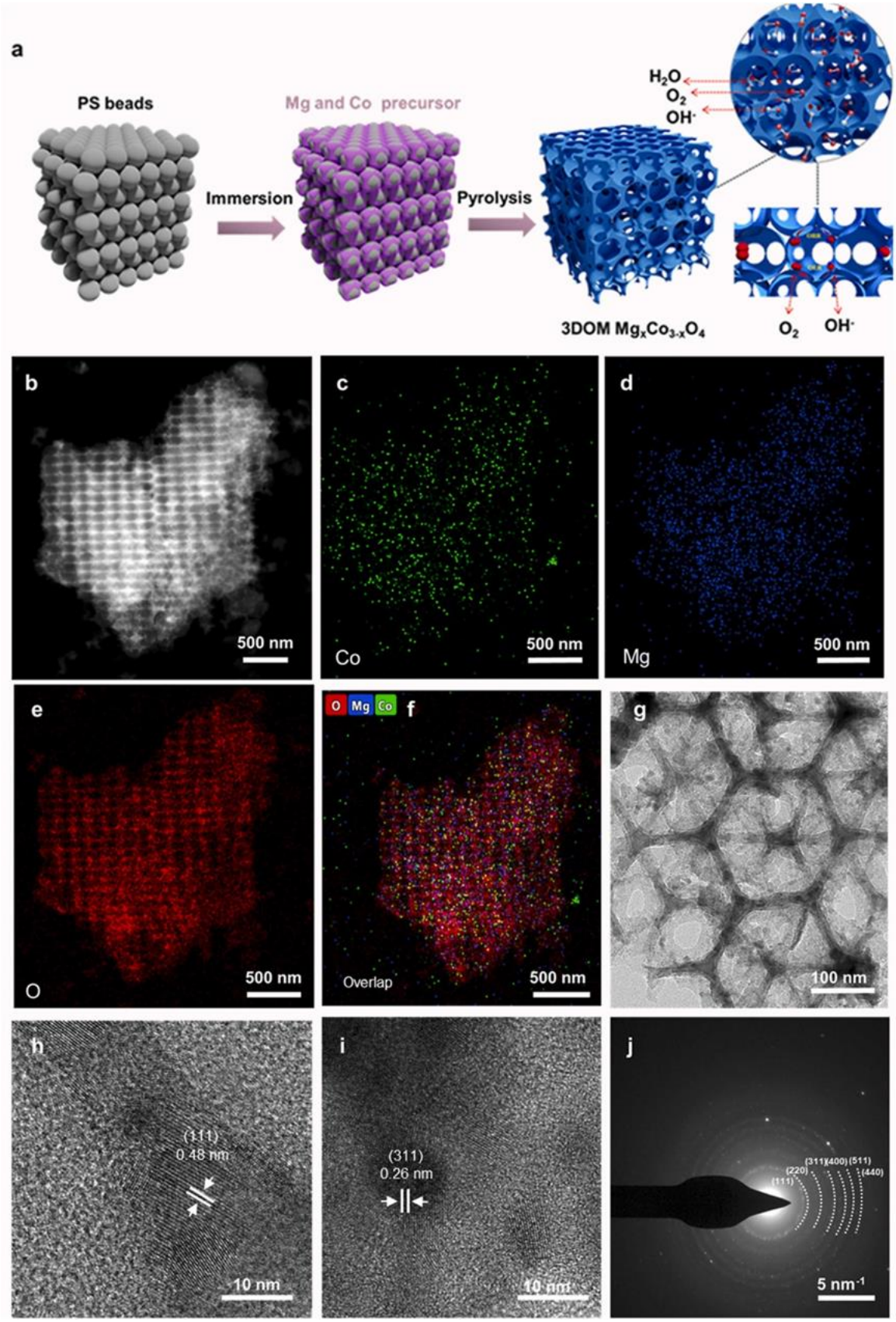


**Figure 22.** (**a**) Schematic illustration of the preparation procedure of 3DOM $Mg_xCo_{3-x}O_4$. (**b**) STEM image, (**c**–**f**) corresponding EDS elemental mapping, (**g**–**i**) TEM and HRTEM images, and (**j**) corresponding SAED pattern of 3DOM $Mg_xCo_{3-x}O_4$. (Reprinted with permission from [289]. Copyright 2022, Elsevier).

Based on this, Mabrook Saleh Amer [297] synthesized highly active bifunctional OER/ORR of cobalt oxide-doped low-symmetry mesoporous titanium oxide ($Co_3O_{4(x)}$/lsm-$TiO_2$) catalysts using a self-assembled surfactant templating method. Physicochemical characterization of the $Co_3O_4$(x)/lsm-$TiO_2$ hybrid by scanning and transmission electron microscopy (Figure 23), X-ray diffraction, $N_2$ adsorption-desorption isotherms, and X-ray photoelectron spectroscopy confirmed the successful incorporation of cobalt oxide nanoparticles (2–3 nm in diameter) and the retention of the highly mesoporous structure of the titanium dioxide substrate. The catalysts exhibit a low-symmetry mesoporous structure, as shown in Figure 23a, and the FESEM images in Figure 23b show the typical surface morphology of mesoporous $Co_3O_4$(3)/hm-$TiO_2$. Figure 23c,d shows representative TEM images of $Co_3O_4$(3)/lsm-$TiO_2$ and $Co_3O_4$(3)/hm-$TiO_2$ catalysts, respectively. Figure 23e shows a high-resolution TEM image of the prepared catalyst, indicating the crystalline nature of the catalyst. The above results indicate that the $Co_3O_4$(3)/hm-$TiO_2$ shows a complex disordered mesoporous structure, and that this morphology is favorable for catalytic ORR behavior. Among these mesoporous hybrids, ~3.0 wt.% of $Co_3O_4$/lsm-$TiO_2$ showed the best performance in oxygen evolution (OER) and reduction (ORR) reactions in alkaline solutions. For ORR, an onset potential of 0.84 V vs. RHE and an OER/ORR overpotential gap (ΔE) of 0.92 V were achieved, which is significantly lower than commercial Pt/C, hexagonal mesoporous, and bulk titanium dioxide analogs. The $Co_3O_4$/lsm-$TiO_2$ hybrid showed significantly higher long-term durability than $IrO_2$. The excellent catalytic performance of the catalyst can be attributed to the synergistic effect between $Co_3O_4$ and $TiO_2$ substrates and the presence of disordered mesopores based on higher charge carrier density and short ion diffusion paths in the electrocatalytic process. The results of this study provide a method for the fabrication of novel $TiO_2$-based bifunctional OER and ORR catalysts modified with non-precious metal oxides for energy production, storage, and conversion technologies. Along with the successive development of excellent ORR catalysts such as composite catalysts ($Fe_3O_4$/$Co_3O_4$-CN) [298], bimetallic ZIFs-derived $Co_3O_4$@NPC@CuO [299], and WCoO-NP [300], this further illustrates the potential of transition metal oxide-based catalysts to replace Pt/C.

On the other hand, the formation of spinel structures by compounding transition metal oxides with different valence states is the focus of transition metal oxide research, for example, the $MnCo_2O_4$ spinel structure, which can be obtained by replacing part of $Co^{3+}$ with $Mn^{3+}$, a catalyst with strong ORR activity [301]. In addition, monodisperse $M_xFe_xO_4$ nanoparticles (M = Mn, Fe, Co, Cu) with crystals smaller than 10 nm have been synthesized by pyrolyzing precursors such as acetylacetonate salts of transition metals [302] using oleylamine-oleic acid as a stabilizer. Even when these nanoparticles were loaded on conventional carbon carriers, they were able to exhibit ORR catalytic activity comparable to that of commercial Pt/C. Other metal oxides, such as $Ta_2O_5$, $NbO_2$, and $TiO_2$, have been shown to possess ORR catalytic activity as well [303–306]. In recent years, chalcogenide oxides have been investigated by many researchers as ORR catalysts in metal–air batteries thanks to their advantages of ionic and electronic conductivity. $ABO_3$ is a class of brass oxides with rare earth elements occupying the A-site and transition metals occupying the B-site, and possesses good ORR catalytic activity [307,308].

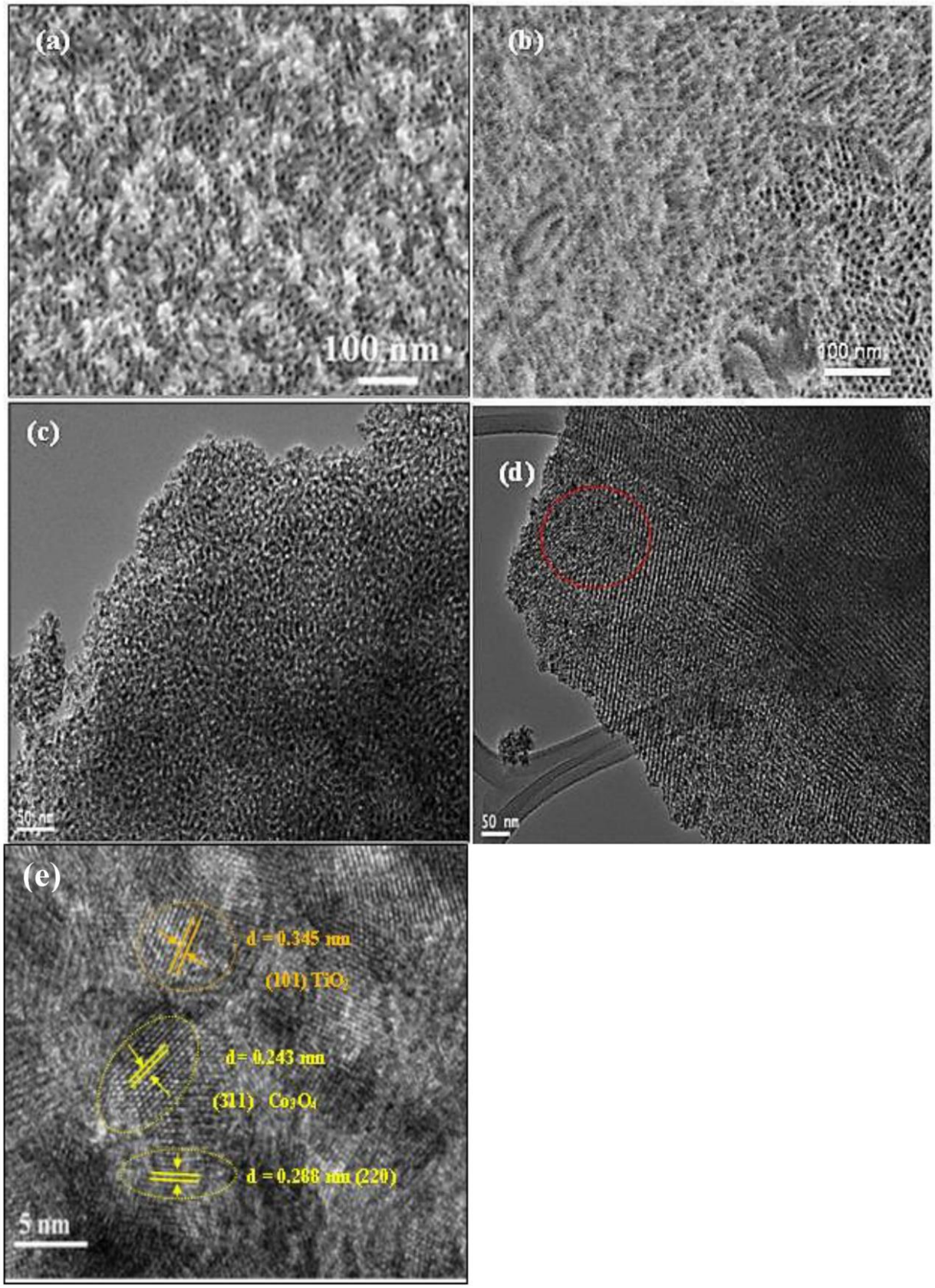


**Figure 23.** SEM images of (**a**) $Co_3O_4$(3)/lsm-$TiO_2$ and (**b**) $Co_3O_4$(3)/hm-$TiO_2$; typical TEM images of (**c**) $Co_3O_4$(3)/lsm-$TiO_2$ and (**d**) $Co_3O_4$(3)/hm-$TiO_2$; and (**e**) high resolution TEM of $Co_3O_4$(3)/hm-$TiO_2$ hybrid. (Reprinted with permission from [297]. Copyright 2019, MDPI).

*6.2. Transition Metal Sulfide Catalysts*

In recent years, a variety of transition metal sulfide compounds M-X (M = Co, Ni, Fe, Ru, or Re, X = S or Se) have been shown to exhibit similar ORR catalytic activity to Pt/C when used as ORR catalytic materials [309,310]. In particular, nanocrystals formed from transition metal sulfide compounds after high-temperature treatment [311] can exhibit excellent ORR catalytic activity in acidic media [312,313]. For example, Gao et al. reported a simple polyol reduction strategy to successfully load $Fe_3O_4$-NP onto surface $CoSe_2$ to obtain $Fe_3O_4$-NP-modified $CoSe_2$ hybrid nanoribbon ORR catalysts, which exhibited better catalytic activity than unmodified $CoSe_2$-DETA nanoribbons and $CoSe_2$ [314].

Among these sulfides, cobalt sulfide has the best ORR catalytic activity in acidic media. Theoretical studies have shown that $Co_9S_8$ exhibits similar catalytic activity to Pt/C in the ORR catalytic process, with both acting through a four-electron transfer pathway. This superior catalytic activity can be attributed to the fact that $S^{2-}$ provides an effective adsorption site for the breakage of the O-O bond. Based on this, Wu et al. developed a $Co_9S_8$-N-C catalyst that exhibited excellent ORR catalytic activity in alkaline media. The high ORR catalytic activity of the $Co_9S_8$-N-C catalyst in 0.1 M NaOH solution was higher than that of commercial Pt/C [315], with strong electrochemical coupling [316]. The above research results illustrate that the catalytic materials of transition metal–sulfur compounds exhibit excellent ORR activity, which greatly broadens the potential types of ORR catalysts.

*6.3. Other Types of Fuel Cell Catalysts*

In addition to the transition metal compound-type ORR catalysts introduced above, there are transition metal nitrides, oxynitrides, transition metal carbides (TMCs), transition metal phosphides, and less common ORR catalyst types such as heteroatom-doped types, rare earth element compound catalysts, etc., which show good catalytic activity. These are described in detail in the following section.

Recently, Vicky et al. reported $Co_2$PNRs for ORR [317], and their experimental results showed a complete four-electron oxygen reduction reaction process. The half-wave potential ($E_{1/2}$) of the $Co_2$PNRs catalyst was 0.196 V, which is very close to the $E_{1/2}$ of the Pt/C catalyst. Moreover, its stability test results showed that after 25,000 s of use of the catalyst, the $Co_2$PNRs maintained 75% of its current density, while the Pt/C maintained only 48%. These results indicate that $Co_2$PNRs have comparable activity to Pt/C for ORR catalytic activity and better stability than Pt/C.

The excellent ORR catalytic activity of transition metal nitrides is due to the good electrical conductivity and chemical resistance of transition metal nitrides (TMN) and oxynitrides. The formation of nitrides facilitates the alteration of the electronic structure of the catalyst, leading to contraction of the d-band of the TMN and increasing the electron density near the Fermi energy level; thus, TMNs have the electronic properties of noble metals and contribute to the transfer of electrons to the oxygen intermediary. The formation of nitride or oxynitride on the transition metal surface can accelerate the kinetics of the ORR. For example, Huang et al. [318] found that $VO_xN_y$-CNTs exhibit good stability and catalytic activity in a KOH medium, with the porous structure of $VO_xN_y$-CNTs facilitating sufficient contact between oxygen and catalyst in the electrolyte and the formation of carbon and nitrogen bonds further improving the overall conductivity and reducing the overpotential. The results of the K-L equation analysis indicate that ORR mainly follows the ideal of the 4e-pathway. Compared with monometallic oxynitrides, bimetallic oxynitrides have better catalytic performance due to the synergistic effect of multiple materials.

Furthermore, although there have been many reports on $Co_2N$, CoP, and heteroatom-doped carbon for electrocatalytic applications, these results have many shortcomings in terms of ORR, and generally require improvements in electrocatalytic activity or stability. In this regard, Zhang et al. [319] reported a layered core–shell ORR catalyst

($Co_2N$/CoP@PNCNTs) which embeds cobalt phosphide and/or cobalt nitride as a core into N, P-doped carbon nanotubes (PNCNTs) as a shell layer via one-step carbonization, nitridation, and phosphorylation of a pyrolytic Co-MOF precursor. Co@C, CoP@PC, $Co_2N$@NCNTs, and $Co_2N$/CoP@PNCNTs were constructed by pyrolysis of Co-MOF precursors using dicyandiamide as the N-doping source and $NaH_2PO_2$ as the P-doping source. Among all the synthesized samples, $Co_2N$/CoP@PNCNTs showed the best electrocatalytic activity and stability for ORR and zinc–air batteries. The excellent catalytic performance and stability of $Co_2N$/CoP@PNCNTs resulted from the synergistic interaction between $Co_2N$/CoP and mesoporous N, P-doped carbon nanotubes. This work provides a new strategy for high-performance ORR electrocatalysis in sustainable energy conversion systems by combining multicomponent cobalt phosphide with heteroatom-doped carbon nanotubes.

In addition, TMCs are susceptible to corrosion in acidic and oxidizing media, which affects their stability as catalysts. Among the transition metal carbides, TiC has attracted a great deal of attention from researchers for its high electrical conductivity and corrosion resistance [320]. Recent studies have shown that N doping improves the ORR performance of TiC, and the introduction of metals (e.g., Fe and Co) in TiC powders further improves the ORR performance [321]. Fe-N/TiC has the highest ORR activity in alkaline media, with a reaction path of 4e-. Dai et al. [322] developed porous core shells with high ORR activity in alkaline and acidic media, and good $Fe_3C$@NCNF-900 electrocatalysts with porous core-shell $Fe_3C$-embedded nitrogen-doped carbon nanofibers exhibited efficient electrocatalytic performance towards ORR in both alkaline and acidic solutions, which was attributed to the synergistic interaction between the $Fe_3C$ and N-doped carbon as the catalytic active site and the protection of $Fe_3C$ from leaching by the carbon shell. This suggests that the doping modification of transition metal carbons may be a future research direction for such electrocatalysts.

The doping of heteroatoms (S, P, N, O) contributes significantly to the enhancement of the electrocatalytic activity of the ORR, where the electronegativity of P (2.19) is lower than that of C (2.55) and N (3.04). Moreover, the addition of P results in an asymmetric spin density, which leads to effective electron modulation and charge redistribution in the system. Because P is highly susceptible to oxidation to P-O, P-O is effective in modulating specific active sites to a certain extent. For this purpose, Sun et al. [323] modified the catalytic activity of single-atom sites by introducing P-O bonds. DFT simulations verified that P-O doping altered the charge density distribution and electronic structure of the Fe active site and improved its catalytic activity towards ORR. The prepared P-O/$FeN_4$-CNS reached a half-wave potential of 0.89 V (vs. RHE) in an alkaline environment (0.1 mol/L KOH), which was better than the P/$FeN_4$-CNS doped with P only ($E_{1/2}$ = 0.87 V vs. RHE) and exceeded the commercial Pt/C catalyst ($E_{1/2}$ = 0.85 V vs. RHE), showing good ORR catalytic activity.

Recently, although many excellent ORR catalyst research results such as Co-CNT/$Ti_3C_2$ [324], Co@TPA-PDI [325], $NGS_4$-900 [326], O-N-CNs [327], and Fe-N-CNFs [15] have been reported, there have been very limited reports on the use of rare earth compounds as modifiers to improve the electrocatalytic performance of carbon-based materials for ORR. Meanwhile, rare earth elements have unique electronic, optical, and chemical properties based on their 4f electrons. Wang [328] developed a $YF_3$-doped nitrogen-containing carbon ($YF_3$@NC) catalytic material and prepared electrocatalysts using m-phenylenediamine as the nitrogen and carbon sources. Yttrium chloride, ammonium fluoride, and L-arginine were used as the Y source, F source, and auxiliary, respectively. The spherical $YF_3$ precursor was obtained by a simple arginine-assisted hydrothermal method, then covered with nitrogen-containing carbon and pyrolyzed at high temperatures to prepare $YF_3$@NC. It had a positive starting potential ($E_{Onset}$ = 0.943 V), half-wave potential ($E_{1/2}$ = 0.836 V), high current density, and good cycling stability (10 h degradation: 13%). When $YF_3$@NC was used as an air-cathode electrode for ZABs, the obtained cell had a high open-circuit potential (1.478 V) and peak power density (75 mW

$cm^{-2}$). This approach makes $YF_3$@NC a promising candidate for future ZAB cathode catalysts. Encouragingly, the half-wave potential of the prepared $YF_3$@NC was comparable to that of commercial Pt/C, with good cycling stability. This type of $YF_3$@NC provides a good reference for the preparation of other advanced and efficient carbon-based cathode catalysts in the future.

In addition, metal oxide clusters are known redox mediators [329], and have been used in processes ranging from (photo)electrochemical decomposition of water reactions [330] to selective organic conversion [331], solar cells [332], and fuel cells [333]. For example, Cang, Ye, and Carsten Streb [334] et al. reported significantly improved performance of commercial Pt/C electrocatalysts for ORR reactions at pH 5.6 in solutions containing polycations $[Fe_{28}(\mu_3\text{-}O)_8(L\text{-}(-)\text{-}tart)_{16}(CH_3COO)_{24}]^{20-}$. The structure of this catalytic material is shown in Figure 24. The results of the reaction mechanism study showed that the iron oxide clusters play a significant effect in improving the ORR. The use of this iron oxide cluster complex for direct formate microfluidic fuel cell (DFMFC) was found to significantly improve performance compared to a control dye cell.

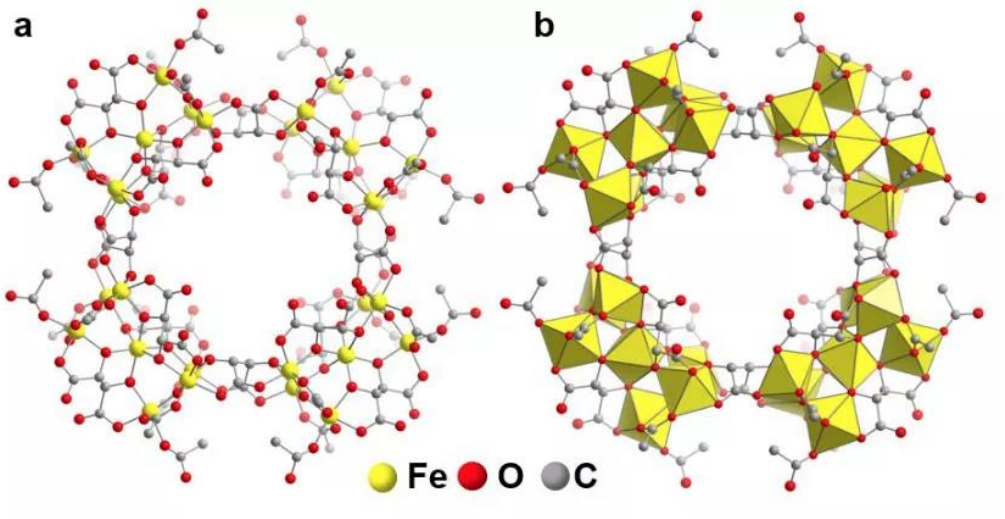


**Figure 24.** (**a**) Ball-and-stick representation of $Fe_{28}$. (**b**) Polyhedral representation of $Fe_{28}$, showing the wheel-like structure assembled from tartrate-linked $Fe_7$ building units. (Reprinted with permission from [334]. Copyright 2022, John Wiley and Sons).

In recent years, good results have been achieved in the study of two-dimensional (2D) materials embedded in non-precious transition metals, which has established a foundation for the development of high-performance electrocatalysts such as OER and ORR [335,336]. TM carbon-based 2D materials exhibit excellent electrocatalytic performance for OER and ORR due to the increased conductivity and electron transfer rate between the reaction center and intermediates [337,338]. For example, Lu [339] reported the synthesis of a new binary material, $MoSi_2N_4$, using first nature theory, and analyzed the effect of TM (tri-D transition metal) embedded in $MoSi_2N_4$ in TM@MSN on the ORR reaction of the system, which has attracted attention for its unique properties and application prospects. The author analyzed the electrochemical stability of TM atoms on the surface of $MoSi_2N_4$. Among the TM sites, Cr@MSN was the most active ORR catalyst, with an overpotential of 0.48 V. The results show that the 3D-TM atoms can play an activating role (as the active center) and activate the carrier, improving its OER/ORR properties. The results show that in $MoSi_2N_4$, all TM atoms could be stably embedded in the defective $MoSi_2N_4$ without being in an aggregated state. It was found that all TM atoms had good electrochemical stability in $MoSi_2N_4$. This work opens a new window of opportunity for the development of novel catalysts that go beyond noble metal-based electrocatalysts for efficient energy conversion and storage and expands the process of ORR catalyst preparation, providing a possible way to replace noble metal catalysts.

Moreover, due to the synergistic effect between ORR effective Fe ($Fe_3O_4$, $Fe_2C$, etc.) and N (pyridine nitrogen, graphite nitrogen) species, and carbon substrates with good conductivity and moderate defects, Fe-based carbon composites are expected to exhibit good activity in ORR, as confirmed by recently reported studies [340–343]. Conventional MOF synthesis methods consume heat and organic solvents, which is not conducive to large-scale synthesis. Therefore, it would be advantageous, though challenging, to develop a more environmentally friendly MOF synthesis method by combining the advantages of physical blending and porosity in the final carbon structure. Based on this, Zhang [344] reported a BM-Fe@NC-120 catalyst to provide a novel green synthesis method for redox reactions. This method involves grinding an organic ligand (1,4-benzene dicarboxylic acid) with a metal salt (hexahydrate) in a trace solvent at room temperature, followed by thermal annealing in an $N_2$ environment. The introduced metal salt acts as a double effect. One type is used as a kind of hard template, which produces a layered porous structure, helping to control the whole reaction mechanism and the kinetics of the reaction process. Another is a metal source, which drives the active centers of $Fe_3O_4$ and $Fe_2C$ and promotes redox. With the combination of porosity and the advantages of MOF, the ORR characteristics of BM-Fe@NC-120 in 0.1 M KOH are good, with a half-wave potential of 0.80 V and an ultimate current density of 5.08 $mAcm^{-2}$. The excellent long-term durability and methanol resistance show that this green process can be promoted for the synthesis of catalysts in future practical fuel cell applications.

In addition, heterostructured catalytic materials exhibit outstanding performance in electrochemical reactions, which is closely related to their beneficial interfacial properties. However, the development of heterostructured catalytic materials with special interfacial properties and charge transfer characteristics remains difficult. Based on this, Liu [345] reported ORR catalytic materials with heterostructured $SrMn_3O_{6-x}$-$SrMnO_3$ ($SMO_x$-SMO) prepared by epitaxial growth and $SrMn_3O_{6-x}$-$Mn_3O_4$ ($SMO_x$-MO) prepared by non-epitaxial synthesis. The experimental results showed that $SMO_x$-SMO exhibits superior ORR performance in alkaline media, with a half-wave potential ($E_{1/2}$) of 0.74 V and an ultimate current density ($J_L$) of 5.46 mA $cm^{-2}$. It was found that the abundant presence of $SrMn_3O_{6-x}$ in $SMO_x$-SMO formed the Mn-O-Mn electron transport channel, which facilitated the electron transport through the $SMO_x$-SMO heterostructure. Density flooding theory calculations indicate that the Mn d-band center of the interfacial phase is close to the Fermi energy level, leading to the formation of high-valence $Mn^{3+}/Mn^{4+}$, which promotes the ORR performance of $SMO_x$-SMO. the generation of OH* is the rate-determining step in the ORR process on $SMO_x$-SMO. The results show that the construction of thermodynamically stable $SMO_x$-SMO heterojunctions promotes the rapid transport of interfacial electrons and reduces the hindrance of strong adsorption intermediates to the reaction, achieving near-ideal adsorption and desorption kinetics. This study provides a new way to develop efficient chalcogenide catalytic materials to replace Pt-based ORR catalysts using the construction of different types of heterojunction interfaces.

### *6.4. Summary and Outlook*

Transition metal catalysts are abundant and economical, and their potential catalytic activity is comparable to that of precious metals. Most transition metal compounds have high potential for ORR catalysis; thus, efforts have been devoted to the development of transition metal catalysts. Although transition metal compound catalysts such as metal oxides, metal sulfides, metal nitrides, metal carbides, metal phosphides, and oxynitride type ORR catalysts are difficult to apply in acidic media, certain transition metal compounds such as TMC are susceptible to corrosion in acidic and oxidizing media, which affects their stability as catalysts. However, studies have shown that they exhibit good performance in alkaline media, and the ORR kinetics in alkaline environments are greatly improved compared to acidic media. The activity of certain transition metal compound catalysts is even comparable to that of Pt-based catalysts, which is achieved

through reasonable structural design. Based on the above-mentioned good conditions of such compounds, it is not enough to apply them only in alkaline conditions. Therefore, in the future, more research needs to be focused on the stability aspects of transition metal compound-like catalysts in acidic media, the optimization of their performance, and other areas of application, such as OER and HER.

In summary, it can be seen that there are many other non-Pt fuel cell ORR catalyst types which have opened up horizons and provided new ways of thinking for subsequent electrocatalytic workers. Different synthesis processes have different characteristics, and electrocatalysts with excellent ORR performance can be synthesized using non-traditional preparation processes. This can inspire future development of new types of catalysts. Regardless of the type of ORR catalysts, all of them are developed with the goal of reducing or replacing precious metals, simplifying preparation processes, improving metal utilization efficiency, and achieving excellent performance, stability, or multifunctional direction. In the context of carbon neutrality, it is particularly important to broaden the preparation process of ORR catalysts for energy saving and emissions reduction.

## 7. Conclusions and Outlook

This article has systematically reviewed the recent research progress on a wide variety of non-Pt-based fuel cell ORR catalysts, including non-Pt-based ORR SACs, non-metallic ORR catalysts, alloy-based ORR catalysts, high-entropy alloy ORR catalysts, and other non-Pt-based fuel cell ORR catalysts. The following conclusions have been obtained. (1) The type, structure, and doping of heteroatoms and doping mode of catalyst carriers play an important role in the performance of catalysts; therefore, it is necessary to expand the type of carriers and suitable doping of non-metallic elements to enhance catalytic performance or even construct bifunctional catalysts. (2) It is necessary to expand the preparation and application of non-Pt catalysts other than transition metals such as Fe, Co and Ni, and to enhance the loading of active metals. (3) The design of high-efficiency ORR catalysts should be based on the combination of ML technology and high-throughput experiments to predict the optimal active sites and active metal combinations of catalysts, in addition to experience. (4) New characterization techniques must be developed, emphasizing the combination of theoretical calculations and experiments, along with more accurate simulation of the catalyst action mechanism through theoretical calculations, based on which cost-saving, high-performance, and high-loading non-Pt ORR catalysts can be designed. (5) In addition to the preparation of highly active and stable non-Pt metal fuel cell catalysts, it is necessary to develop low-cost and large-scale synthesis techniques, which are directly related to the practical application value of the catalysts. Most of the synthesis strategies reported thus far for non-precious metal catalysts are complex and time-consuming. Therefore, developing simple and inexpensive methods for large-scale preparation of electrocatalysts is key to realize their industrial applications. (6) Improving the stability and durability of catalysts is another the main task, for which it is necessary to enhance the interaction between metal and carrier, inhibit the migration and aggregation of metal atoms, and develop new catalysts with high efficiency and stability. (7) The low efficiency of catalyst utilization in general is because ORR usually occurs on the surface of catalysts with active central sites, while most of the catalyst materials are not involved in the reaction. In addition, it is related to the diversity of catalyst surface structure and morphology, which usually lead to the difference of active sites, that is, the real state of active sites is not consistent with the state of catalyst carriers, which in turn leads to the difference of various catalytic products. In order to solve this problem, it is necessary to develop 2D\3D materials and new preparation processes, as these multi-dimensional materials are ideal for supporting the active sites and surface reaction of catalytic materials. In addition, they can effectively prevent the aggregation of transition metal atoms, as evidenced by the many examples cited in the body of this review. (8) Conventional catalysts can cause pollution in the environment,

especially non-metallic ORR catalysts; for this reason, it is important to focus on this issue in future research promoting the development of green, clean, non-polluting, and low-cost catalysts. Although many issues need to be studied in more depth, the successful development of the catalysts described above has made it possible to replace conventional Pt/C catalysts with non-Pt catalyst materials, which is beneficial to the further development of non-Pt fuel cell ORR catalysts.

**Supplementary Materials:** The following supporting information can be downloaded at: https://www.mdpi.com/article/10.3390/pr11020361/s1, Table S1: Data on E1/2 ORR catalysts from the literature.

**Author Contributions:** Q.C., Z.Z. and R.Z. co-wrote the manuscript. M.H., L.S. and Z.Y. reviewed and edited the manuscript. Z.Y. and M.H. acquired the funding. All authors have read and agreed to the published version of the manuscript.

**Funding:** This work was partially supported by the Natural Science Foundation of China (52102256) and Jianghan University Science Research Project (2021-95). The APC is fully waived.

**Conflicts of Interest:** The authors declare no conflict of interest.

## References

1. Kendall, M. Fuel cell development for New Energy Vehicles (NEVs) and clean air in China. *Prog. Nat. Sci. Mater. Int.* **2018**, *28*, 113–120. https://doi.org/10.1016/j.pnsc.2018.03.001.
2. Tian, X.; Lu, X.F.; Xia, B.Y.; Lou, X.W. Advanced Electrocatalysts for the Oxygen Reduction Reaction in Energy Conversion Technologies. *Joule* **2020**, *4*, 45–68. https://doi.org/10.1016/j.joule.2019.12.014.
3. Debe, M.K. Electrocatalyst approaches and challenges for automotive fuel cells. *Nature* **2012**, *486*, 43–51.
4. Banham, D.; Ye, S. Current status and future development of catalyst materials and catalyst layers for proton exchange membrane fuel cells: An industrial perspective. *ACS Energy Lett.* **2017**, *2*, 629–638.
5. You, P.Y.; Kamarudin, S.K. Recent progress of carbonaceous materials in fuel cell applications: An overview. *Chem. Eng. J.* **2017**, *309*, 489–502. https://doi.org/10.1016/j.cej.2016.10.051.
6. Seh, Z.W.; Kibsgaard, J.; Dickens, C.F.; Chorkendorff, I.; Nørskov, J.K.; Jaramillo, T.F. Combining theory and experiment in electrocatalysis: Insights into materials design. *Science* **2017**, *355*, eaad4998.
7. Jiao, Y.; Zheng, Y.; Jaroniec, M.; Qiao, S.Z. Design of electrocatalysts for oxygen- and hydrogen-involving energy conversion reactions. *Chem. Soc. Rev.* **2015**, *44*, 2060–2086. https://doi.org/10.1039/C4CS00470A.
8. Guo, S.; Zhang, S.; Sun, S. Tuning Nanoparticle Catalysis for the Oxygen Reduction Reaction. *Angew. Chem. Int. Ed.* **2013**, *52*, 8526–8544. https://doi.org/10.1002/anie.201207186.
9. Wroblowa, H.S.; Yen Chi, P.; Razumney, G. Electroreduction of oxygen: A new mechanistic criterion. *J. Electroanal. Chem. Interfacial Electrochem.* **1976**, *69*, 195–201. https://doi.org/10.1016/S0022-0728(76)80250-1.
10. Masa, J.; Andronescu, C.; Schuhmann, W. Electrocatalysis as the nexus for sustainable renewable energy: The gordian knot of activity, stability, and selectivity. *Angew. Chem. Int. Ed.* **2020**, *59*, 15298–15312.
11. Gong, M.; Li, Y.; Wang, H.; Liang, Y.; Wu, J.Z.; Zhou, J.; Wang, J.; Regier, T.; Wei, F.; Dai, H. An Advanced Ni–Fe Layered Double Hydroxide Electrocatalyst for Water Oxidation. *J. Am. Chem. Soc.* **2013**, *135*, 8452–8455. https://doi.org/10.1021/ja4027715.
12. Qiao, J.; Liu, Y.; Hong, F.; Zhang, J. A review of catalysts for the electroreduction of carbon dioxide to produce low-carbon fuels. *Chem. Soc. Rev.* **2014**, *43*, 631–675.
13. Shao, M.; Chang, Q.; Dodelet, J.-P.; Chenitz, R. Recent Advances in Electrocatalysts for Oxygen Reduction Reaction. *Chem. Rev.* **2016**, *116*, 3594–3657. https://doi.org/10.1021/acs.chemrev.5b00462.
14. Zhong, K.; Li, M.; Yang, Y.; Zhang, H.; Zhang, B.; Tang, J.; Yan, J.; Su, M.; Yang, Z. Nitrogen-doped biochar derived from watermelon rind as oxygen reduction catalyst in air cathode microbial fuel cells. *Appl. Energy* **2019**, *242*, 516–525. https://doi.org/10.1016/j.apenergy.2019.03.050.
15. Hu, B.-C.; Wu, Z.-Y.; Chu, S.-Q.; Zhu, H.-W.; Liang, H.-W.; Zhang, J.; Yu, S.-H. $SiO_2$-protected shell-mediated templating synthesis of Fe–N-doped carbon nanofibers and their enhanced oxygen reduction reaction performance. *Energy Environ. Sci.* **2018**, *11*, 2208–2215.
16. Sharifi, T.; Gracia-Espino, E.; Chen, A.; Hu, G.; Wågberg, T. Oxygen Reduction Reactions on Single- or Few-Atom Discrete Active Sites for Heterogeneous Catalysis. *Adv. Energy Mater.* **2020**, *10*, 1902084. https://doi.org/10.1002/aenm.201902084.
17. Puthiyapura, V.K.; Brett, D.J.; Russell, A.E.; Lin, W.-F.; Hardacre, C. Biobutanol as Fuel for Direct Alcohol Fuel Cells◎ Investigation of Sn-Modified Pt Catalyst for Butanol Electro-oxidation. *ACS Appl. Mater. Interfaces* **2016**, *8*, 12859–12870.
18. Ma, Z.; Cano, Z.P.; Yu, A.; Chen, Z.; Jiang, G.; Fu, X.; Yang, L.; Wu, T.; Bai, Z.; Lu, J. Enhancing Oxygen Reduction Activity of Pt-based Electrocatalysts: From Theoretical Mechanisms to Practical Methods. *Angew. Chem.* **2020**, *132*, 18490–18504.

19. Kong, F.; Ren, Z.; Norouzi Banis, M.; Du, L.; Zhou, X.; Chen, G.; Zhang, L.; Li, J.; Wang, S.; Li, M.; et al. Active and Stable Pt–Ni Alloy Octahedra Catalyst for Oxygen Reduction via Near-Surface Atomical Engineering. *ACS Catal.* **2020**, *10*, 4205–4214. https://doi.org/10.1021/acscatal.9b05133.
20. Ye, C.-W.; Xu, L. Recent advances in the design of a high-performance metal–nitrogen–carbon catalyst for the oxygen reduction reaction. *J. Mater. Chem.* **2021**, *9*, 22218–22247. https://doi.org/10.1039/d1ta05605k.
21. Bhoyate, S.D.; Kim, J.; de Souza, F.M.; Lin, J.; Lee, E.; Kumar, A.; Gupta, R.K. Science, and engineering for non-noble-metal-based electrocatalysts to boost their ORR performance: A critical review. *Coord. Chem. Rev.* **2023**, *474*, 214854. https://doi.org/10.1016/j.ccr.2022.214854.
22. Niu, W.J.; He, J.Z.; Gu, B.N.; Liu, M.C.; Chueh, Y.L. Opportunities and Challenges in Precise Synthesis of Transition Metal Single-Atom Supported by 2D Materials as Catalysts toward Oxygen Reduction Reaction. *Adv. Funct. Mater.* **2021**, *31*, 2103558. https://doi.org/10.1002/adfm.202103558.
23. Zhang, Z.; Hu, J.; Li, B.; Qi, Q.; Zhang, Y.; Chen, J.; Dong, P.; Zhang, C.; Zhang, Y.; Leung, M.K.H. Recent research progress on high-entropy alloys as electrocatalytic materials. *J. Alloys Compd.* **2022**, *918*, 165585. https://doi.org/10.1016/j.jallcom.2022.165585.
24. Huang, X.; Yang, G.; Li, S.; Wang, H.; Cao, Y.; Peng, F.; Yu, H. Noble-metal-based high-entropy-alloy nanoparticles for electrocatalysis. *J. Energy Chem.* **2022**, *68*, 721–751. https://doi.org/10.1016/j.jechem.2021.12.026.
25. Huo, X.; Yu, H.; Xing, B.; Zuo, X.; Zhang, N. Review of High Entropy Alloys Electrocatalysts for Hydrogen Evolution, Oxygen Evolution, and Oxygen Reduction Reaction. *Chem. Rec.* **2022**, *22*, e202200175. https://doi.org/10.1002/tcr.202200175.
26. Hossen, S.; Hossain, M.K.; Basher, M.K.; Mia, M.N.H.; Rahman, M.T.; Uddin, M.J. Smart nanocarrier-based drug delivery systems for cancer therapy and toxicity studies: A review. *J. Adv. Res* **.2019**, *15*, 1-18. https://doi.org/10.1016/j.jare.2018.06.005.
27. Hossain, M.K.; Rubel, M.; Akbar, M.A.; Ahmed, M.H.; Haque, N.; Rahman, M.F.; Hossain, J.; Hossain, K.M. A review on recent applications and future prospects of rare earth oxides in corrosion and thermal barrier coatings, catalysts, tribological, and environmental sectors. *Ceram. Int*. **2022**, *48*, 32588–32612 . https://doi.org/10.1016/j.ceramint.2022.07.220.
28. Hossain, M.K.; Hasan, S.K.; Hossain, M.I.; Das, R.C.; Bencherif, H.; Rubel, M.; Rahman, M.F.; Emrose, T.; Hashizume, K. A Review of Applications, Prospects, and Challenges of Proton-Conducting Zirconates in Electrochemical Hydrogen Devices. *Nanomaterials* **2022**, *12*, 3581. https://doi.org/10.3390/nano12203581.
29. Afzal, M.J.; Tayyaba, S.; Ashraf, M.W.; Khan, M.; Javaid, F.; Basher, M.K.; Hossain, M.K. A Review on Microchannel Fabrication Methods and Applications in Large-Scale and Prospective Industries. *Evergreen* **2022**, *9*, 764–808.
30. Khan, S.; Hossain, M.K. Classification and properties of nanoparticles. *In Nanoparticle-Based Polymer Composites*; Elsevier: Amsterdam, The Netherlands, 2022; pp. 15–54. https://doi.org/10.1016/B978-0-12-824272-8.00009-9.
31. Jasinski, R. A New Fuel Cell Cathode Catalyst. *Nature* **1964**, *201*, 1212–1213. https://doi.org/10.1038/2011212a0.
32. Gupta, S.; Tryk, D.; Bae, I.; Aldred, W.; Yeager, E. Heat-treated polyacrylonitrile-based catalysts for oxygen electroreduction. *J. Appl. Electrochem.* **1989**, *19*, 19–27. https://doi.org/10.1007/BF01039385.
33. Jahnke, H.; Schönborn, M.; Zimmermann, G. Organic dyestuffs as catalysts for fuel cells. *Phys. Chem. Appl. Dyest.* **1976**, *61*, 133–181.
34. Bagotzky, V.; Tarasevich, M.; Radyushkina, K.; Levina, O.; Andrusyova, S. Electrocatalysis of the oxygen reduction process on metal chelates in acid electrolyte. *J. Power Sources* **1978**, *2*, 233–240.
35. Qiao, B.; Wang, A.; Yang, X.; Allard, L.F.; Jiang, Z.; Cui, Y.; Liu, J.; Li, J.; Zhang, T. Single-atom catalysis of CO oxidation using $Pt_1/FeO_x$. *Nat. Chem.* **2011**, *3*, 634–641. https://doi.org/10.1038/nchem.1095.
36. Zhao, C.X.; Li, B.Q.; Liu, J.N.; Zhang, Q. Intrinsic Electrocatalytic Activity Regulation of M-N-C Single-Atom Catalysts for the Oxygen Reduction Reaction. *Angew Chem. Int. Ed. Engl.* **2021**, *60*, 4448–4463. https://doi.org/10.1002/anie.202003917.
37. Zhao, X.; Yang, X.; Wang, M.; Hwang, S.; Karakalos, S.G.; Chen, M.; Qiao, Z.; Wang, L.; Liu, B.; Ma, Q.; et al. Single-Iron Site Catalysts with Self-Assembled Dual-size Architecture and Hierarchical Porosity for Proton-Exchange Membrane Fuel Cells. *Appl. Catal. B-Environ.* **2020**, *279*, 119400.
38. Yao, Y.; You, Y.; Zhang, G.; Liu, J.; Sun, H.; Zou, Z.; Sun, S. Highly Functional Bioinspired Fe/N/C Oxygen Reduction Reaction Catalysts: Structure-Regulating Oxygen Sorption. *ACS Appl. Mater. Interfaces* **2016**, *8*, 6464–6471. https://doi.org/10.1021/acsami.5b11870.
39. Hanif, S.; Shi, X.; Iqbal, N.; Noor, T.; Anwar, R.; Kannan, A.M. ZIF derived PtNiCo/NC cathode catalyst for proton exchange membrane fuel cell. *Appl. Catal. B: Environ.* **2019**, *258*, 117947. https://doi.org/10.1016/j.apcatb.2019.117947.
40. Kramm, U.I. Non Precious Catalysts for Fuel Cells-A short review on Mößbauer spectroscopy of Fe-NC catalysts for ORR. *ECS Trans.* **2013**, *58*, 119.
41. Martens, I.; Melo, L.G.A.; West, M.M.; Wilkinson, D.P.; Bizzotto, D.; Hitchcock, A.P. Imaging Reactivity of the Pt–Ionomer Interface in Fuel-Cell Catalyst Layers. *ACS Catal.* **2020**, *10*, 8285–8292. https://doi.org/10.1021/acscatal.0c01594.
42. Suryanarayana, C. Mechanical alloying and milling. *Prog. Mater. Sci.* **2001**, *46*, 1–184. https://doi.org/10.1016/S0079-6425(99)00010-9.
43. Mun, Y.; Lee, S.; Kim, K.; Kim, S.; Lee, S.; Han, J.W.; Lee, J. Versatile Strategy for Tuning ORR Activity of a Single Fe-$N_4$ Site by Controlling Electron-Withdrawing/Donating Properties of a Carbon Plane. *J. Am. Chem. Soc.* **2019**, *141*, 6254–6262. https://doi.org/10.1021/jacs.8b13543.
44. He, Y.; Hwang, S.; Cullen, D.A.; Uddin, M.A.; Langhorst, L.; Li, B.; Karakalos, S.; Kropf, A.J.; Wegener, E.C.; Sokolowski, J.; et al. Highly active atomically dispersed $CoN_4$ fuel cell cathode catalysts derived from surfactant-assisted MOFs: Carbon-shell confinement strategy. *Energy Environ. Sci.* **2019**, *12*, 250–260. https://doi.org/10.1039/c8ee02694g.

45. Peng, H.; Liu, F.; Liu, X.; Liao, S.; You, C.; Tian, X.; Nan, H.; Luo, F.; Song, H.; Fu, Z.; et al. Effect of Transition Metals on the Structure and Performance of the Doped Carbon Catalysts Derived From Polyaniline and Melamine for ORR Application. *ACS Catal.* **2014**, *4*, 3797–3805. https://doi.org/10.1021/cs500744x.
46. Fu, X.; Li, N.; Ren, B.; Jiang, G.; Liu, Y.; Hassan, F.M.; Su, D.; Zhu, J.; Yang, L.; Bai, Z.; et al. Tailoring $FeN_4$ Sites with Edge Enrichment for Boosted Oxygen Reduction Performance in Proton Exchange Membrane Fuel Cell. *Adv. Energy Mater.* **2019**, *9*, 1803737. https://doi.org/10.1002/aenm.201803737.
47. Wang, M.; Qian, T.; Liu, S.; Zhou, J.; Yan, C. Unprecedented Activity of Bifunctional Electrocatalyst for High Power Density Aqueous Zinc–Air Batteries. *ACS Appl. Mater. Interfaces* **2017**, *9*, 21216–21224. https://doi.org/10.1021/acsami.7b02346.
48. Wang, J.; Wu, H.; Gao, D.; Miao, S.; Wang, G.; Bao, X. High-density iron nanoparticles encapsulated within nitrogen-doped carbon nanoshell as efficient oxygen electrocatalyst for zinc-air battery. *Nano Energy* **2015**, *13*, 387–396.
49. Zhang, J.; Zhang, M.; Zeng, Y.; Chen, J.; Qiu, L.; Zhou, H.; Sun, C.; Yu, Y.; Zhu, C.; Zhu, Z. Single Fe Atom on Hierarchically Porous S, N-Codoped Nanocarbon Derived from Porphyra Enable Boosted Oxygen Catalysis for Rechargeable Zn-Air Batteries. *Small* **2019**, *15*, e1900307. https://doi.org/10.1002/smll.201900307.
50. Hu, X.; Chen, S.; Chen, L.; Tian, Y.; Yao, S.; Lu, Z.; Zhang, X.; Zhou, Z. What is the Real Origin of the Activity of Fe–N–C Electrocatalysts in the $O_2$ Reduction Reaction? Critical Roles of Coordinating Pyrrolic N and Axially Adsorbing Species. *J. Am. Chem. Soc.* **2022**, *144*, 18144–18152.
51. Xie, X.; Shang, L.; Xiong, X.; Shi, R.; Zhang, T. Fe Single-Atom Catalysts on MOF-5 Derived Carbon for Efficient Oxygen Reduction Reaction in Proton Exchange Membrane Fuel Cells. *Adv. Energy Mater.* **2022**, *12*, 2102688. https://doi.org/10.1002/aenm.202102688.
52. Jiao, L.; Zhang, R.; Wan, G.; Yang, W.; Wan, X.; Zhou, H.; Shui, J.; Yu, S.-H.; Jiang, H.-L. Nanocasting $SiO_2$ into metal–organic frameworks imparts dual protection to high-loading Fe single-atom electrocatalysts. *Nat. Commun.* **2020**, *11*, 2831. https://doi.org/10.1038/s41467-020-16715-6.
53. Lu, F.; Fan, K.; Cui, L.; Li, B.; Yang, Y.; Zong, L.; Wang, L. Engineering FeN4 active sites onto nitrogen-rich carbon with tubular channels for enhanced oxygen reduction reaction performance. *Appl. Catal. B Environ.* **2022**, *313*, 121464. https://doi.org/10.1016/j.apcatb.2022.121464.
54. Gupta, S.; Zhao, S.; Ogoke, O.; Lin, Y.; Xu, H.; Wu, G. Engineering Favorable Morphology and Structure of Fe-N-C Oxygen-Reduction Catalysts through Tuning of Nitrogen/Carbon Precursors. *ChemSusChem* **2017**, *10*, 774–785. https://doi.org/10.1002/cssc.201601397.
55. Fang, X.; Jiao, L.; Yu, S.H.; Jiang, H.L. Metal-Organic Framework-Derived FeCo-N-Doped Hollow Porous Carbon Nanocubes for Electrocatalysis in Acidic and Alkaline Media. *ChemSusChem* **2017**, *10*, 3019–3024. https://doi.org/10.1002/cssc.201700864.
56. Zhang, H.; Hwang, S.; Wang, M.; Feng, Z.; Karakalos, S.; Luo, L.; Qiao, Z.; Xie, X.; Wang, C.; Su, D.; et al. Single Atomic Iron Catalysts for Oxygen Reduction in Acidic Media: Particle Size Control and Thermal Activation. *J. Am. Chem. Soc.* **2017**, *139*, 14143–14149. https://doi.org/10.1021/jacs.7b06514.
57. Zhao, L.; Zhang, Y.; Huang, L.-B.; Liu, X.-Z.; Zhang, Q.-H.; He, C.; Wu, Z.-Y.; Zhang, L.-J.; Wu, J.; Yang, W.; et al. Cascade anchoring strategy for general mass production of high-loading single-atomic metal-nitrogen catalysts. *Nat. Commun.* **2019**, *10*, 1278. https://doi.org/10.1038/s41467-019-09290-y.
58. Ge, X.; Su, G.; Che, W.; Yang, J.; Zhou, X.; Wang, Z.; Qu, Y.; Yao, T.; Liu, W.; Wu, Y. Atomic filtration by graphene oxide membranes to access atomically dispersed single atom catalysts. *ACS Catal.* **2020**, *10*, 10468–10475.
59. Gu, W.; Wu, M.; Xu, J.; Zhao, T. MXene boosted metal-organic framework-derived Fe–N–C as an efficient electrocatalyst for oxygen reduction reactions. *Int. J. Hydrogen Energy* **2022**, *47*, 17224–17232.
60. Li, Z.; Zhuang, Z.; Lv, F.; Zhu, H.; Zhou, L.; Luo, M.; Zhu, J.; Lang, Z.; Feng, S.; Chen, W.; et al. The Marriage of the FeN4 Moiety and MXene Boosts Oxygen Reduction Catalysis: Fe 3d Electron Delocalization Matters. *Adv. Mater.* **2018**, *30*, 1803220. https://doi.org/10.1002/adma.201803220.
61. Yang, L.; Huang, N.; Luo, C.; Yu, H.; Sun, P.; Lv, X.; Sun, X. Atomically dispersed and nanoscaled Co species embedded in micro-/mesoporous carbon nanosheet/nanotube architecture with enhanced oxygen reduction and evolution bifunction for Zn-Air batteries. *Chem. Eng. J.* **2021**, *404*, 127112.
62. Su, C.; Liu, Y.; Luo, Z.; Veder, J.-P.; Zhong, Y.; Shao, Z. Defects-rich porous carbon microspheres as green electrocatalysts for efficient and stable oxygen-reduction reaction over a wide range of pH values. *Chem. Eng. J.* **2021**, *406*, 126883.
63. Zhang, Y.; Wang, P.; Yang, J.; Li, K.; Long, X.; Li, M.; Zhang, K.; Qiu, J. Fabrication of core-shell nanohybrid derived from iron-based metal-organic framework grappled on nitrogen-doped graphene for oxygen reduction reaction. *Chem. Eng. J.* **2020**, *401*, 126001.
64. Gu, W.; Hu, L.; Hong, W.; Jia, X.; Li, J.; Wang, E. Noble-metal-free $Co_3S_4$–S/G porous hybrids as an efficient electrocatalyst for oxygen reduction reaction. *Chem. Sci.* **2016**, *7*, 4167–4173.
65. Liu, Y.; Shen, Y.; Zhu, S.; Li, D. TiN nanoparticles hybridized with Fe, N co-doped carbon nanosheets composites as highly efficient electrocatalyst for oxygen reduction reaction. *Chem. Eng. J.* **2020**, *400*, 125968.
66. Yang, H.; Li, Z.; Kou, S.; Lu, G.; Liu, Z. A complex-sequestered strategy to fabricate Fe single-atom catalyst for efficient oxygen reduction in a broad pH-range. *Appl. Catal. B Environ.* **2020**, *278*, 119270.
67. Li, Z.; Shao, M.; Zhou, L.; Zhang, R.; Zhang, C.; Wei, M.; Evans, D.G.; Duan, X. Directed Growth of Metal-Organic Frameworks and Their Derived Carbon-Based Network for Efficient Electrocatalytic Oxygen Reduction. *Adv. Mater.* **2016**, *28*, 2337–2344. https://doi.org/10.1002/adma.201505086.

68. Lin, L.; Zhu, Q.; Xu, A.-W. Noble-Metal-Free Fe–N/C Catalyst for Highly Efficient Oxygen Reduction Reaction under Both Alkaline and Acidic Conditions. *J. Am. Chem. Soc.* **2014**, *136*, 11027–11033. https://doi.org/10.1021/ja504696r.
69. Jin, H.; Zhao, X.; Liang, L.; Ji, P.; Liu, B.; Hu, C.; He, D.; Mu, S. Sulfate Ions Induced Concave Porous S-N Co-Doped Carbon Confined FeCx Nanoclusters with Fe-$N_4$ Sites for Efficient Oxygen Reduction in Alkaline and Acid Media. *Small* **2021**, *17*, 2101001. https://doi.org/10.1002/smll.202101001.
70. Gao, L.; Xiao, M.; Jin, Z.; Liu, C.; Ge, J.; Xing, W. Hydrogen etching induced hierarchical meso/micro-pore structure with increased active density to boost ORR performance of Fe-NC catalyst. *J. Energy Chem.* **2019**, *35*, 17–23.
71. Qin, F.; Chen, W. Copper-based single-atom alloys for heterogeneous catalysis. *Chem. Commun.* **2021**, *57*, 2710–2723. https://doi.org/10.1039/d1cc00062d.
72. Kang, L.; Wang, B.; Güntner, A.T.; Xu, S.; Wan, X.; Liu, Y.; Marlow, S.; Ren, Y.; Gianolio, D.; Tang, C.C.; et al. The Electrophilicity of Surface Carbon Species in the Redox Reactions of CuO-$CeO_2$ Catalysts. *Angew. Chem. Int. Ed.* **2021**, *60*, 14420–14428. https://doi.org/10.1002/anie.202102570.
73. Jiang, Z.; Sun, W.; Shang, H.; Chen, W.; Sun, T.; Li, H.; Dong, J.; Zhou, J.; Li, Z.; Wang, Y.; et al. Atomic Interface Effect of Single Atom Copper Catalyst for Enhanced Oxygen Reduction Reaction. *Energy Environ. Sci.* **2019**, *12*, 3508–3514. https://doi.org/10.1039/C9EE02974E.
74. Cui, L.; Cui, L.; Li, Z.; Zhang, J.; Wang, H.; Lu, S.; Xiang, Y. A copper single-atom catalyst towards efficient and durable oxygen reduction for fuel cells. *J. Mater. Chem. A* **2019**, *7*, 16690–16695.
75. Qu, Y.; Li, Z.; Chen, W.; Lin, Y.; Yuan, T.; Yang, Z.; Zhao, C.; Wang, J.; Zhao, C.; Wang, X. Direct transformation of bulk copper into copper single sites via emitting and trapping of atoms. *Nat. Catal.* **2018**, *1*, 781–786.
76. Wang, D.; Ao, C.-c.; Liu, X.; Fang, S.-M.; Lin, Y.; Liu, W.; Zhang, W.; Zheng, X.; Zhang, L.; Yao, T. Coordination-Engineered Cu–Nx Single-Site Catalyst for Enhancing Oxygen Reduction Reaction. *ACS Appl. Energy Mater.* **2019**, *2*, 6497–6504.
77. Yang, Y.; Mao, K.; Gao, S.; Huang, H.; Xia, G.; Lin, Z.; Jiang, P.; Wang, C.; Wang, H.; Chen, Q. O-, N-atoms-coordinated Mn cofactors within a graphene framework as bioinspired oxygen reduction reaction electrocatalysts. *Adv. Mater.* **2018**, *30*, 1801732.
78. Xu, Q.; Guo, C.; Tian, S.; Zhang, J.; Chen, W.; Cheong, W.-C.; Gu, L.; Zheng, L.; Xiao, J.; Liu, Q.; et al. Coordination structure dominated performance of single-atomic Pt catalyst for anti-Markovnikov hydroboration of alkenes. *Sci. China Mater.* **2020**, *63*, 972–981. https://doi.org/10.1007/s40843-020-1334-6.
79. Shang, H.; Zhou, X.; Dong, J.; Li, A.; Zhao, X.; Liu, Q.; Lin, Y.; Pei, J.; Li, Z.; Jiang, Z.; et al. Engineering unsymmetrically coordinated Cu-S(1)N(3) single atom sites with enhanced oxygen reduction activity. *Nat. Commun.* **2020**, *11*, 3049. https://doi.org/10.1038/s41467-020-16848-8.
80. Li, J.; Chen, M.; Cullen, D.A.; Hwang, S.; Wang, M.; Li, B.; Liu, K.; Karakalos, S.; Lucero, M.; Zhang, H.; et al. Atomically dispersed manganese catalysts for oxygen reduction in proton-exchange membrane fuel cells. *Nat. Catal.* **2018**, *1*, 935–945. https://doi.org/10.1038/s41929-018-0164-8.
81. Gupta, S.; Zhao, S.; Wang, X.X.; Hwang, S.; Karakalos, S.; Devaguptapu, S.V.; Mukherjee, S.; Su, D.; Xu, H.; Wu, G. Quaternary FeCoNiMn-Based Nanocarbon Electrocatalysts for Bifunctional Oxygen Reduction and Evolution: Promotional Role of Mn Doping in Stabilizing Carbon. *ACS Catal.* **2017**, *7*, 8386–8393. https://doi.org/10.1021/acscatal.7b02949.
82. Zhong, Y.; Liang, X.; He, Z.; Tan, W.; Zhu, J.; Yuan, P.; Zhu, R.; He, H. The constraints of transition metal substitutions (Ti, Cr, Mn, Co and Ni) in magnetite on its catalytic activity in heterogeneous Fenton and UV/Fenton reaction: From the perspective of hydroxyl radical generation. *Appl. Catal. B-Environ.* **2014**, *150*, 612–618.
83. Bai, L.; Duan, Z.; Wen, X.; Si, R.; Guan, J. Atomically dispersed manganese-based catalysts for efficient catalysis of oxygen reduction reaction. *Appl. Catal. B: Environ.* **2019**, *257*, 117930.
84. Zhu, X.; Amal, R.; Lu, X. N,P Co-Coordinated Manganese Atoms in Mesoporous Carbon for Electrochemical Oxygen Reduction. *Small* **2019**, *15*, 1804524. https://doi.org/10.1002/smll.201804524.
85. Wang, J.; Li, H.; Liu, S.; Hu, Y.; Zhang, J.; Xia, M.; Hou, Y.; Tse, J.; Zhang, J.; Zhao, Y. Turning on Zn 4s electrons in a $N_2$-Zn-$B_2$ configuration to stimulate remarkable ORR performance. *Angew. Chem.* **2021**, *133*, 183–187. https://doi.org/10.1002/ange.202009991.
86. Li, J.; Chen, S.; Yang, N.; Deng, M.; Ibraheem, S.; Deng, J.; Li, J.; Li, L.; Wei, Z. Ultrahigh-Loading Zinc Single-Atom Catalyst for Highly Efficient Oxygen Reduction in Both Acidic and Alkaline Media. *Angew. Chem. Int. Ed.* **2019**, *58*, 7035–7039. https://doi.org/10.1002/anie.201902109.
87. Song, P.; Luo, M.; Liu, X.; Xing, W.; Xu, W.; Jiang, Z.; Gu, L. Zn Single Atom Catalyst for Highly Efficient Oxygen Reduction Reaction. *Adv. Funct. Mater.* **2017**, *27*, 1700802. https://doi.org/10.1002/adfm.201700802.
88. Chen, M.; He, Y.; Spendelow, J.S.; Wu, G. Atomically Dispersed Metal Catalysts for Oxygen Reduction. *ACS Energy Lett.* **2019**, *4*, 1619–1633. https://doi.org/10.1021/acsenergylett.9b00804.
89. Olson, T.S.; Pylypenko, S.; Fulghum, J.E.; Atanassov, P. Bifunctional Oxygen Reduction Reaction Mechanism on Non-Platinum Catalysts Derived from Pyrolyzed Porphyrins. *J. Electrochem. Soc.* **2010**, *157*, B54. https://doi.org/10.1149/1.3248003.
90. Liu, K.; Qiao, Z.; Hwang, S.; Liu, Z.; Zhang, H.; Su, D.; Xu, H.; Wu, G.; Wang, G. Mn- and N- doped carbon as promising catalysts for oxygen reduction reaction: Theoretical prediction and experimental validation. *Appl. Catal. B: Environ.* **2019**, *243*, 195–203. https://doi.org/10.1016/j.apcatb.2018.10.034.
91. Wang, X.X.; Cullen, D.A.; Pan, Y.-T.; Hwang, S.; Wang, M.; Feng, Z.; Wang, J.; Engelhard, M.H.; Zhang, H.; He, Y.; et al. Nitrogen-Coordinated Single Cobalt Atom Catalysts for Oxygen Reduction in Proton Exchange Membrane Fuel Cells. *Adv. Mater.* **2018**, *30*, 1706758. https://doi.org/10.1002/adma.201706758.

92. Wang, A.L.; Sun, Y.; Liang, Z.X.; Chen, S.L. Particle Size Effects of Pt Nanocatalyst in the Catalyst Layer of Proton Exchange Membrane Fuel Cell. *Acta Chim. Sin.* **2009**, *67*, 2554–2558.
93. Chen, Z.; Gong, W.; Liu, Z.; Cong, S.; Zheng, Z.; Wang, Z.; Zhang, W.; Ma, J.; Yu, H.; Li, G.; et al. Coordination-controlled single-atom tungsten as a non-3d-metal oxygen reduction reaction electrocatalyst with ultrahigh mass activity. *Nano Energy* **2019**, *60*, 394–403. https://doi.org/10.1016/j.nanoen.2019.03.045.
94. Luo, E.; Zhang, H.; Wang, X.; Gao, L.; Gong, L.; Zhao, T.; Jin, Z.; Ge, J.; Jiang, Z.; Liu, C.; et al. Single-Atom Cr-N(4) Sites Designed for Durable Oxygen Reduction Catalysis in Acid Media. *Angew Chem. Int. Ed. Engl.* **2019**, *58*, 12469–12475. https://doi.org/10.1002/anie.201906289.
95. Calle-Vallejo, F.; Martínez, J.I.; Rossmeisl, J. Density functional studies of functionalized graphitic materials with late transition metals for Oxygen Reduction Reactions. *Phys. Chem. Chem. Phys.* **2011**, *13*, 15639–15643. https://doi.org/10.1039/c1cp21228a.
96. Liu, S.; Li, Z.; Wang, C.; Tao, W.; Huang, M.; Zuo, M.; Yang, Y.; Yang, K.; Zhang, L.; Chen, S.; et al. Turning main-group element magnesium into a highly active electrocatalyst for oxygen reduction reaction. *Nat. Commun.* **2020**, *11*, 938. https://doi.org/10.1038/s41467-020-14565-w.
97. Wang, Y.; Wang, D.; Li, Y. Rational Design of Single-Atom Site Electrocatalysts: From Theoretical Understandings to Practical Applications. *Adv. Mater.* **2021**, *33*, 2008151. https://doi.org/10.1002/adma.202008151.
98. Jiang, R.; Li, L.; Sheng, T.; Hu, G.; Chen, Y.; Wang, L. Edge-Site Engineering of Atomically Dispersed Fe–$N_4$ by Selective C–N Bond Cleavage for Enhanced Oxygen Reduction Reaction Activities. *J. Am. Chem. Soc.* **2018**, *140*, 11594–11598. https://doi.org/10.1021/jacs.8b07294.
99. Zhang, J.; Zhao, Y.; Chen, C.; Huang, Y.-C.; Dong, C.-L.; Chen, C.-J.; Liu, R.-S.; Wang, C.; Yan, K.; Li, Y.; et al. Tuning the Coordination Environment in Single-Atom Catalysts to Achieve Highly Efficient Oxygen Reduction Reactions. *J. Am. Chem. Soc.* **2019**, *141*, 20118–20126. https://doi.org/10.1021/jacs.9b09352.
100. Duraisamy, V.; Senthil Kumar, S.M. N and P dual heteroatom doped mesoporous hollow carbon as an efficient oxygen reduction reaction catalyst in alkaline electrolyte. *Int. J. Hydrogen Energy* **2022**, *47*, 17992–18006. https://doi.org/10.1016/j.ijhydene.2022.03.284**.**
101. Yuan, K.; Lützenkirchen-Hecht, D.; Li, L.; Shuai, L.; Li, Y.; Cao, R.; Qiu, M.; Zhuang, X.; Leung, M.K.H.; Chen, Y.; et al. Boosting Oxygen Reduction of Single Iron Active Sites via Geometric and Electronic Engineering: Nitrogen and Phosphorus Dual Coordination. *J. Am. Chem. Soc.* **2020**, *142*, 2404–2412. https://doi.org/10.1021/jacs.9b11852.
102. Han, A.; Wang, X.; Tang, K.; Zhang, Z.; Ye, C.; Kong, K.; Hu, H.; Zheng, L.; Jiang, P.; Zhao, C.; et al. An Adjacent Atomic Platinum Site Enables Single-Atom Iron with High Oxygen Reduction Reaction Performance. *Angew. Chem. Int. Ed.* **2021**, *60*, 19262–19271. https://doi.org/10.1002/anie.202105186.
103. Jiao, L.; Wan, G.; Zhang, R.; Zhou, H.; Yu, S.-H.; Jiang, H.-L. From Metal–Organic Frameworks to Single-Atom Fe Implanted N-doped Porous Carbons: Efficient Oxygen Reduction in Both Alkaline and Acidic Media. *Angew. Chem. Int. Ed.* **2018**, *57*, 8525–8529. https://doi.org/10.1002/anie.201803262.
104. Wang, X.; An, Y.; Liu, L.; Fang, L.; Liu, Y.; Zhang, J.; Qi, H.; Heine, T.; Li, T.; Kuc, A.; et al. Atomically Dispersed Pentacoordinated-Zirconium Catalyst with Axial Oxygen Ligand for Oxygen Reduction Reaction. *Angew. Chem. Int. Ed.* **2022**, *61*, e202209746. https://doi.org/10.1002/anie.202209746.
105. Yang, H.; Wang, X.; Zheng, T.; Cuello, N.C.; Goenaga, G.; Zawodzinski, T.A.; Tian, H.; Wright, J.T.; Meulenberg, R.W.; Wang, X. CrN-Encapsulated hollow Cr-NC capsules boosting oxygen reduction catalysis in PEMFC. *CCS Chem.* **2021**, *3*, 208–218. https://doi.org/10.31635/ccschem.020.202000645.
106. Wang, G.; Deng, Y.; Yu, J.; Zheng, L.; Du, L.; Song, H.; Liao, S. From Chlorella to Nestlike Framework Constructed with Doped Carbon Nanotubes: A Biomass-Derived, High-Performance, Bifunctional Oxygen Reduction/Evolution Catalyst. *ACS Appl. Mater. Interfaces* **2017**, *9*, 32168–32178. https://doi.org/10.1021/acsami.7b10668.
107. Wei, Y.-S.; Sun, L.; Wang, M.; Hong, J.; Zou, L.; Liu, H.; Wang, Y.; Zhang, M.; Liu, Z.; Li, Y.; et al. Fabricating Dual-Atom Iron Catalysts for Efficient Oxygen Evolution Reaction: A Heteroatom Modulator Approach. *Angew. Chem. Int. Ed.* **2020**, *59*, 16013–16022. https://doi.org/10.1002/anie.202007221.
108. Xu, J.; Lai, S.; Qi, D.; Hu, M.; Peng, X.; Liu, Y.; Liu, W.; Hu, G.; Xu, H.; Li, F.; et al. Atomic Fe-Zn dual-metal sites for high-efficiency pH-universal oxygen reduction catalysis. *Nano Res.* **2021**, *14*, 1374–1381. https://doi.org/10.1007/s12274-020-3186-x.
109. Zhang, W.; Chao, Y.; Zhang, W.; Zhou, J.; Lv, F.; Wang, K.; Lin, F.; Luo, H.; Li, J.; Tong, M.; et al. Emerging Dual-Atomic-Site Catalysts for Efficient Energy Catalysis. *Adv. Mater.* **2021**, *33*, 2102576. https://doi.org/10.1002/adma.202102576.
110. Yu, D.; Ma, Y.; Hu, F.; Lin, C.-C.; Li, L.; Chen, H.-Y.; Han, X.; Peng, S. Dual-Sites Coordination Engineering of Single Atom Catalysts for Flexible Metal–Air Batteries. *Adv. Energy Mater.* **2021**, *11*, 2101242. https://doi.org/10.1002/aenm.202101242.
111. Zhong, X.; Ye, S.; Tang, J.; Zhu, Y.; Wu, D.; Gu, M.; Pan, H.; Xu, B. Engineering Pt and Fe dual-metal single atoms anchored on nitrogen-doped carbon with high activity and durability towards oxygen reduction reaction for zinc-air battery. *Appl. Catal. B: Environ.* **2021**, *286*, 119891. https://doi.org/10.1016/j.apcatb.2021.119891.
112. Zhang, J.; Huang, Q.-A.; Wang, J.; Wang, J.; Zhang, J.; Zhao, Y. Supported dual-atom catalysts: Preparation, characterization, and potential applications. *Chin. J. Catal.* **2020**, *41*, 783–798. https://doi.org/10.1016/S1872-2067(20)63536-7.
113. Cao, L.; Shao, Y.; Pan, H.; Lu, Z. Designing Efficient Dual-Metal Single-Atom Electrocatalyst TMZnN6 (TM = Mn, Fe, Co, Ni, Cu, Zn) for Oxygen Reduction Reaction. *J. Phys. Chem. C* **2020**, *124*, 11301–11307. https://doi.org/10.1021/acs.jpcc.0c01045.

114. Sun, H.; Wang, M.; Zhang, S.; Liu, S.; Shen, X.; Qian, T.; Niu, X.; Xiong, J.; Yan, C. Boosting Oxygen Dissociation over Bimetal Sites to Facilitate Oxygen Reduction Activity of Zinc-Air Battery. *Adv. Funct. Mater.* **2021**, *31*, 2006533. https://doi.org/10.1002/adfm.202006533.
115. Chen, H.Q.; Ze, H.; Yue, M.F.; Wei, D.Y.; Wu, Y.F.; Dong, J.C.; Zhang, Y.J.; Zhang, H.; Tian, Z.Q.; Li, J.F.; et al. Unmasking the Critical Role of the Ordering Degree of Bimetallic Nanocatalysts on Oxygen Reduction Reaction by In Situ Raman Spectroscopy. *Angew Chem. Int. Ed. Engl.* **2022**, *61*, e202117834. https://doi.org/10.1002/anie.202117834.
116. Shu, C.; Chen, Y.; Yang, X.-D.; Liu, Y.; Chong, S.; Fang, Y.; Liu, Y.; Yang, W.-H. Enhanced Fe dispersion via "pinning" effect of thiocyanate ion on ferric ion in Fe-NS-doped catalyst as an excellent oxygen reduction reaction electrode. *J. Power Sources* **2018**, *376*, 161–167.
117. Zhang, D.; Chen, W.; Li, Z.; Chen, Y.; Zheng, L.; Gong, Y.; Li, Q.; Shen, R.; Han, Y.; Cheong, W.-C. Isolated Fe and Co dual active sites on nitrogen-doped carbon for a highly efficient oxygen reduction reaction. *Chem. Commun.* **2018**, *54*, 4274–4277.
118. Yan, Z.; Zhang, Y.; Jiang, Z.; Jiang, D.; Wei, W.; Hu, Z. Nitrogen-Doped Bimetallic Carbide-Graphite Composite as Highly Active and Extremely Stable Electrocatalyst for Oxygen Reduction Reaction in Alkaline Media. *Adv. Funct. Mater.* **2022**, *32*, 2204031. https://doi.org/10.1002/adfm.202204031.
119. Wang, B.; Zou, J.; Shen, X.; Yang, Y.; Hu, G.; Li, W.; Peng, Z.; Banham, D.; Dong, A.; Zhao, D. Nanocrystal super crystal-derived atomically dispersed Mn-Fe catalysts with enhanced oxygen reduction activity. *Nano Energy* **2019**, *63*, 103851. https://doi.org/10.1016/j.nanoen.2019.06.047.
120. Lin, L.; Yang, Z.K.; Jiang, Y.-F.; Xu, A.-W. Nonprecious Bimetallic (Fe,Mo)–N/C Catalyst for Efficient Oxygen Reduction Reaction. *ACS Catal.* **2016**, *6*, 4449–4454. https://doi.org/10.1021/acscatal.6b00535.
121. Jiao, P.; Ye, D.; Zhu, C.; Wu, S.; Qin, C.; An, C.; Hu, N.; Deng, Q. Non-precious transition metal single-atom catalysts for the oxygen reduction reaction: Progress and prospects. *Nanoscale* **2022**, *14*, 14322–14340. https://doi.org/10.1039/D2NR03687H.
122. Chen, G.; Liu, P.; Liao, Z.; Sun, F.; He, Y.; Zhong, H.; Zhang, T.; Zschech, E.; Chen, M.; Wu, G.; et al. Zinc-Mediated Template Synthesis of Fe-N-C Electrocatalysts with Densely Accessible Fe-Nx Active Sites for Efficient Oxygen Reduction. *Adv. Mater.* **2020**, *32*, 1907399. https://doi.org/10.1002/adma.201907399.
123. Zhao, D.; Wang, P.; Di, H.; Zhang, P.; Hui, X.; Yin, L. Single Semi-Metallic Selenium Atoms on $Ti_3C_2$ MXene Nanosheets as Excellent Cathode for Lithium–Oxygen Batteries. *Adv. Funct. Mater.* **2021**, *31*, 2010544. https://doi.org/10.1002/adfm.202010544.
124. Chen, Z.; Su, X.; Ding, J.; Yang, N.; Zuo, W.; He, Q.; Wei, Z.; Zhang, Q.; Huang, J.; Zhai, Y. Boosting oxygen reduction reaction with Fe and Se dual-atom sites supported by nitrogen-doped porous carbon. *Appl. Catal. B: Environ.* **2022**, *308*, 121206. https://doi.org/10.1016/j.apcatb.2022.121206.
125. Wang, J.; Huang, Z.; Liu, W.; Chang, C.; Tang, H.; Li, Z.; Chen, W.; Jia, C.; Yao, T.; Wei, S.; et al. Design of N-Coordinated Dual-Metal Sites: A Stable and Active Pt-Free Catalyst for Acidic Oxygen Reduction Reaction. *J. Am. Chem. Soc.* **2017**, *139*, 17281–17284. https://doi.org/10.1021/jacs.7b10385.
126. Chen, Z.; Liao, X.; Sun, C.; Zhao, K.; Ye, D.; Li, J.; Wu, G.; Fang, J.; Zhao, H.; Zhang, J. Enhanced performance of atomically dispersed dual-site Fe-Mn electrocatalysts through cascade reaction mechanism. *Appl. Catal. B Environ.* **2021**, *288*, 120021. https://doi.org/10.1016/j.apcatb.2021.120021.
127. Kong, F.; Si, R.; Chen, N.; Wang, Q.; Li, J.; Yin, G.; Gu, M.; Wang, J.; Liu, L.-M.; Sun, X. Origin of hetero-nuclear Au-Co dual atoms for efficient acidic oxygen reduction. *Appl. Catal. B: Environ.* **2022**, *301*, 120782.
128. Yue, L.; Chen, L.; Wang, X.; Lu, D.; Zhou, W.; Shen, D.; Yang, Q.; Xiao, S.; Li, Y. Ni/Co-MOF@ aminated MXene hierarchical electrodes for high-stability supercapacitors. *Chem. Eng. J.* **2023,** *451*, 138687. https://doi.org/10.1016/j.cej.2022.138687.
129. Yang, L.; Zeng, X.; Wang, W.; Cao, D. Recent Progress in MOF-Derived, Heteroatom-Doped Porous Carbons as Highly Efficient Electrocatalysts for Oxygen Reduction Reaction in Fuel Cells. *Adv. Funct. Mater.* **2018**, *28*, 1704537. https://doi.org/10.1002/adfm.201704537.
130. Xue, Y.; Guo, Y.; Zhang, Q.; Xie, Z.; Wei, J.; Zhou, Z. MOF-Derived Co and Fe Species Loaded on N-Doped Carbon Networks as Efficient Oxygen Electrocatalysts for Zn-Air Batteries. *Nano-Micro. Lett.* **2022**, *14*, 162. https://doi.org/10.1007/s40820-022-00890-w.
131. Ahsan, M.A.; Puente Santiago, A.R.; Hong, Y.; Zhang, N.; Cano, M.; Rodriguez-Castellon, E.; Echegoyen, L.; Sreenivasan, S.T.; Noveron, J.C. Tuning of trifunctional NiCu bimetallic nanoparticles confined in a porous carbon network with surface composition and local structural distortions for the electrocatalytic oxygen reduction, oxygen and hydrogen evolution reactions. *J. Am. Chem. Soc.* **2020**, *142*, 14688–14701.
132. Wei, C.; Sun, Y.; Scherer, G.G.; Fisher, A.C.; Sherburne, M.; Ager, J.W.; Xu, Z.J. Surface Composition Dependent Ligand Effect in Tuning the Activity of Nickel-Copper Bimetallic Electrocatalysts toward Hydrogen Evolution in Alkaline. *J. Am. Chem. Soc.* **2020**, *142*, 7765–7775. https://doi.org/10.1021/jacs.9b12005.
133. Deng, J.; Ren, P.; Deng, D.; Bao, X. Enhanced electron penetration through an ultrathin graphene layer for highly efficient catalysis of the hydrogen evolution reaction. *Angew Chem. Int. Ed. Engl.* **2015**, *54*, 2100–2104. https://doi.org/10.1002/anie.201409524.
134. Su, C.-Y.; Cheng, H.; Li, W.; Liu, Z.-Q.; Li, N.; Hou, Z.; Bai, F.-Q.; Zhang, H.-X.; Ma, T.-Y. Atomic Modulation of FeCo–Nitrogen–Carbon Bifunctional Oxygen Electrodes for Rechargeable and Flexible All-Solid-State Zinc–Air Battery. *Adv. Energy Mater.* **2017**, *7*, 1602420. https://doi.org/10.1002/aenm.201602420.

135. Hao, X.; Jiang, Z.; Zhang, B.; Tian, X.; Song, C.; Wang, L.; Maiyalagan, T.; Hao, X.; Jiang, Z.J. N-Doped Carbon Nanotubes Derived from Graphene Oxide with Embedment of FeCo Nanoparticles as Bifunctional Air Electrode for Rechargeable Liquid and Flexible All-Solid-State Zinc–Air Batteries. *Adv. Sci.* **2021**, *8*, 2004572.
136. Wang, Z.; Jin, X.; Zhu, C.; Liu, Y.; Tan, H.; Ku, R.; Zhang, Y.; Zhou, L.; Liu, Z.; Hwang, S.-J.; et al. Atomically Dispersed $Co_2$–$N_6$ and Fe–$N_4$ Costructures Boost Oxygen Reduction Reaction in Both Alkaline and Acidic Media. *Adv. Mater.* **2021**, *33*, 2104718. https://doi.org/10.1002/adma.202104718.
137. Xiao, M.; Chen, Y.; Zhu, J.; Zhang, H.; Zhao, X.; Gao, L.; Wang, X.; Zhao, J.; Ge, J.; Jiang, Z.; et al. Climbing the Apex of the ORR Volcano Plot via Binuclear Site Construction: Electronic and Geometric Engineering. *J. Am. Chem. Soc.* **2019**, *141*, 17763–17770. https://doi.org/10.1021/jacs.9b08362.
138. Guo, X.; Gu, J.; Lin, S.; Zhang, S.-L.; Chen, Z.; Huang, S. Tackling the Activity and Selectivity Challenges of Electrocatalysts towards Nitrogen Reduction Reaction via Atomically Dispersed Bi-Atom Catalysts. *J. Am. Chem. Soc.* **2020**, *142*, 5709–5721.
139. Hunter, M.A.; Fischer, J.M.T.A.; Yuan, Q.; Hankel, M.; Searles, D.J. Evaluating the Catalytic Efficiency of Paired, Single-Atom Catalysts for the Oxygen Reduction Reaction. *ACS Catal.* **2019**, *9*, 7660–7667.
140. Sa, Y.J.; Joo, S.H. Dimeric Fe Sites Effectively Activate Oxygen Molecule. *Chemistry* **2019**, *5*, 3006–3007. https://doi.org/10.1016/j.chempr.2019.11.005.
141. Ouyang, Y.; Shi, L.; Bai, X.; Li, Q.; Wang, J. Breaking scaling relations for efficient CO<sub>2</sub> electrochemical reduction through dual-atom catalysts. *Chem. Sci.* **2020**, *11*, 1807–1813.
142. Chen, Z.W.; Chen, L.X.; Yang, C.C.; Jiang, Q. Atomic (single, double, and triple atoms) catalysis: Frontiers, opportunities, and challenges. *J. Mater. Chem. A.* **201**9, 7: 3492-3515.
143. Huang, Z.-F.; Wang, J.; Peng, Y.; Jung, C.-Y.; Fisher, A.; Wang, X. Design of Efficient Bifunctional Oxygen Reduction/Evolution Electrocatalyst: Recent Advances and Perspectives. *Adv. Energy Mater.* **2017**, *7*, 1700544. https://doi.org/10.1002/aenm.201700544.
144. Liu, J.; Jiao, M.; Mei, B.; Tong, Y.; Li, Y.; Ruan, M.; Song, P.; Sun, G.; Jiang, L.; Wang, Y.; et al. Carbon-Supported Divacancy-Anchored Platinum Single-Atom Electrocatalysts with Superhigh Pt Utilization for the Oxygen Reduction Reaction. *Angew. Chem.* **2019**, *58*, 1163–1167.
145. Zhang, C.; Sha, J.; Fei, H.; Liu, M.; Yazdi, S.; Zhang, J.; Zhong, Q.; Zou, X.; Zhao, N.; Yu, H.; et al. Single-Atomic Ruthenium Catalytic Sites on Nitrogen-Doped Graphene for Oxygen Reduction Reaction in Acidic Medium. *ACS Nano* **2017**, *11*, 6930–6941.
146. Xiao, M.; Gao, L.; Wang, Y.; Wang, X.; Zhu, J.; Jin, Z.; Liu, C.; Chen, H.; Li, G.; Ge, J.; et al. Engineering Energy Level of Metal Center: Ru Single-Atom Site for Efficient and Durable Oxygen Reduction Catalysis. *J. Am. Chem. Soc.* **2019**, *141*, 19800–19806. https://doi.org/10.1021/jacs.9b09234.
147. Liu, Q.; Li, Y.; Zheng, L.; Shang, J.; Liu, X.; Yu, R.; Shui, J. Sequential Synthesis and Active-Site Coordination Principle of Precious Metal Single-Atom Catalysts for Oxygen Reduction Reaction and PEM Fuel Cells. *Adv. Energy Mater.* **2020**, *10*, 2000689. https://doi.org/10.1002/aenm.202000689.
148. Sa, Y.J.; Seo, D.J.; Woo, J.; Lim, J.T.; Cheon, J.Y.; Yang, S.Y.; Lee, J.M.; Kang, D.; Shin, T.J.; Shin, H.S.; et al. A General Approach to Preferential Formation of Active Fe-N(x) Sites in Fe-N/C Electrocatalysts for Efficient Oxygen Reduction Reaction. *J. Am. Chem. Soc.* **2016**, *138*, 15046–15056. https://doi.org/10.1021/jacs.6b09470.
149. Zhang, B.; Chen, R.; Yang, Z.; Chen, Y.; Zhou, L.; Yuan, Y. Rapeseed meal-based autochthonous N and S-doped non-metallic porous carbon electrode material for oxygen reduction reaction catalysis. *Int. J. Hydrogen Energy* **2021**, *46*, 508–517. https://doi.org/10.1016/j.ijhydene.2020.09.198.
150. Barkholtz, H.M.; Chong, L.; Kaiser, Z.B.; Xu, T.; Liu, D.-J. Highly Active Non-PGM Catalysts Prepared from Metal Organic Frameworks. *Catalysts* **2015**, *5*, 955–965.
151. Matter, P.H.; Ozkan, U.S. Non-metal Catalysts for Dioxygen Reduction in an Acidic Electrolyte. *Catal. Lett.* **2006**, *109*, 115–123. https://doi.org/10.1007/s10562-006-0067-1.
152. Gong, K.; Du, F.; Xia, Z.; Durstock, M.; Dai, L. Nitrogen-Doped Carbon Nanotube Arrays with High Electrocatalytic Activity for Oxygen Reduction. *Science* **2009**, *323*, 760–764, https://doi.org/10.1126/science.1168049.
153. Qian, Y.; Hu, Z.; Ge, X.; Yang, S.; Peng, Y.; Kang, Z.; Liu, Z.; Lee, J.Y.; Zhao, D. A metal-free ORR/OER bifunctional electrocatalyst derived from metal-organic frameworks for rechargeable Zn-Air batteries. *Carbon* **2017**, *111*, 641–650. https://doi.org/10.1016/j.carbon.2016.10.046.
154. Chung, H.T.; Cullen, D.A.; Higgins, D.; Sneed, B.T.; Holby, E.F.; More, K.L.; Zelenay, P. Direct atomic-level insight into the active sites of a high-performance PGM-free ORR catalyst. *Science* **2017**, *357*, 479–484. https://doi.org/10.1126/science.aan2255.
155. Yang, L.; Jiang, S.; Zhao, Y.; Zhu, L.; Chen, S.; Wang, X.; Wu, Q.; Ma, J.; Ma, Y.; Hu, Z. Boron-Doped Carbon Nanotubes as Metal-Free Electrocatalysts for the Oxygen Reduction Reaction. *Angew. Chem. Int. Ed.* **2011**, *50*, 7132–7135. https://doi.org/10.1002/anie.201101287.
156. Liu, Z.W.; Peng, F.; Wang, H.J.; Yu, H.; Zheng, W.X.; Yang, J. Phosphorus-doped graphite layers with high electrocatalytic activity for the $O_2$ reduction in an alkaline medium. *Angew Chem. Int. Ed. Engl.* **2011**, *50*, 3257–3261. https://doi.org/10.1002/anie.201006768.
157. Jeon, I.-Y.; Zhang, S.; Zhang, L.; Choi, H.-J.; Seo, J.-M.; Xia, Z.; Dai, L.; Baek, J.-B. Edge-Selectively Sulfurized Graphene Nanoplatelets as Efficient Metal-Free Electrocatalysts for Oxygen Reduction Reaction: The Electron Spin Effect. *Adv. Mater.* **2013**, *25*, 6138–6145. https://doi.org/10.1002/adma.201302753.

158. Yao, Z.; Nie, H.; Yang, Z.; Zhou, X.; Liu, Z.; Huang, S. Catalyst-free synthesis of iodine-doped graphene via a facile thermal annealing process and its use for electrocatalytic oxygen reduction in an alkaline medium. *Chem. Commun.* **2012**, *48*, 1027–1029. https://doi.org/10.1039/c2cc16192c.
159. Jeon, I.-Y.; Choi, H.-J.; Choi, M.; Seo, J.-M.; Jung, S.-M.; Kim, M.-J.; Zhang, S.; Zhang, L.; Xia, Z.; Dai, L.; et al. Facile, scalable synthesis of edge-halogenated graphene nanoplatelets as efficient metal-free eletrocatalysts for oxygen reduction reaction. *Sci. Rep.* **2013**, *3*, 1810. https://doi.org/10.1038/srep01810.
160. Liu, X.; Dai, L. Carbon-Based Metal Free Catalysts. *Nat. Rev. Mater.* **2016**, *1*, 16064.
161. Ferrero, G.A.; Fuertes, A.B.; Sevilla, M.; Titirici, M.-M. Efficient metal-free N-doped mesoporous carbon catalysts for ORR by a template-free approach. *Carbon* **2016**, *106*, 179–187. https://doi.org/10.1016/j.carbon.2016.04.080.
162. Quílez-Bermejo, J.; Morallón, E.; Cazorla-Amorós, D. Metal-free heteroatom-doped carbon-based catalysts for ORR: A critical assessment about the role of heteroatoms. *Carbon* **2020**, *165*, 434–454. https://doi.org/10.1016/j.carbon.2020.04.068.
163. Yu, L.; Yang, C.; Zhang, W.; Liu, W.; Wang, H.; Qi, J.; Xu, L. Solvent-free synthesis of N-doped nanoporous carbon materials as durable high-performance pH-universal ORR catalysts. *J. Colloid Interface Sci.* **2020**, *575*, 406–415. https://doi.org/10.1016/j.jcis.2020.05.012.
164. Li, J.-C.; Hou, P.-X.; Cheng, M.; Liu, C.; Cheng, H.M.; Shao, M. Carbon nanotube encapsulated in nitrogen and phosphorus co-doped carbon as a bifunctional electrocatalyst for oxygen reduction and evolution reactions. *Carbon* **2018**, 139, 156–163.
165. Wood, K.N.; O'Hayre, R.; Pylypenko, S. Recent progress on nitrogen/carbon structures designed for use in energy and sustainability applications. *Energy Environ. Sci.* **2014**, *7*, 1212–1249.
166. Jeon, I.-Y.; Choi, H.-J.; Ju, M.J.; Choi, I.T.; Lim, K.; Ko, J.; Kim, H.K.; Kim, J.C.; Lee, J.-J.; Shin, D.; et al. Direct nitrogen fixation at the edges of graphene nanoplatelets as efficient electrocatalysts for energy conversion. *Sci. Rep.* **2013**, *3*, 2260. https://doi.org/10.1038/srep02260.
167. Sasaki, K.; Naohara, H.; Cai, Y.; Choi, Y.M.; Liu, P.; Vukmirovic, M.B.; Wang, J.X.; Adzic, R.R. Core-protected platinum monolayer shell high-stability electrocatalysts for fuel-cell cathodes. *Angew Chem. Int. Ed. Engl.* **2010**, *49*, 8602–8607. https://doi.org/10.1002/anie.201004287.
168. Parvez, K.; Yang, S.; Hernandez, Y.; Winter, A.; Turchanin, A.; Feng, X.; Müllen, K. Nitrogen-doped graphene and its iron-based composite as efficient electrocatalysts for oxygen reduction reaction. *ACS Nano* **2012**, *6*, 9541–9550. https://doi.org/10.1021/nn302674k.
169. He, W.; Jiang, C.; Wang, J.; Lu, L. High-rate oxygen electroreduction over graphitic-N species exposed on 3D hierarchically porous nitrogen-doped carbons. *Angew Chem. Int. Ed. Engl.* **2014**, *53*, 9503–9507. https://doi.org/10.1002/anie.201404333.
170. Xing, T.; Zheng, Y.; Li, L.H.; Cowie, B.C.; Gunzelmann, D.; Qiao, S.Z.; Huang, S.; Chen, Y. Observation of active sites for oxygen reduction reaction on nitrogen-doped multilayer graphene. *ACS Nano* **2014**, *8*, 6856–6862. https://doi.org/10.1021/nn501506p.
171. Tuci, G.; Zafferoni, C.; Rossin, A.; Luconi, L.; Milella, A.; Ceppatelli, M.; Innocenti, M.; Liu, Y.; Liu, Y.; Pham-Huu, C.; et al. Chemical functionalization of N-doped carbon nanotubes: A powerful approach to cast light on the electrochemical role of specific N-functionalities in the oxygen reduction reaction. *Catal. Sci. Technol.* **2016**, *6*, 6226–6236.
172. Yasuda, S.; Yu, L.; Kim, J.; Murakoshi, K. Selective nitrogen doping in graphene for oxygen reduction reactions. *Chem. Commun.* **2013**, *49*, 9627–9629.
173. Saputro, A.G.; Kasai, H. Oxygen reduction reaction on neighboring Fe–N 4 and quaternary-N sites of pyrolized Fe/N/C catalyst. *Phys. Chem. Chem. Phys.* **2015**, *17*, 3059–3071.
174. Kou, Z.; Guo, B.; He, D.; Zhang, J.; Mu, S. Transforming Two-Dimensional Boron Carbide into Boron and Chlorine Dual-Doped Carbon Nanotubes by Chlorination for Efficient Oxygen Reduction. *ACS Energy Lett.* **2018**, *3*, 184–190. https://doi.org/10.1021/acsenergylett.7b01133.
175. Tam, T.V.; Kang, S.G.; Kim, M.H.; Lee, S.G.; Hur, S.H.; Chung, J.S.; Choi, W.M. Novel Graphene Hydrogel/B-Doped Graphene Quantum Dots Composites as Trifunctional Electrocatalysts for Zn−Air Batteries and Overall Water Splitting. *Adv. Energy Mater.* **2019**, *9*, 1900945. https://doi.org/10.1002/aenm.201900945.
176. Zhao, Y.; Yang, L.; Chen, S.; Wang, X.; Ma, Y.; Wu, Q.; Jiang, Y.; Qian, W.; Hu, Z. Can Boron and Nitrogen Co-doping Improve Oxygen Reduction Reaction Activity of Carbon Nanotubes? *J. Am. Chem. Soc.* **2013**, *135*, 1201–1204. https://doi.org/10.1021/ja310566z.
177. Wang , S.; Iyyamperumal , E.; Roy, A.; Xue, Y.; Yu, D.; Dai, L. Vertically Aligned BCN Nanotubes as Efficient Metal-Free Electrocatalysts for the Oxygen Reduction Reaction: A Synergetic Effect by Co-Doping with Boron and Nitrogen. *Angew. Chem. Int. Ed.* **2011**, *50*, 11756–11760. https://doi.org/10.1002/anie.201105204.
178. Wang, D.W.; Su, D.S. Heterogeneous nanocarbon materials for oxygen reduction reaction. *Energy Environ. Sci.* **2014**, *7*, 576–591.
179. Wei, P.; Li, X.; He, Z.; Sun, X.; Liang, Q.; Wang, Z.; Fang, C.; Li, Q.; Yang, H.; Han, J.; et al. Porous N, B co-doped carbon nanotubes as efficient metal-free electrocatalysts for ORR and Zn-air batteries. *Chem. Eng. J.* **2021**, *422*, 130134. https://doi.org/10.1016/j.cej.2021.130134.
180. Yan, P.; Liu, J.; Yuan, S.; Liu, Y.; Cen, W.; Chen, Y. The promotion effects of graphitic and pyridinic N combinational doping on graphene for ORR. *Appl. Surf. Sci.* **2018**, *445*, 398–403. https://doi.org/10.1016/j.apsusc.2018.03.106.
181. Higgins, D.C.; Hoque, M.A.; Hassan, F.; Choi, J.-Y.; Kim, B.; Chen, Z. Oxygen Reduction on Graphene–Carbon Nanotube Composites Doped Sequentially with Nitrogen and Sulfur. *ACS Catal.* **2014**, *4*, 2734–2740. https://doi.org/10.1021/cs5003806.

182. Meng, Y.; Voiry, D.; Goswami, A.; Zou, X.; Huang, X.; Chhowalla, M.; Liu, Z.; Asefa, T. N-, O-, and S-Tridoped Nanoporous Carbons as Selective Catalysts for Oxygen Reduction and Alcohol Oxidation Reactions. *J. Am. Chem. Soc.* **2014**, *136*, 13554–13557. https://doi.org/10.1021/ja507463w.
183. Zhao, S.; Liu, J.; Li, C.; Ji, W.; Yang, M.; Huang, H.; Liu, Y.; Kang, Z. Tunable Ternary (N, P, B)-Doped Porous Nanocarbons and Their Catalytic Properties for Oxygen Reduction Reaction. *ACS Appl. Mater. Interfaces* **2014**, *6*, 22297–22304. https://doi.org/10.1021/am506284k.
184. Yan, Z.; Gao, L.; Dai, C.; Zhang, M.; Lv, X.; Shen, P.K. Metal-free mesoporous carbon with higher contents of active N and S codoping by template method for superior ORR efficiency to Pt/C. *Int. J. Hydrogen Energy* **2018**, *43*, 3705–3715. https://doi.org/10.1016/j.ijhydene.2018.01.013.
185. Hua, Y.; Jiang, T.; Wang, K.; Wu, M.; Song, S.; Wang, Y. Efficient Pt-free Electrocatalysts for Oxygen Reduction Reaction: Highly Ordered Mesoporous N- and S- Co-doped Carbon with Saccharin as Single-source Molecular Precursor. *Appl. Catal. B: Environ.* **2016**, *194*, 202–208. https://doi.org/10.1016/j.apcatb.2016.04.056.
186. Larijani, H.T.; Khorshidian, M. Theoretical insight into the role of pyridinic nitrogen on the catalytic activity of boron-doped graphene towards oxygen reduction reaction. *Appl. Surf. Sci.* **2019**, *492*, 826–842. https://doi.org/10.1016/j.apsusc.2019.05.149.
187. Cheng, C.; Li, Y.; Maouche, C.; Li, B.; Zhou, Y.; Wang, S.; Cheng, X.; Yang, J. Green synthesis of N, P-co doped porous reduced graphene oxide as an active metal-free electrocatalyst toward oxygen reduction reaction. *J. Electroanal. Chem.* **2021**, *883*, 115058. https://doi.org/10.1016/j.jelechem.2021.115058.
188. Zhou, Z.; Chen, A.; Fan, X.; Kong, A.; Shan, Y. Hierarchical porous N-P-coupled carbons as metal-free bifunctional electrocatalysts for oxygen conversion. *Appl. Surf. Sci.* **2019**, *464*, 380–387. https://doi.org/10.1016/j.apsusc.2018.09.095.
189. Dong, F.; Cai, Y.; Liu, C.; Liu, J.; Qiao, J. Heteroatom (B, N and P) doped porous graphene foams for efficient oxygen reduction reaction electrocatalysis. *Int. J. Hydrogen Energy* **2018**, *43*, 12661–12670.
190. Wang, L.; Wang, Y.; Wu, M.; Wei, Z.; Cui, C.; Mao, M.; Zhang, J.; Han, X.; Liu, Q.; Ma, J. Nitrogen, Fluorine, and Boron Ternary Doped Carbon Fibers as Cathode Electrocatalysts for Zinc–Air Batteries. *Small* **2018**, *14*, 1800737. https://doi.org/10.1002/smll.201800737.
191. Kong, D.; Liu, L.; Yuan, W.; Xie, A.; Shen, Y. Facile synthesis and excellent catalytic performance of nitrogen-doped porous carbons derived from banana peel towards oxygen reduction reaction. *Mater. Res. Bull.* **2018**, *103*, 63–69. https://doi.org/10.1016/j.materresbull.2018.03.019.
192. Lai, F.; Zhou, G.; Li, F.; He, Z.; Yong, D.; Bai, W.; Huang, Y.; Tjiu, W.W.; Miao, Y.-E.; Pan, B.; et al. Highly Dual-Heteroatom-Doped Ultrathin Carbon Nanosheets with Expanded Interlayer Distance for Efficient Energy Storage. *ACS Sustain. Chem. Eng.* **2018**, *6*, 3143–3153. https://doi.org/10.1021/acssuschemeng.7b03161.
193. Zhang, Q.; Luo, F.; Ling, Y.; Guo, L.; Qu, K.; Hu, H.; Yang, Z.; Cai, W.; Cheng, H. Constructing Successive Active Sites for Metal-free Electrocatalyst with Boosted Electrocatalytic Activities Toward Hydrogen Evolution and Oxygen Reduction Reactions. *ChemCatChem* **2018**, *10*, 5194–5200. https://doi.org/10.1002/cctc.201801455.
194. Jin, J.-t.; Qiao, X.-c.; Cheng, F.-l.; Fan, H.-b.; Cui, L.-f. Direct synthesis of interconnected N, S-codoped porous exfoliated carbon nanosheets as advanced electrocatalysts for oxygen reduction reaction. *Carbon* **2017**, *122*, 114–121. https://doi.org/10.1016/j.carbon.2017.06.044.
195. Li, Y.; Yang, J.; Huang, J.; Zhou, Y.; Xu, K.; Zhao, N.; Cheng, X. Soft template-assisted method for synthesis of nitrogen and sulfur co-doped three-dimensional reduced graphene oxide as an efficient metal free catalyst for oxygen reduction reaction. *Carbon* **2017**, *122*, 237–246. https://doi.org/10.1016/j.carbon.2017.06.046.
196. Lee, M.S.; Whang, D.R.; Choi, H.-J.; Yang, M.H.; Kim, B.-G.; Baek, J.-B.; Chang, D.W. A facile approach to tailoring electrocatalytic activities of imine-rich nitrogen-doped graphene for oxygen reduction reaction. *Carbon* **2017**, *122*, 515–523. https://doi.org/10.1016/j.carbon.2017.07.001.
197. Jia, S.; Wang, Y.; Xin, G.; Zhou, S.; Tian, P.; Zang, J. An efficient preparation of N-doped mesoporous carbon derived from milk powder for supercapacitors and fuel cells. *Electrochim. Acta* **2016**, *196*, 527–534. https://doi.org/10.1016/j.electacta.2016.02.196.
198. Zhou, S.; Zang, J.; Gao, H.; Tian, X.; Tian, P.; Song, S.; Wang, Y. Deflagration method synthesizing N, S co-doped oxygen-functionalized carbons as a bifunctional catalyst for oxygen reduction and oxygen evolution reaction. *Carbon* **2021**, *181*, 234–245. https://doi.org/10.1016/j.carbon.2021.05.034.
199. Jiang, Y.; Yang, L.; Sun, T.; Zhao, J.; Lyu, Z.; Zhuo, O.; Wang, X.; Wu, Q.; Ma, J.; Hu, Z. Significant Contribution of Intrinsic Carbon Defects to Oxygen Reduction Activity. *ACS Catal.* **2015**, *5*, 6707–6712. https://doi.org/10.1021/acscatal.5b01835.
200. Jin, H.; Huang, H.; He, Y.; Feng, X.; Wang, S.; Dai, L.; Wang, J. Graphene Quantum Dots Supported by Graphene Nanoribbons with Ultrahigh Electrocatalytic Performance for Oxygen Reduction. *J. Am. Chem. Soc.* **2015**, *137*, 7588–7591. https://doi.org/10.1021/jacs.5b03799.
201. Li, H.; Zhu, H.; Zhang, S.; Zhang, N.; Du, M.; Chai, Y. Nano High-Entropy Materials: Synthesis Strategies and Catalytic Applications. *Small Struct.* **2020**, *1*, 2000033. https://doi.org/10.1002/sstr.202000033.
202. Wang, H.-F.; Chen, L.; Pang, H.; Kaskel, S.; Xu, Q. MOF-derived electrocatalysts for oxygen reduction, oxygen evolution and hydrogen evolution reactions. *Chem. Soc. Rev.* **2020**, *49*, 1414–1448. https://doi.org/10.1039/C9CS00906J.
203. Lee, J.-S.M.; Fujiwara, Y.-i.; Kitagawa, S.; Horike, S. Homogenized Bimetallic Catalysts from Metal–Organic Framework Alloys. *Chem. Mater.* **2019**, *31*, 4205–4212. https://doi.org/10.1021/acs.chemmater.9b01093.
204. Herron, J.A.; Tonelli, S.; Mavrikakis, M. Atomic and molecular adsorption on Pd (111). *Surf. Sci.* **2012**, *606*, 1670–1679.

205. Rajesh, D.; Mahendiran, C.; Suresh, C. The Promotional Effect of Ag in Pd-Ag/Carbon Nanotube-Graphene Electrocatalysts for Alcohol and Formic Acid Oxidation Reactions. *ChemElectroChem* **2020**, *7*, 2629–2636. https://doi.org/10.1002/celc.202000642.
206. Xu, W.; Yoon, D.; Yang, Y.; Xiong, Y.; Li, H.; Zeng, R.; Muller, D.A.; Abruña, H.D. MOF-Derived Bimetallic Pd–Co Alkaline ORR Electrocatalysts. *ACS Appl. Mater. Interfaces* **2022**, *14*, 44735–44744. https://doi.org/10.1021/acsami.2c10074.
207. Zhu, G.; Yang, H.; Jiang, Y.; Sun, Z.; Li, X.; Yang, J.; Wang, H.; Zou, R.; Jiang, W.; Qiu, P.; et al. Modulating the Electronic Structure of FeCo Nanoparticles in N-Doped Mesoporous Carbon for Efficient Oxygen Reduction Reaction. *Adv. Sci.* **2022**, *9*, 2200394. https://doi.org/10.1002/advs.202200394.
208. Chen, C.; Cheng, D.; Liu, S.; Wang, Z.; Hu, M.; Zhou, K. Engineering the multiscale structure of bifunctional oxygen electrocatalyst for highly efficient and ultrastable zinc-air battery. *Energy Storage Mater.* **2020**, *24*, 402–411. https://doi.org/10.1016/j.ensm.2019.07.028.
209. Zheng, Y.; He, F.; Wu, J.; Ma, D.; Fan, H.; Zhu, S.; Li, X.; Lu, Y.; Liu, Q.; Hu, X. Nitrogen-Doped Carbon Nanotube–Graphene Frameworks with Encapsulated Fe/Fe3N Nanoparticles as Catalysts for Oxygen Reduction. *ACS Appl. Nano Mater.* **2019**, *2*, 3538–3547. https://doi.org/10.1021/acsanm.9b00506.
210. Lei, Y.; Huang, R.; Xie, H.; Zhang, D.; Liu, X.; Si, Y.; Li, N. Electronic structure tuning of FeCo nanoparticles embedded in multi-dimensional carbon matrix for enhanced bifunctional oxygen electrocatalysis. *J. Alloys Compd.* **2021**, *853*, 157070. https://doi.org/10.1016/j.jallcom.2020.157070.
211. Park, M.-S.; Kim, J.; Kim, K.; Lee, J.-W.; Kim, J.H.; Yamauchi, Y. Porous nanoarchitectures of spinel-type transition metal oxides for electrochemical energy storage systems. *Phys. Chem. Chem. Phys. PCCP* **2015**, *17*, 30963–30977 https://doi.org/10.1039/c5cp05936d.
212. Tang, R.; Wang, L.; Ying, M.; Yang, W.; Kheradmand, A.; Jiang, Y.; Li, Z.; Cui, Y.; Zheng, R.; Huang, J. Multigraded Heterojunction Hole Extraction Layer of ZIF-$Co_xZn_{1-x}$ on $Co_3O_4/TiO_2$ Skeleton for a New Photoanode Architecture in Water Oxidation. *Small Sci.* **2021**, *1*, 2000033. https://doi.org/10.1002/smsc.202000033.
213. Peng, L.; Chen, S.; Yu, C.; Wei, C.; Liao, C.; Wu, Z.; Wang, H.-L.; Cheng, S.; Xie, J. Enhancing Moisture and Electrochemical Stability of the Li5.5PS4.5Cl1.5 Electrolyte by Oxygen Doping. *ACS Appl. Mater. Interfaces* **2022**, *14*, 4179–4185. https://doi.org/10.1021/acsami.1c21561.
214. Wen, S.; Liu, Y.; Bai, H.; Shao, R.; Xu, W.; Shi, W. Full synergistic effect of hydrothermal $NiCo_2O_4$ nanosheets/$CuCo_2O_4$ nanocones supported on Ni foam for high-performance asymmetric supercapacitors. *J. Solid State Chem.* **2018**, *262*, 327–334. https://doi.org/10.1016/j.jssc.2018.03.023.
215. Osgood, H.; Devaguptapu, S.V.; Xu, H.; Cho, J.; Wu, G. Transition metal (Fe, Co, Ni, and Mn) oxides for oxygen reduction and evolution bifunctional catalysts in alkaline media. *Nano Today* **2016**, *11*, 601–625. https://doi.org/10.1016/j.nantod.2016.09.001.
216. Liu, F.; Zhang, L.; Wang, L.; Cheng, F. The Electrochemical Tuning of Transition Metal-Based Materials for Electrocatalysis. *Electrochem. Energy Rev.* **2021**, *4*, 146–168. https://doi.org/10.1007/s41918-020-00089-w.
217. Prabu, M.; Ketpang, K.; Shanmugam, S. Hierarchical nanostructured NiCo2O4 as an efficient bifunctional non-precious metal catalyst for rechargeable zinc-air batteries. *Nanoscale* **2014**, *6*, 3173–3181.
218. Chakrabarty, S.; Mukherjee, A.; Su, W.-N.; Basu, S. Improved bi-functional ORR and OER catalytic activity of reduced graphene oxide supported $ZnCo_2O_4$ microsphere. *Int. J. Hydrogen Energy* **2019**, *44*, 1565–1578. https://doi.org/10.1016/j.ijhydene.2018.11.163.
219. Prabu, M.; Ramakrishnan, P.; Shanmugam, S. $CoMn_2O_4$ nanoparticles anchored on nitrogen-doped graphene nanosheets as bifunctional electrocatalyst for rechargeable zinc–air battery. *Electrochem. Commun.* **2014**, *41*, 59–63. https://doi.org/10.1016/j.elecom.2014.01.027.
220. Ding, K.; Han, J.; Gao, X.; Wang, L.; Zhou, L.; Qu, R.; He, X. An ionic liquid-present hydrothermal method for preparing hawthorn sherry ball shaped palladium (Pd)-based composite catalysts for ethanol oxidation reaction (EOR). *Int. J. Hydrogen Energy* **2020**, *45*, 1930–1939. https://doi.org/10.1016/j.ijhydene.2019.11.110.
221. Sahoo, L.; Garg, R.; Kaur, K.; Vinod, C.P.; Gautam, U.K. Ultrathin Twisty PdNi Alloy Nanowires as Highly Active ORR Electrocatalysts Exhibiting Morphology-Induced Durability over 200 K Cycles. *Nano Lett.* **2022**, *22*, 246–254. https://doi.org/10.1021/acs.nanolett.1c03704.
222. Chang, Z.; Yu, F.; Liu, Z.; Peng, S.; Guan, M.; Shen, X.; Zhao, S.; Liu, N.; Wu, Y.; Chen, Y. Co–Ni Alloy Encapsulated by N-doped Graphene as a Cathode Catalyst for Rechargeable Hybrid Li–Air Batteries. *ACS Appl. Mater. Interfaces* **2020**, *12*, 4366–4372. https://doi.org/10.1021/acsami.9b12213.
223. Zhang, W.; Zhu, J.; Cheng, D.; Zeng, X.C. PtCoNi Alloy Nanoclusters for Synergistic Catalytic Oxygen Reduction Reaction. *ACS Appl. Nano Mater.* **2020**, *3*, 2536–2544. https://doi.org/10.1021/acsanm.9b02604.
224. Pavko, L.; Gatalo, M.; Križan, G.; Križan, J.; Ehelebe, K.; Ruiz-Zepeda, F.; Šala, M.; Dražić, G.; Geuß, M.; Kaiser, P.; et al. Toward the Continuous Production of Multigram Quantities of Highly Uniform Supported Metallic Nanoparticles and Their Application for Synthesis of Superior Intermetallic Pt-Alloy ORR Electrocatalysts. *ACS Appl. Energy Mater.***2021**, *4*, 13819-13829. https://doi.org/10.1021/acsaem.1c02570.
225. Sial, M.; Lin, H.; Zulfiqar, M.; Ullah, S.; Ni, B.; Wang, X. Trimetallic PtCoFe Alloy Monolayer Superlattices as Bifunctional Oxygen-Reduction and Ethanol-Oxidation Electrocatalysts. *Small* **2017**, *13*, 1700250. https://doi.org/10.1002/smll.201700250.
226. Zhu, J.; Xie, M.; Chen, Z.; Lyu, Z.; Chi, M.; Jin, W.; Xia, Y. Pt-Ir-Pd Trimetallic Nanocages as a Dual Catalyst for Efficient Oxygen Reduction and Evolution Reactions in Acidic Media. *Adv. Energy Mater.* **2020**, *10*, 1904114. https://doi.org/10.1002/aenm.201904114.

227. Li, X.; Zhao, J.; Su, D. Structural Changes of Intermetallic Catalysts under Reaction Conditions. *Small Struct.* **2021**, *2*, 2100011. https://doi.org/10.1002/sstr.202100011.
228. Li, S.; Chen, W.; Pan, H.; Cao, Y.; Jiang, Z.; Tian, X.; Hao, X.; Maiyalagan, T.; Jiang, Z.-J. FeCo Alloy Nanoparticles Coated by an Ultrathin N-Doped Carbon Layer and Encapsulated in Carbon Nanotubes as a Highly Efficient Bifunctional Air Electrode for Rechargeable Zn-Air Batteries. *ACS Sustain. Chem. Eng.* **2019**, *7*, 8530–8541. https://doi.org/10.1021/acssuschemeng.9b00307.
229. Wang, J.; Ciucci, F. Boosting Bifunctional Oxygen Electrolysis for N-Doped Carbon via Bimetal Addition. *Small* **2017**, *13*, 1604103. https://doi.org/10.1002/smll.201604103.
230. Barman, B.K.; Nanda, K.K. CoFe Nanoalloys Encapsulated in N-Doped Graphene Layers as a Pt-Free Multifunctional Robust Catalyst: Elucidating the Role of Co-Alloying and N-Doping. *ACS Sustain. Chem. Eng.* **2018**, *6*, 12736–12745. https://doi.org/10.1021/acssuschemeng.8b01861.
231. Yan, Q.; Duan, X.; Liu, Y.; Ge, F.; Zheng, H. A hybridization cage-confinement pyrolysis strategy for ultrasmall Ni $_3$ Fe alloy coated with N-doped carbon nanotubes as bifunctional oxygen electrocatalysts for Zn–air batteries. *J. Mater. Chem. A* 2023. https://doi.org/10.1039/D2TA08319A.
232. Wang, Z.; Cheng, L.; Zhang, R.; Lv, W.; Wang, W. Surface-oxidized Fe–Co–Ni alloys anchored to N-doped carbon nanotubes as efficient catalysts for oxygen reduction reaction. *J. Alloys Compd.* **2021**, *857*, 158249.
233. Bu, L.; Zhang, N.; Guo, S.; Zhang, X.; Li, J.; Yao, J.; Wu, T.; Lu, G.; Ma, J.-Y.; Su, D.; et al. Biaxially strained PtPb/Pt core/shell nanoplate boosts oxygen reduction catalysis. *Science* **2016**, *354*, 1410–1414, doi:doi:10.1126/science.aah6133.
234. Lai, J.; Huang, B.; Tang, Y.; Lin, F.; Zhou, P.; Chen, X.; Sun, Y.; Lv, F.; Guo, S. Barrier-free Interface Electron Transfer on PtFe-$Fe_2C$ Janus-like Nanoparticles Boosts Oxygen Catalysis. *Chemistry* **2018**, *4*, 1153–1166. https://doi.org/10.1016/j.chempr.2018.02.010.
235. Ud Din, M.A.; Saleem, F.; Ni, B.; Yong, Y.; Wang, X. Porous Tetrametallic PtCuBiMn Nanosheets with a High Catalytic Activity and Methanol Tolerance Limit for Oxygen Reduction Reactions. *Adv. Mater.* **2017**, *29*, 1604994. https://doi.org/10.1002/adma.201604994.
236. Papanikolaou, K.G.; Darby, M.T.; Stamatakis, M. CO-induced aggregation and segregation of highly dilute alloys: A density functional theory study. *J. Phys. Chem. C* **2019**, *123*, 9128–9138.
237. Darby, M.T.; Sykes, E.C.H.; Michaelides, A.; Stamatakis, M. Carbon monoxide poisoning resistance and structural stability of single atom alloys. *Top. Catal.* **2018**, *61*, 428–438.
238. Darby, M.T.; Stamatakis, M. Single-Atom Alloys for the Electrochemical Oxygen Reduction Reaction. *Chemphyschem* **2021**, *22*, 499–508. https://doi.org/10.1002/cphc.202000869.
239. Arán-Ais, R.M.; Dionigi, F.; Merzdorf, T.; Gocyla, M.; Heggen, M.; Dunin-Borkowski, R.E.; Gliech, M.; Solla-Gullón, J.; Herrero, E.; Feliu, J.M.; et al. Elemental Anisotropic Growth and Atomic-Scale Structure of Shape-Controlled Octahedral Pt–Ni–Co Alloy Nanocatalysts. *Nano Lett.* **2015**, *15*, 7473–7480. https://doi.org/10.1021/acs.nanolett.5b03057.
240. George, E.P.; Raabe, D.; Ritchie, R.O. High-entropy alloys. *Nat. Rev. Mater.* **2019**, *4*, 515–534. https://doi.org/10.1038/s41578-019-0121-4.
241. Xin, Y.; Li, S.; Qian, Y.; Zhu, W.; Yuan, H.; Jiang, P.; Guo, R.; Wang, L. High-Entropy Alloys as a Platform for Catalysis: Progress, Challenges, and Opportunities. *ACS Catal.* **2020**, *10*, 11280–11306. https://doi.org/10.1021/acscatal.0c03617.
242. Li, H.; Lai, J.; Li, Z.; Wang, L. Multi-Sites Electrocatalysis in High-Entropy Alloys. *Adv. Funct. Mater.* **2021**, *31*, 2106715. https://doi.org/10.1002/adfm.202106715.
243. Shi, P.; Ren, W.; Zheng, T.; Ren, Z.; Hou, X.; Peng, J.; Hu, P.; Gao, Y.; Zhong, Y.; Liaw, P.K. Enhanced strength–ductility synergy in ultrafine-grained eutectic high-entropy alloys by inheriting microstructural lamellae. *Nat. Commun.* **2019**, *10*, 489. https://doi.org/10.1038/s41467-019-08460-2.
244. Yao, Y.; Huang, Z.; Xie, P.; Lacey, S.D.; Jacob, R.J.; Xie, H.; Chen, F.; Nie, A.; Pu, T.; Rehwoldt, M.; et al. Carbothermal shock synthesis of high-entropy-alloy nanoparticles. *Science* **2018**, *359*, 1489–1494, doi:doi:10.1126/science.aan5412.
245. Murty, B.; Ranganathan, S. Novel materials synthesis by mechanical alloying/milling. *Int. Mater. Rev.* **1998**, *43*, 101–141. https://doi.org/10.1179/095066098790105654.
246. Tsai, C.F.; Wu, P.W.; Lin, P.; Chao, C.G.; Yeh, K.Y. Sputter deposition of multi-element nanoparticles as electrocatalysts for methanol oxidation. *JPN. J. Appl. Phys.* **2008**, *47*, 5755–5761.
247. Shih, C.-Y.; Wu, C.; Shugaev, M.V.; Zhigilei, L.V. Atomistic modeling of nanoparticle generation in short pulse laser ablation of thin metal films in water. *J. Colloid Interface Sci.* **2017**, *489*, 3–17. https://doi.org/10.1016/j.jcis.2016.10.029.
248. Bondesgaard, M.; Broge, N.L.N.; Mamakhel, A.; Bremholm, M.; Iversen, B.B. General Solvothermal Synthesis Method for Complete Solubility Range Bimetallic and High-Entropy Alloy Nanocatalysts. *Adv. Funct. Mater.* **2019**, *29*, 1905933. https://doi.org/10.1002/adfm.201905933.
249. Lu, D.; Zhang, Y.; Lin, S.; Wang, L.; Wang, C. Synthesis of PtAu bimetallic nanoparticles on graphene–carbon nanotube hybrid nanomaterials for nonenzymatic hydrogen peroxide sensor. *Talanta* **2013**, *112*, 111–116. https://doi.org/10.1016/j.talanta.2013.03.010.
250. Gao, S.; Hao, S.; Huang, Z.; Yuan, Y.; Han, S.; Lei, L.; Zhang, X.; Shahbazian-Yassar, R.; Lu, J. Synthesis of high-entropy alloy nanoparticles on supports by the fast moving bed pyrolysis. *Nat. Commun.* **2020**, *11*, 2016. https://doi.org/10.1038/s41467-020-15934-1.
251. Kumar, N.; Tiwary, C.S.; Biswas, K. Preparation of nanocrystalline high-entropy alloys via cryomilling of cast ingots. *J. Mater. Sci.* **2018**, *53*, 13411–13423. https://doi.org/10.1007/s10853-018-2485-z.

252. Cui, X.; Li, W.; Ryabchuk, P.; Junge, K.; Beller, M. Bridging homogeneous and heterogeneous catalysis by heterogeneous single-metal-site catalysts. *Nat. Catal.* **2018**, *1*, 385–397. https://doi.org/10.1038/s41929-018-0090-9.
253. Zhang, G.; Ming, K.; Kang, J.; Huang, Q.; Zhang, Z.; Zheng, X.; Bi, X. High entropy alloy as a highly active and stable electrocatalyst for hydrogen evolution reaction. *Electrochim. Acta* **2018**, *279*, 19–23. https://doi.org/10.1016/j.electacta.2018.05.035.
254. Glasscott, M.W.; Pendergast, A.D.; Goines, S.; Bishop, A.R.; Hoang, A.T.; Renault, C.; Dick, J.E. Electrosynthesis of high-entropy metallic glass nanoparticles for designer, multi-functional electrocatalysis. *Nat. Commun.* **2019**, *10*, 2650. https://doi.org/10.1038/s41467-019-10303-z.
255. Jin, Z.; Lv, J.; Jia, H.; Liu, W.; Li, H.; Chen, Z.; Lin, X.; Xie, G.; Liu, X.; Sun, S.; et al. Nanoporous Al-Ni-Co-Ir-Mo High-Entropy Alloy for Record-High Water Splitting Activity in Acidic Environments. *Small* **2019**, *15*, 1904180. https://doi.org/10.1002/smll.201904180.
256. Xie, P.; Yao, Y.; Huang, Z.; Liu, Z.; Zhang, J.; Li, T.; Wang, G.; Shahbazian-Yassar, R.; Hu, L.; Wang, C. Highly efficient decomposition of ammonia using high-entropy alloy catalysts. *Nat. Commun.* **2019**, *10*, 4011. https://doi.org/10.1038/s41467-019-11848-9.
257. Cui, C.; Gan, L.; Heggen, M.; Rudi, S.; Strasser, P. Compositional segregation in shaped Pt alloy nanoparticles and their structural behaviour during electrocatalysis. *Nat. Mater.* **2013**, *12*, 765–771. https://doi.org/10.1038/nmat3668.
258. Batchelor, T.A.A.; Pedersen, J.K.; Winther, S.H.; Castelli, I.E.; Jacobsen, K.W.; Rossmeisl, J. High-Entropy Alloys as a Discovery Platform for Electrocatalysis. *Joule* **2019**, *3*, 834–845. https://doi.org/10.1016/j.joule.2018.12.015.
259. Zhang, Y.; Zhou, Y.J.; Lin, J.P.; Chen, G.L.; Liaw, P.K. Solid-Solution Phase Formation Rules for Multi-component Alloys. *Adv. Eng. Mater.* **2008**, *10*, 534–538. https://doi.org/10.1002/adem.200700240.
260. Yang, X.; Zhang, Y. Prediction of high-entropy stabilized solid-solution in multi-component alloys. *Mater. Chem. Phys.* **2012**, *132*, 233–238. https://doi.org/10.1016/j.matchemphys.2011.11.021.
261. Mizutani, U. Hume-Rothery rules for structurally complex alloy phases. *MRS Bull.* **2012**, *37*, 169–169. https://doi.org/10.1557/mrs.2012.45.
262. Che, M. Nobel Prize in chemistry 1912 to Sabatier: Organic chemistry or catalysis? *Catal. Today* **2013**, *218*, 162–171. https://doi.org/10.1016/j.cattod.2013.07.006.
263. Lu, Z.; Chen, Z.W.; Singh, C.V. Neural Network-Assisted Development of High-Entropy Alloy Catalysts: Decoupling Ligand and Coordination Effects. *Matter* **2020**, *3*, 1318–1333. https://doi.org/10.1016/j.matt.2020.07.029.
264. Kulkarni, A.; Siahrostami, S.; Patel, A.; Nørskov, J.K. Understanding Catalytic Activity Trends in the Oxygen Reduction Reaction. *Chem. Rev.* **2018**, *118*, 2302–2312. https://doi.org/10.1021/acs.chemrev.7b00488.
265. Yao, C.-Z.; Zhang, P.; Liu, M.; Li, G.-R.; Ye, J.-Q.; Liu, P.; Tong, Y.-X. Electrochemical preparation and magnetic study of Bi–Fe–Co–Ni–Mn high entropy alloy. *Electrochim. Acta* **2008**, *53*, 8359–8365. https://doi.org/10.1016/j.electacta.2008.06.036.
266. Soare, V.; Burada, M.; Constantin, I.; Mitrică, D.; Bădiliţă, V.; Caragea, A.; Târcolea, M. Electrochemical deposition and microstructural characterization of AlCrFeMnNi and AlCrCuFeMnNi high entropy alloy thin films. *Appl. Surf. Sci.* **2015**, *358*, 533–539. https://doi.org/10.1016/j.apsusc.2015.07.142.
267. Nellaiappan, S.; Katiyar, N.K.; Kumar, R.; Parui, A.; Malviya, K.D.; Pradeep, K.G.; Singh, A.K.; Sharma, S.; Tiwary, C.S.; Biswas, K. High-Entropy Alloys as Catalysts for the $CO_2$ and CO Reduction Reactions: Experimental Realization. *ACS Catal.* **2020**, *10*, 3658–3663. https://doi.org/10.1021/acscatal.9b04302.
268. Pedersen, J.K.; Batchelor, T.A.A.; Bagger, A.; Rossmeisl, J. High-Entropy Alloys as Catalysts for the $CO_2$ and CO Reduction Reactions. *ACS Catal.* **2020**, *10*, 2169–2176. https://doi.org/10.1021/acscatal.9b04343.
269. Snyder, J.; Asanithi, P.; Dalton, A.B.; Erlebacher, J. Stabilized Nanoporous Metals by Dealloying Ternary Alloy Precursors. *Adv. Mater.* **2008**, *20*, 4883–4886. https://doi.org/10.1002/adma.200702760.
270. Qiu, H.-J.; Fang, G.; Wen, Y.; Liu, P.; Xie, G.; Liu, X.; Sun, S. Nanoporous high-entropy alloys for highly stable and efficient catalysts. *J. Mater. Chem. A* **2019**, *7*, 6499–6506. https://doi.org/10.1039/c9ta00505f.
271. Wang, D.; Xin, H.L.; Hovden, R.; Wang, H.; Yu, Y.; Muller, D.A.; DiSalvo, F.J.; Abruña, H.D. Structurally ordered intermetallic platinum–cobalt core–shell nanoparticles with enhanced activity and stability as oxygen reduction electrocatalysts. *Nat. Mater.* **2013**, *12*, 81–87.
272. Li, Q.; Wu, L.; Wu, G.; Su, D.; Lv, H.; Zhang, S.; Zhu, W.; Casimir, A.; Zhu, H.; Mendoza-Garcia, A.; et al. New Approach to Fully Ordered fct-FePt Nanoparticles for Much Enhanced Electrocatalysis in Acid. *Nano Lett.* **2015**, *15*, 2468–2473. https://doi.org/10.1021/acs.nanolett.5b00320.
273. Wang, X.X.; Hwang, S.; Pan, Y.-T.; Chen, K.; He, Y.; Karakalos, S.; Zhang, H.; Spendelow, J.S.; Su, D.; Wu, G. Ordered $Pt_3Co$ Intermetallic Nanoparticles Derived from Metal–Organic Frameworks for Oxygen Reduction. *Nano Lett.* **2018**, *18*, 4163–4171. https://doi.org/10.1021/acs.nanolett.8b00978.
274. Zhu, G.; Jiang, Y.; Yang, H.; Wang, H.; Fang, Y.; Wang, L.; Xie, M.; Qiu, P.; Luo, W. Constructing Structurally Ordered High-Entropy Alloy Nanoparticles on Nitrogen-Rich Mesoporous Carbon Nanosheets for High-Performance Oxygen Reduction. *Adv. Mater.* **2022**, *34*, 2110128. https://doi.org/10.1002/adma.202110128.
275. Zuo, X.; Yan, R.; Zhao, L.; Long, Y.; Shi, L.; Cheng, Q.; Liu, D.; Hu, C. A hollow PdCuMoNiCo high-entropy alloy as an efficient bi-functional electrocatalyst for oxygen reduction and formic acid oxidation. *J. Mater. Chem. A* **2022**, *10*, 14857–14865. https://doi.org/10.1039/d2ta02597c.
276. Zuo, Y.; Rao, D.; Li, S.; Li, T.; Zhu, G.; Chen, S.; Song, L.; Chai, Y.; Han, H. Atomic Vacancies Control of Pd-Based Catalysts for Enhanced Electrochemical Performance. *Adv. Mater.* **2018**, *30*, 1704171. https://doi.org/10.1002/adma.201704171.

277. He, C.; Tao, J.; Shen, P.K. Solid Synthesis of Ultrathin Palladium and Its Alloys' Nanosheets on RGO with High Catalytic Activity for Oxygen Reduction Reaction. *ACS Catal.* **2018**, *8*, 910–919. https://doi.org/10.1021/acscatal.7b03190.
278. Chen, Z.; Zhang, J.; Zhang, Y.; Liu, Y.; Han, X.; Zhong, C.; Hu, W.; Deng, Y. NiO-induced synthesis of PdNi bimetallic hollow nanocrystals with enhanced electrocatalytic activities toward ethanol and formic acid oxidation. *Nano Energy* **2017**, *42*, 353–362. https://doi.org/10.1016/j.nanoen.2017.11.033.
279. Löffler, T.; Meyer, H.; Savan, A.; Wilde, P.; Garzón Manjón, A.; Chen, Y.-T.; Ventosa, E.; Scheu, C.; Ludwig, A.; Schuhmann, W. Discovery of a Multinary Noble Metal–Free Oxygen Reduction Catalyst. *Adv. Energy Mater.* **2018**, *8*, 1802269. https://doi.org/10.1002/aenm.201802269.
280. Rao, P.; Deng, Y.; Fan, W.; Luo, J.; Deng, P.; Li, J.; Shen, Y.; Tian, X. Movable type printing method to synthesize high-entropy single-atom catalysts. *Nat. Commun.* **2022**, *13*, 5071. https://doi.org/10.1038/s41467-022-32850-8.
281. Hu, J.; Cao, L.; Wang, Z.; Liu, J.; Zhang, J.; Cao, Y.; Lu, Z.; Cheng, H. Hollow high-entropy metal organic framework derived nanocomposite as efficient electrocatalyst for oxygen reduction reaction. *Compos. Commun.* **2021**, *27*, 100866. https://doi.org/10.1016/j.coco.2021.100866.
282. Wu, S.; Zhu, Y.; Huo, Y.; Luo, Y.; Zhang, L.; Wan, Y.; Nan, B.; Cao, L.; Wang, Z.; Li, M.; et al. Bimetallic organic frameworks derived CuNi/carbon nanocomposites as efficient electrocatalysts for oxygen reduction reaction. *Sci. China Mater.* **2017**, *60*, 654–663. https://doi.org/10.1007/s40843-017-9041-0.
283. Sun, Y.; Shen, Z.; Xin, S.; Ma, L.; Xiao, C.; Ding, S.; Li, F.; Gao, G. Ultrafine Co-doped ZnO nanoparticles on reduced graphene oxide as an efficient electrocatalyst for oxygen reduction reaction. *Electrochim. Acta* **2017**, *224*, 561–570. https://doi.org/10.1016/j.electacta.2016.12.021.
284. Hao, R.; Chen, J.; Wang, Z.; Zhang, J.; Gan, Q.; Wang, Y.; Li, Y.; Luo, W.; Wang, Z.; Yuan, H.; et al. Iron polyphthalocyanine-derived ternary-balanced $Fe_3O_4$/$Fe_3N$/Fe-N-C@PC as a high-performance electrocatalyst for the oxygen reduction reaction. *Sci. China Mater.* **2021**, *64*, 2987–2996. https://doi.org/10.1007/s40843-021-1699-4.
285. Bockris, J.O.M.; Otagawa, T. The electrocatalysis of oxygen evolution on perovskites. *J. Electrochem. Soc.* **1984**, *131*, 290.
286. Meng, Y.; Song, W.; Huang, H.; Ren, Z.; Chen, S.-Y.; Suib, S.L. Structure–Property Relationship of Bifunctional $MnO_2$ Nanostructures: Highly Efficient, Ultra-Stable Electrochemical Water Oxidation and Oxygen Reduction Reaction Catalysts Identified in Alkaline Media. *J. Am. Chem. Soc.* **2014**, *136*, 11452–11464. https://doi.org/10.1021/ja505186m.
287. Liang, Y.; Li, Y.; Wang, H.; Zhou, J.; Wang, J.; Regier, T.; Dai, H. $Co_3O_4$ nanocrystals on graphene as a synergistic catalyst for oxygen reduction reaction. *Nat. Mater.* **2011**, *10*, 780–786. https://doi.org/10.1038/nmat3087.
288. Liang, Y.; Wang, H.; Diao, P.; Chang, W.; Hong, G.; Li, Y.; Gong, M.; Xie, L.; Zhou, J.; Wang, J.; et al. Oxygen Reduction Electrocatalyst Based on Strongly Coupled Cobalt Oxide Nanocrystals and Carbon Nanotubes. *J. Am. Chem. Soc.* **2012**, *134*, 15849–15857. https://doi.org/10.1021/ja305623m.
289. Zhang, Y.; Zhang, Z.; Jiang, G.; Mamaghani, A.H.; Sy, S.; Gao, R.; Jiang, Y.; Deng, Y.; Bai, Z.; Yang, L.; et al. Three-dimensionally ordered mesoporous $Co_3O_4$ decorated with Mg as bifunctional oxygen electrocatalysts for high-performance zinc-air batteries. *Nano Energy* **2022**, *100*, 107425. https://doi.org/10.1016/j.nanoen.2022.107425.
290. Tong, X.; Chen, S.; Guo, C.; Xia, X.; Guo, X.-Y. Mesoporous $NiCo_2O_4$ Nanoplates on Three-Dimensional Graphene Foam as an Efficient Electrocatalyst for the Oxygen Reduction Reaction. *ACS Appl. Mater. Interfaces* **2016**, *8*, 28274–28282. https://doi.org/10.1021/acsami.5b10044.
291. Qian, M.; Cheng, X.; Sun, T.; Tian, J.; Isimjan, T.T.; Shi, Z.; Yang, X. Synergistic catalytic effect of N-doped carbon embedded with CoFe-rich $CoFe_2O_4$ clusters as highly efficient catalyst towards oxygen reduction. *J. Alloys Compd.* **2020**, *819*, 153015. https://doi.org/10.1016/j.jallcom.2019.153015.
292. Wan, H.; Lv, M.; Liu, X.; Chen, G.; Zhang, N.; Cao, Y.; Wang, H.; Ma, R.; Qiu, G. Activating Hematite Nanoplates via Partial Reduction for Electrocatalytic Oxygen Reduction Reaction. *ACS Sustain. Chem. Eng.* **2019**, *7*, 11841–11849. https://doi.org/10.1021/acssuschemeng.9b02352.
293. Shang, L.; Yu, H.; Huang, X.; Bian, T.; Shi, R.; Zhao, Y.; Waterhouse, G.I.N.; Wu, L.-Z.; Tung, C.-H.; Zhang, T. Well-Dispersed ZIF-Derived Co,N-Co-doped Carbon Nanoframes through Mesoporous-Silica-Protected Calcination as Efficient Oxygen Reduction Electrocatalysts. *Adv. Mater.* **2016**, *28*, 1668–1674. https://doi.org/10.1002/adma.201505045.
294. Hu, Y.; Liu, Y.; Sun, Y. Superparticles: Mesoporous Colloidal Superparticles of Platinum-Group Nanocrystals with Surfactant-Free Surfaces and Enhanced Heterogeneous Catalysis (Adv. Funct. Mater. 11/2015). *Adv. Funct. Mater.* **2015**, *25*, 1613. https://doi.org/10.1002/adfm.201570074.
295. Knossalla, J.; Mezzavilla, S.; Schüth, F. Continuous synthesis of nanostructured silica based materials in a gas–liquid segmented flow tubular reactor. *New J. Chem.* **2016**, *40*, 4361–4366.
296. Mosa, I.M.; Biswas, S.; El-Sawy, A.M.; Botu, V.; Guild, C.J.; Song, W.; Ramprasad, R.; Rusling, J.F.; Suib, S.L. Tunable mesoporous manganese oxide for high performance oxygen reduction and evolution reactions. *J. Mater. Chem.* **2016**, *4*, 620–631.
297. Amer, M.S.; Ghanem, M.A.; Arunachalam, P.; Al-Mayouf, A.M.; Hadadi, S.M. Bifunctional Electrocatalyst of Low-Symmetry Mesoporous Titanium Dioxide Modified with Cobalt Oxide for Oxygen Evolution and Reduction Reactions. *Catalysts* **2019**, *9*, 836.
298. Wang, Z.; Yang, J.; Tang, Y.; Chen, Z.; Lu, Q.; Shen, G.; Wen, Y.; Liu, X.; Liu, F.; Chen, R. $Fe_3O_4$/$Co_3O_4$ binary oxides as bifunctional electrocatalysts for rechargeable Zn–air batteries by one-pot pyrolysis of zeolitic imidazolate frameworks. *Sustain. Energy Fuels* **2021**, *5*, 2985–2993.

299. Zhang, Y.; Sun, Y.; Cai, Z.; You, S.; Li, X.; Zhang, Y.; Yu, Y.; Ren, N.; Zou, J. Stable CuO with variable valence states cooperated with active $Co^{2+}$ as catalyst/co-catalyst for oxygen reduction/methanol oxidation reactions. *J. Colloid Interface Sci.* **2021**, *593*, 345–358. https://doi.org/10.1016/j.jcis.2021.02.125.
300. Amer, M.S.; Arunachalam, P.; Ghanem, M.A.; Al-Mayouf, A.M.; Shar, M.A. Enriched active surface structure in nanosized tungsten-cobalt oxides electrocatalysts for efficient oxygen redox reactions. *Appl. Surf. Sci.* **2020**, *513*, 145831. https://doi.org/10.1016/j.apsusc.2020.145831.
301. Liang, Y.; Wang, H.; Zhou, J.; Li, Y.; Wang, J.; Regier, T.; Dai, H. Covalent Hybrid of Spinel Manganese–Cobalt Oxide and Graphene as Advanced Oxygen Reduction Electrocatalysts. *J. Am. Chem. Soc.* **2012**, *134*, 3517–3523. https://doi.org/10.1021/ja210924t.
302. Zhu, H.; Zhang, S.; Huang, Y.-X.; Wu, L.; Sun, S. Monodisperse $M_xFe_{3-x}O_4$ (M = Fe, Cu, Co, Mn) Nanoparticles and Their Electrocatalysis for Oxygen Reduction Reaction. *Nano Lett.* **2013**, *13*, 2947–2951. https://doi.org/10.1021/nl401325u.
303. Wang, Y.; Ding, W.; Chen, S.; Nie, Y.; Xiong, K.; Wei, Z. Cobalt carbonate hydroxide/C: An efficient dual electrocatalyst for oxygen reduction/evolution reactions. *Chem. Commun.* **2014**, *50*, 15529–15532. https://doi.org/10.1039/c4cc07722a.
304. Wu, G.; Nelson, M.A.; Mack, N.H.; Ma, S.; Sekhar, P.; Garzon, F.H.; Zelenay, P. Titanium dioxide-supported non-precious metal oxygen reduction electrocatalyst. *Chem. Commun.* **2010**, *46*, 7489–7491. https://doi.org/10.1039/c0cc03088k.
305. Imai, H.; Matsumoto, M.; Miyazaki, T.; Fujieda, S.; Ishihara, A.; Tamura, M.; Ota, K.-i. Structural defects working as active oxygen-reduction sites in partially oxidized Ta-carbonitride core-shell particles probed by using surface-sensitive conversion-electron-yield x-ray absorption spectroscopy. *Appl. Phys. Lett.* **2010**, *96*, 191905–191905. https://doi.org/10.1063/1.3430543.
306. Sasaki, K.; Zhang, L.; Adzic, R.R. Niobium oxide-supported platinum ultra-low amount electrocatalysts for oxygen reduction. *Phys. Chem. Chem. Phys.* **2008**, *10*, 159–167. https://doi.org/10.1039/b709893f.
307. Beall, C.E.; Fabbri, E.; Schmidt, T.J. Perovskite Oxide Based Electrodes for the Oxygen Reduction and Evolution Reactions: The Underlying Mechanism. *ACS Catal.* **2021**, *11*, 3094–3114. https://doi.org/10.1021/acscatal.0c04473.
308. Suntivich, J.; Gasteiger, H.A.; Yabuuchi, N.; Nakanishi, H.; Goodenough, J.B.; Shao-Horn, Y. Design principles for oxygen-reduction activity on perovskite oxide catalysts for fuel cells and metal-air batteries. *Nat. Chem.* **2011**, *3*, 546–550. https://doi.org/10.1038/nchem.1069.
309. Lang, P.; Yuan, N.; Jiang, Q.; Zhang, Y.; Tang, J. Recent Advances and Prospects of Metal-Based Catalysts for Oxygen Reduction Reaction. *Energy Technol.* **2020**, *8*, 1900984. https://doi.org/10.1002/ente.201900984.
310. Gao, M.R.; Jiang, J.; Yu, S.H. Solution-based synthesis and design of late transition metal chalcogenide materials for oxygen reduction reaction (ORR). *Small* **2012**, *8*, 13–27. https://doi.org/10.1002/smll.201101573.
311. Feng, Y.; Alonso-Vante, N. Nonprecious metal catalysts for the molecular oxygen-reduction reaction. *Phys. Status Solidi (B)* **2008**, *245*, 1792–1806. https://doi.org/10.1002/pssb.200879537.
312. Behret, H.; Binder, H.; Sandstede, G. Electrocatalytic oxygen reduction with thiospinels and other sulphides of transition metals. *Electrochim. Acta* **1975**, *20*, 111–117. https://doi.org/10.1016/0013-4686(75)90047-X.
313. He, T.; Alonso-Vante, N. In situ Free-Surfactant Synthesis and ORR- Electrochemistry of Carbon-Supported $Co_3S_4$ and $CoSe_2$ Nanoparticles. *Chem. Mater.* **2008**, *20*, 26–28. https://doi.org/10.1021/cm7024763.
314. Gao, M.-R.; Liu, S.; Jiang, J.; Cui, C.; Yao, W.T.; Yu, S.-H. In Situ Controllable Synthesis of Magnetite Nanocrystals/$CoSe_2$ Hybrid Nanobelts and Their Enhanced Catalytic Performance. *J. Mater. Chem.* **2010**, *20*, 9355–9361. https://doi.org/10.1039/C0JM01547D.
315. Wu, G.; Zelenay, P. Nanostructured Nonprecious Metal Catalysts for Oxygen Reduction Reaction. *Acc. Chem. Res.* **2013**, *46*, 1878–1889. https://doi.org/10.1021/ar400011z.
316. Huang, N.; Yan, S.; Zhang, M.; Ding, Y.; Yang, L.; Sun, P.; Sun, X. A $MoS_2$-$Co_9S_8$-NC heterostructure as an efficient bifunctional electrocatalyst towards hydrogen and oxygen evolution reaction. *Electrochim. Acta* **.2019**, *327*, 134942. https://doi.org/10.1016/j.electacta.2019.134942.
317. Doan-Nguyen, V.V.T.; Zhang, S.; Trigg, E.B.; Agarwal, R.; Li, J.; Su, D.; Winey, K.I.; Murray, C.B. Synthesis and X-ray Characterization of Cobalt Phosphide (Co2P) Nanorods for the Oxygen Reduction Reaction. *ACS Nano* **2015**, *9*, 8108–8115. https://doi.org/10.1021/acsnano.5b02191.
318. Huang, K.; Bi, K.; Lu, Y.K.; Zhang, R.; Liu, J.; Wang, W.J.; Tang, H.L.; Wang, Y.G.; Lei, M. Porous VOxNy nanoribbons supported on CNTs as efficient and stable non-noble electrocatalysts for the oxygen reduction reaction. *Sci. Rep.* **2015**, *5*, 17385. https://doi.org/10.1038/srep17385.
319. Yao, C.; Li, J.; Zhang, Z.; Gou, C.; Zhang, Z.; Pan, G.; Zhang, J. Hierarchical Core–Shell $Co_2N$/CoP Embedded in N, P-doped Carbon Nanotubes as Efficient Oxygen Reduction Reaction Catalysts for Zn-air Batteries. *Small* **2022**, *18*, 2108094. https://doi.org/10.1002/smll.202108094.
320. Yang, L.; Kimmel, Y.C.; Lu, Q.; Chen, J.G. Effect of pretreatment atmosphere on the particle size and oxygen reduction activity of low-loading platinum impregnated titanium carbide powder electrocatalysts. *J. Power Sources* **2015**, *287*, 196–202. https://doi.org/10.1016/j.jpowsour.2015.03.146.
321. Cui, X.; Meng, L.; Zhang, X.; Wang, X.; Shi, J. Heterogeneous atoms-doped titanium carbide as a precious metal-free electrocatalyst for oxygen reduction reaction. *Electrochim. Acta* **2019**, *295*, 384–392. https://doi.org/10.1016/j.electacta.2018.10.169.
322. Ren, G.; Lu, X.; Li, Y.; Zhu, Y.; Dai, L.; Jiang, L. Porous Core–Shell $Fe_3C$ Embedded N-doped Carbon Nanofibers as an Effective Electrocatalysts for Oxygen Reduction Reaction. *ACS Appl. Mater. Interfaces* **2016**, *8*, 4118–4125. https://doi.org/10.1021/acsami.5b11786.

323. Sun, H.; Liu, S.; Wang, M.; Qian, T.; Xiong, J.; Yan, C. Updating the Intrinsic Activity of a Single-Atom Site with a P–O Bond for a Rechargeable Zn–Air Battery. *ACS Appl. Mater. Interfaces* **2019**, *11*, 33054–33061. https://doi.org/10.1021/acsami.9b11337.
324. Chen, J.; Yuan, X.; Lyu, F.; Zhong, Q.; Hu, H.; Pan, Q.; Zhang, Q. Integrating MXene nanosheets with cobalt-tipped carbon nanotubes for an efficient oxygen reduction reaction. *J. Mater. Chem. A* **2019**, *7*, 1281–1286.
325. Bhattacharyya, S.; Samanta, D.; Roy, S.; Haveri Radhakantha, V.P.; Maji, T.K. In situ Stabilization of Au and Co Nanoparticles in a Redox-Active Conjugated Microporous Polymer Matrix: Facile Heterogeneous Catalysis and Electrocatalytic Oxygen Reduction Reaction Activity. *ACS Appl. Mater. Interfaces* **2019**, *11*, 5455–5461. https://doi.org/10.1021/acsami.8b20610.
326. Xiang, Q.; Liu, Y.; Zou, X.; Hu, B.; Qiang, Y.; Yu, D.; Yin, W.; Chen, C. Hydrothermal Synthesis of a New Kind of N-Doped Graphene Gel-like Hybrid As an Enhanced ORR Electrocatalyst. *ACS Appl. Mater. Interfaces* **2018**, *10*, 10842–10850. https://doi.org/10.1021/acsami.7b19122.
327. Lv, J.-J.; Li, Y.; Wu, S.; Fang, H.; Li, L.-L.; Song, R.-B.; Ma, J.; Zhu, J.-J. Oxygen Species on Nitrogen-Doped Carbon Nanosheets as Efficient Active Sites for Multiple Electrocatalysis. *ACS Appl. Mater. Interfaces* **2018**, *10*, 11678–11688. https://doi.org/10.1021/acsami.8b00240.
328. Wang, W.; Mi, Y.; Kang, Y.; Liu, X.; Imhanria, S.; Lei, Z. Yttrium fluoride doped nitrogen-contained carbon as an efficient cathode catalyst in zinc-air battery. *J. Power Sources* **2020**, *472*, 228451. https://doi.org/10.1016/j.jpowsour.2020.228451.
329. Li, N.; Liu, J.; Dong, B.-X.; Lan, Y.-Q. Polyoxometalate-Based Compounds for Photo- and Electrocatalytic Applications. *Angew. Chem. Int. Ed.* **2020**, *59*, 20779–20793. https://doi.org/10.1002/anie.202008054.
330. Bloor, L.G.; Solarska, R.; Bienkowski, K.; Kulesza, P.J.; Augustynski, J.; Symes, M.D.; Cronin, L. Solar-Driven Water Oxidation and Decoupled Hydrogen Production Mediated by an Electron-Coupled-Proton Buffer. *J. Am. Chem. Soc.* **2016**, *138*, 6707–6710. https://doi.org/10.1021/jacs.6b03187.
331. Stergiou, A.D.; Symes, M.D. Organic transformations using electro-generated polyoxometalate redox mediators. *Catal. Today* **2022**, *384*, 146–155.
332. Bakker, T.M.A.; Mathew, S.; Reek, J.N.H. Lindqvist polyoxometalates as electrolytes in p-type dye sensitized solar cells. *Sustain. Energy Fuels* **2019**, *3*, 96–100. https://doi.org/10.1039/c8se00495a.
333. Anson, C.W.; Stahl, S.S. Mediated Fuel Cells: Soluble Redox Mediators and Their Applications to Electrochemical Reduction of O2 and Oxidation of $H_2$, Alcohols, Biomass, and Complex Fuels. *Chem. Rev.* **2020**, *120*, 3749–3786. https://doi.org/10.1021/acs.chemrev.9b00717.
334. Lv, J.Q.; Lang, Z.L.; Fu, J.Q.; Lan, Q.; Liu, R.; Zang, H.Y.; Li, Y.G.; Ye, D.D.; Streb, C. Molecular Iron Oxide Clusters Boost the Oxygen Reduction Reaction of Platinum Electrocatalysts at Near-Neutral pH. *Angew Chem. Int. Ed. Engl.* **2022**, *61*, e202202650. https://doi.org/10.1002/anie.202202650.
335. Deng, J.; Deng, D.; Bao, X. Robust Catalysis on 2D Materials Encapsulating Metals: Concept, Application, and Perspective. *Adv. Mater.* **2017**, *29*, 1606967. https://doi.org/10.1002/adma.201606967.
336. Zhou, Y.; Gao, G.; Kang, J.; Chu, W.; Wang, L.-W. Transition metal-embedded two-dimensional $C_3N$ as a highly active electrocatalyst for oxygen evolution and reduction reactions. *J. Mater. Chem. A* **2019**, *7*, 12050–12059. https://doi.org/10.1039/c9ta01389j.
337. Wang, X.; Sun, G.; Routh, P.; Kim, D.H.; Huang, W.; Chen, P. Heteroatom-doped graphene materials: Syntheses, properties and applications. *Chem. Soc. Rev.* **2014**, *43*, 7067–7098. https://doi.org/10.1039/c4cs00141a.
338. Kong, X.K.; Chen, C.L.; Chen, Q.W. Doped graphene for metal-free catalysis. *Chem. Soc. Rev.* **2014**, *43*, 2841–2857. https://doi.org/10.1039/c3cs60401b.
339. Lu, S.; Zhang, Y.; Lou, F.; Guo, K.; Yu, Z. Non-precious metal activated MoSi2N4 monolayers for high-performance OER and ORR electrocatalysts: A first-principles study. *Appl. Surf. Sci.* **2022**, *579*, 152234. https://doi.org/10.1016/j.apsusc.2021.152234.
340. Huang, Z.; Pan, H.; Yang, W.; Zhou, H.; Gao, N.; Fu, C.; Li, S.; Li, H.; Kuang, Y. In Situ Self-Template Synthesis of Fe–N-Doped Double-Shelled Hollow Carbon Microspheres for Oxygen Reduction Reaction. *ACS Nano* **2018**, *12*, 208–216. https://doi.org/10.1021/acsnano.7b05832.
341. Li, M.; Xiao, Z.; Fan, L.; Wang, F.; Du, X.; Kang, Z.; Fan, W.; Guo, Z.; Sun, D. Fe/N-doped carbon nanofibers with $Fe_3O_4$/$Fe_2C$ nanocrystals enchased as electrocatalysts for efficient oxygen reduction reaction. *Inorg. Chem. Front.* **2019**, *6*, 2296–2303.
342. Han, J.; Meng, X.; Lu, L.; Bian, J.; Li, Z.; Sun, C. Single-Atom Fe-Nx-C as an Efficient Electrocatalyst for Zinc–Air Batteries. *Adv. Funct. Mater.* **2019**, *29*, 1808872. https://doi.org/10.1002/adfm.201808872.
343. Wen, Z.; Ci, S.; Zhang, F.; Feng, X.; Cui, S.; Mao, S.; Luo, S.; He, Z.; Chen, J. Nitrogen-Enriched Core-Shell Structured Fe/$Fe_3C$-C Nanorods as Advanced Electrocatalysts for Oxygen Reduction Reaction. *Adv. Mater.* **2012**, *24*, 1399–1404. https://doi.org/10.1002/adma.201104392.

344. Zhang, L.; Fan, L.; Yang, P.; Li, M.; Zhang, H.; Tang, Y.; Kang, Z.; Guo, H.; Wang, R.; Sun, D. Green synthesis of hierarchical carbon coupled with $Fe_3O4/Fe_2C$ as an efficient catalyst for the oxygen reduction reaction. *Mater. Adv.* **2020**, *1*, 2010–2018. https://doi.org/10.1039/d0ma00454e.
345. Chen, C.; Wang, X.-T.; Zhong, J.-H.; Liu, J.; Waterhouse, G.I.N.; Liu, Z.-Q. Epitaxially Grown Heterostructured $SrMn_3O_{6-x}$-$SrMnO_3$ with High-Valence $Mn^{3+/4+}$ for Improved Oxygen Reduction Catalysis. *Angew. Chem. Int. Ed.* **2021**, *60*, 22043–22050. https://doi.org/10.1002/anie.202109207.